lek. Julia Dudkiewicz-Garbicz

Inhibicja CDK12/13 jako strategia przełamywania oporności na deksametazon w ostrej białaczce limfoblastycznej

Rozprawa na stopień doktora nauk medycznych i nauk o zdrowiu w dyscyplinie nauki medyczne

Promotor: Prof. dr hab. n. med. Paweł K. Włodarski

Obrona rozprawy doktorskiej przed Radą Dyscypliny Nauk Medycznych Warszawskiego Uniwersytetu Medycznego

Warszawa 2026 r.

Keywords: acute lymphoblastic leukemia, CDK12, CDK13, glucocorticoid resistance, dexamethasone

Słowa kluczowe: ostra białaczka limfoblastyczna, CDK12, CDK13, glikokortykosteroidy, oporność, deksametazon

This work was funded by mini-grant (1MN/4/ M/MG/N/20) from Medical University of Warsaw.

Julia Dudkiewicz-Garbicz, M.D.

Targeting CDK12/13 to Overcome Glucocorticoid Resistance in Acute Lymphoblastic Leukemia

Dissertation submitted for the degree of

Doctor of Philosophy

In the Discipline of Medical Sciences

Supervisor: Paweł K. Włodarski, M.D., Ph.D.

Ph.D. dissertation presented to the Medical Sciences of Discipline Council of Medical University of Warsaw

Warsaw, 2026

To my loving husband, Filip.

Declaration

I hereby declare that except where specific reference is made to the work of others, the contents of this dissertation are original and have not been submitted in whole or in part for consideration for any other degree or qualification in this, or any other university. This dissertation is my own work and contains nothing which is the outcome of work done in collaboration with others, except as specified in the text and Acknowledgements. The research conducted for this dissertation involving human subjects was carried out in accordance with ethical principles, and all necessary approvals and informed consent were obtained. Any sources, data, or ideas from external sources have been appropriately cited and referenced in accordance with the established academic conventions.

Julia Dudkiewicz-Garbicz, M.D.

Warsaw, 2026

Acknowledgements

I want to sincerely thank Prof. Paweł Włodarski for welcoming me into his laboratory for my PhD. His mentorship, and unwavering support were invaluable. I am especially grateful that he fostered my independence, giving me the freedom to explore unconventional ideas, and encouraging me to think for myself. I also want to thank the other members of the Methodology Department of the Medical University of Warsaw. Special thanks go to Prof. Przemysław Juszczyński, Director at the Institute of Hematology and Transfusion Medicine, for creating an environment that fostered my research pursuits. I extend my deepest appreciation to all members of the Department of Experimental Hematology, especially Ewa Kurtz, Marcin Kaszkowiak, and Paulina Laskowska, for their support throughout this project. I am also thankful to Prof. Aleksandra Banaszkiewicz, the Head of the Department of Pediatrics and Pediatric Gastroenterology, Prof. Marcin Dziekiewicz, Prof. Marcin Banasiuk, Dr. Izabella Łazowska-Przeorek, and Dr. Maria Kotowska for facilitating my growth as a resident. I sincerely thank Monika Sarnecka, Kaja Zawrotny, Tomek Janiga, Aleksandra Warchoł, and Sylwia Dywicka from the Department for their friendship and support. I also wish to thank Prof. Ruben Carrasco from the Dana-Farber Cancer Institute for his steadfast support. Furthermore, I would like to acknowledge all the medical staff, patients, and their families whose participation made this research possible.

On a personal note, I thank my family, especially my brother Jacek, sister-in-law Ola, and my nephews Stefan and Marian, for cheering me up and keeping me going. I would like to thank Zuzanna Handziuk and Paula Łojek for their sense of humor, constant encouragement, and friendship. My gratitude also extends to Ewa Urbańska, my high school biology teacher, under whose guidance I conducted my first scientific project and learned what it means to have a true mentor.

Finally, my deepest gratitude goes to my husband. Thank you for believing in me when I doubted myself, for the daily lessons in perseverance, and for your constant friendship. This journey would not have been possible without you.

Table of Contents

i List of figures

ii List of tables

iii Abbreviations

A

- A3SS: Alternative 3′ splice sites
- A5SS: Alternative 5′ splice sites
- ALE: Alternative last exon
- ALL: Acute lymphoblastic leukemia
- alloSCT / aSCT: Allogeneic stem cell transplantation
- AML: Acute myeloid leukemia
- APA: Alternative polyadenylation
- APL: Acute promyelocytic leukemia

B

- B-ALL: B-cell acute lymphoblastic leukemia/lymphoma
- B-LBL: Lymphomatous presentation of B-ALL
- BM: Bone marrow
- BSA: Bovine serum albumin

C

- CBC: Complete blood count
- CCNK: Cyclin K
- CDK12: Cyclin-dependent kinase 12
- CDK13: Cyclin-dependent kinase 13
- CDS: Coding sequence
- CLL: Chronic lymphocytic leukemia
- CML: Chronic myeloid leukemia
- CNS: Central nervous system
- COG: Children's Oncology Group
- cPARP: Cleaved poly (ADP-ribose) polymerase
- CR: Complete remission
- CR1: First complete remission
- CT: Computed tomography
- CTD: C-terminal domain of RNA polymerase II

D

- DDR: DNA damage response
- DEGs: Differentially expressed genes
- DEXA: Dexamethasone
- DMSO: Dimethyl sulfoxide
- DSMZ: German Collection of Microorganisms and Cell Cultures

E

- ETP: Early T-cell precursor ALL

F

- FAB: French-American-British
- FBS: Fetal bovine serum
- FDR: False discovery rate
- FFPE: Formalin-fixed paraffin-embedded
- FISH: Fluorescence in situ hybridization

G

- GCs: Glucocorticoids
- GR: Glucocorticoid receptor
- GSEA: Gene set enrichment analysis

H

- HLA: Human leukocyte antigen
- HR: Homologous recombination
- HSPCs: Hematopoietic stem and progenitor cells

I

- iAMP21: Intrachromosomal amplification of chromosome 21
- ICC: International Consensus Classification of Myeloid and Lymphoid Neoplasms
- IC_{50}: Half-maximal inhibitory concentration
- IEGs: Immediate early genes
- IGH: Immunoglobulin heavy chain
- IGL: Immunoglobulin light chain
- IHC: Immunohistochemistry
- IPA: Intronic polyadenylation
- IRB: Institutional Review Board

J

- JC: Junction counts

L

- LoF: Loss of function

M

- MDS: Myelodysplastic syndromes
- MDS/MPN-RS-T: Myelodysplastic/myeloproliferative neoplasm with ringed sideroblasts and thrombocytosis
- MLL: Mixed-lineage leukemia
- MPAL: Mixed phenotype acute leukemia

- MRD: Measurable residual disease
- MSigDB: Molecular Signatures Database
- MTS: 3-(4,5-dimethylthiazol-2-yl)-5-(3-carboxymethoxyphenyl)-2-(4-sulfophenyl)-2H-tetrazolium (CellTiter 96 AQueous One Solution)
- MXE: Mutually exclusive exons

N

- NCI: National Cancer Institute
- NES: Normalized enrichment score
- NOS: Not otherwise specified
- ns: Non-significant

P

- PBMCs: Peripheral blood mononuclear cells
- PBS: Phosphate-buffered saline
- PC: Principal component
- PCA: Principal component analysis
- PCR: Polymerase chain reaction
- Ph-like: BCR::ABL1-like / Philadelphia chromosome-like
- PI: Propidium iodide
- PIC: Pre-initiation complex
- Pol II: RNA polymerase II
- pre-RC: Pre-replicative complex
- pSer2: Phosphorylated Serine 2
- pSer5: Phosphorylated Serine 5

R

- RI: Retained introns
- rMATS: Replicate Multivariate Analysis of Transcript Splicing
- RNA-seq: RNA sequencing
- RS: Arginine/serine-rich

S

- SCT: Stem cell transplantation
- SDS-PAGE: SDS–polyacrylamide gel electrophoresis
- SE: Skipped exons
- SEER: Surveillance, Epidemiology, and End Results
- STK: Serine/threonine kinase

T

- T-ALL: T-cell acute lymphoblastic leukemia/lymphoma
- TBST: Tris-buffered saline with Tween 20
- TCR: T-cell receptor
- TdT: Terminal deoxynucleotidyl transferase
- TES: Transcription end site

- TF: Transcription factor
- TKIs: Tyrosine-kinase inhibitors
- TLS: Tumor lysis syndrome
- TMA: Tissue microarray
- TSS: Transcription start site

U

- UTR: Untranslated region

V

- VST: Variance-stabilizing transformation

W

- WBC: White blood cell

iv Streszczenie

Inhibicja CDK12/13 jako strategia przełamywania oporności na deksametazon w ostrej białaczce limfoblastycznej

Lek. Julia Dudkiewicz-Garbicz

Ostra białaczka limfoblastyczna (ALL) jest najczęściej występującym nowotworem złośliwym u dzieci. Mimo znacznej poprawy wskaźników przeżyć w ostatnich dekadach, podgrupa pacjentów z chorobą oporną na leczenie lub jej nawrotem wciąż rokuje niepomyślnie. Głównym czynnikiem predykcyjnym sukcesu terapii jest początkowa odpowiedź pacjenta na glikokortykosteroidy, stanowiące podstawę leczenia indukcyjnego w ALL. Glikokortykosteroidy wiążą się z receptorem glikokortykosteroidowym i inicjują rozległe zmiany transkrypcyjne, które napędzają szlaki proapoptotyczne i przeprogramowanie metaboliczne. Ponieważ komórki oporne na glikokortykosteroidy nie są w stanie uruchomić tych kluczowych programów transkrypcyjnych, postawiłam hipotezę, że zahamowanie kompleksu CDK12/CDK13/CCNK, odpowiedzialnego za podtrzymywanie onkogennej transkrypcji przez regulację polimerazy RNA II, może przywrócić ich podatność na apoptozę. W niniejszej pracy wykazano, że ekspresja CDK12, CDK13 i CCNK jest podwyższona w ALL, a komórki białaczkowe wykazują od nich funkcjonalną zależność. Farmakologiczna inhibicja CDK12/13 jest cytotoksyczna dla komórek ALL, oszczędzając jednocześnie zdrowe komórki jednojądrzaste krwi obwodowej i działa synergistycznie z deksametazonem, głównie w B-ALL. Pod względem mechanistycznym, inhibicja CDK12/13 hamuje programy transkrypcyjne związane ze wzrostem komórki (w tym szlaki zależne od mTORC1, *MYC* i *E2F*), obniża ekspresję genów zaangażowanych w naprawę DNA oraz indukuje zmiany w alternatywnym splicingu RNA. Zaburzenia te aktywują komórkową odpowiedź na stres i w unikalny sposób wzmacniają program transkrypcyjny indukowany przez glikokortykosteroidy w komórkach uprzednio opornych na deksametazon. Dodatkowo, zahamowanie CDK12/13 wywołuje uszkodzenia DNA, zatrzymanie cyklu komórkowego w fazie G2 oraz apoptozę, również w opornych komórkach B-ALL. Tym samym skojarzenie inhibicji CDK12/13 z deksametazonem stanowi racjonalną strategię przełamywania oporności na glikokortykosteroidy w ALL.

v Summary

Targeting CDK12/13 to Overcome Glucocorticoid Resistance in Acute Lymphoblastic Leukemia

Julia Dudkiewicz-Garbicz, M.D.

Acute lymphoblastic leukemia (ALL) is the most common childhood cancer. Although research has dramatically improved survival rates, a subgroup of relapsed or refractory patients continues to experience poor outcomes. A primary predictor of treatment success is the patient's initial response to glucocorticoids, a mainstay of ALL induction therapy. Glucocorticoids bind to the glucocorticoid receptor to initiate a vast transcriptional shift that drives pro-apoptotic pathways and metabolic reprogramming. The failure of resistant cells to execute these programs led to the hypothesis that targeting the CDK12/CDK13/CCNK complex, a master regulator of RNA polymerase II responsible for maintaining oncogenic transcription, could restore pro-apoptotic susceptibility. In this study, we found that CDK12, CDK13, and CCNK are upregulated in B-ALL, with a strong functional dependency on this complex across B- and T-ALL models in CRISPR screen. Pharmacological inhibition of CDK12/13 was highly cytotoxic to ALL cells, sparing healthy peripheral blood mononuclear cells, and acted synergistically with dexamethasone, predominantly in B-ALL. Mechanistically, CDK12/13 inhibition suppressed growth-associated programs (such as mTORC1*,* *MYC*, and *E2F* targets), downregulated DNA repair genes, and induced alternative splicing events. This disruption activated cellular stress responses and uniquely potentiated the glucocorticoid-responsive transcriptional program in otherwise dexamethasone-resistant cells. Ultimately, targeting the CDK12/13 axis induced DNA damage, G2 cell cycle arrest, and apoptosis in dexamethasone-resistant B-ALL cells, establishing combined CDK12/13 inhibition and glucocorticoid therapy as a mechanistically rational strategy to overcome glucocorticoid resistance in ALL.

Chapter 1: Introduction

1.1 Acute Lymphoblastic Leukemia: Epidemiology, subtypes and clinical relevance

Lymphoid neoplasms are a heterogenous group of cancers that originate from cells of the lymphoid lineage. The fundamental distinction based on the stage of maturation divides them into two major categories: precursor lymphoid neoplasms, which arise from immature cells, and mature lymphoid neoplasms, which arise from differentiated cells [1].

Precursor acute lymphoblastic leukemia (ALL) is an aggressive neoplasm of immature lymphoid progenitor cells, known as lymphoblasts. These malignant cells rapidly proliferate and crowd out healthy hematopoietic cells in the bone marrow (BM), disrupting the normal production of red blood cells, white blood cells, and platelets. This leads to common clinical manifestations such as anemia, frequent infections, and bleeding [2]. Based on the cell of origin, ALL is further subclassified as:

- B-lymphoblastic leukemia/lymphoma (B-ALL): Arising from B-cell progenitors, this is the most common form, accounting for approximately 80% of cases. They can be identified based on cell surface expression of CD19 and at least one other recognized B lineage-associated antigen: CD20, CD24, CD22, CD21, or CD79. They may also express CD34 or terminal deoxynucleotidyl transferase (TdT). The most common subtype of precursor B-cell ALL, termed common precursor B-cell ALL, also expresses CD10.
- T-lymphoblastic leukemia/lymphoma (T-ALL): Arising from T-cell progenitors, comprise approximately 15% of ALL cases. These cases can be classified according to the sequence of expression of T-cell-associated surface antigens during normal thymocyte ontogeny [2,3].
- Mixed-Lineage Leukemia (MLL): These leukemias arise from blast cells that express markers of both lymphoid and myeloid lineages. The majority of MLL cases consist of blasts with lymphoid morphology that coexpress myeloid-associated antigens. Conversely, some MLLs exhibit myeloid morphology but express surface antigens typically restricted to lymphoid cells. Bilineal leukemia, in contrast, refers to cases in which two distinct blast populations

coexist - one of lymphoid and one of myeloid origin - rather than a single population with mixed immunophenotypic features [2,4].

An overview of hematopoietic neoplasms classified in a lineage-specific context is presented in Figure 1.

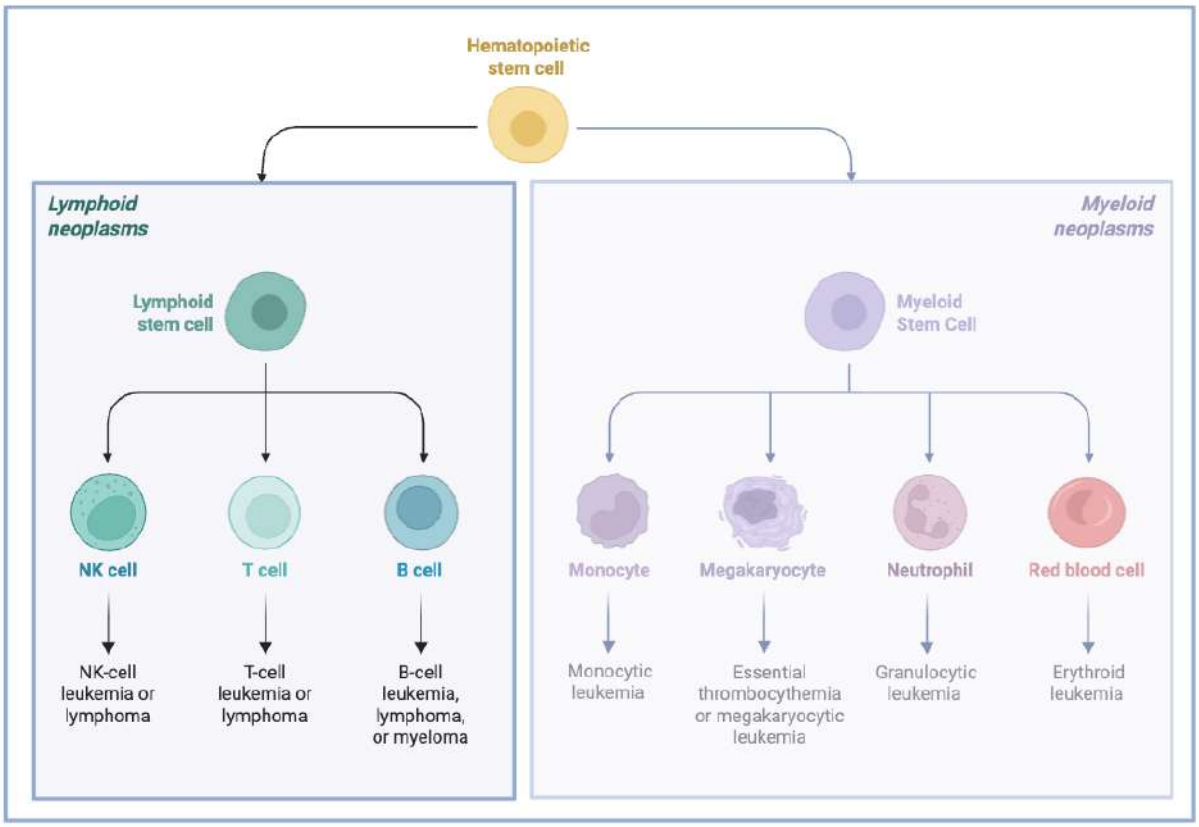

Figure 1. Hematologic neoplasms in the context of normal blood cell development, with the left portion highlighting lymphoid neoplasms.

The clinical terminology – leukemia versus lymphoma – is determined by the primary site of disease presentation. The diagnosis is termed leukemia when the bone marrow contains 20% or more blasts. When the disease primarily manifests as a tumor mass in an extramedullary site, it is termed lymphoma. Nonetheless, they are considered biologically equivalent provided they derive from the same lineage [1]. Lymphomatous presentations of B-ALL (B-LBL, B-lymphoblastic lymphoma) are less common than of T-ALL (T-LBL, T-lymphoblastic lymphoma), occurring predominantly in individuals younger than 20 years [5,6].

ALL is the most common cancer in children, representing approximately 25% of cancer diagnoses in children younger than 15 years, with the peak incidence of approximately

four to five cases per 100,000 children between 2 and 5 years of age. The rate of ALL diagnosis drops significantly after early childhood and stays low for several decades, followed by a slight but notable increase among individuals older than 50 [7].

According to SEER data from 2015-2021, the overall 5-year relative survival rate for ALL is 72.6%; however, this outcome varies significantly with age. Survival is most favorable for children under 15 (~90%) and lower for adolescents aged 15 to 19 (~75 %) [8]. The annual incidence of leukemia in European children aged 0-19 was approximately 40 to 60 cases per 1 million, with minor variation across countries. Comparable rates are reported in the United States, at roughly 34 cases per 1 million. Across all age groups, incidence is consistently higher in boys than in girls, especially in T-ALL [9–11]. Relapsed ALL has low overall survival of only 40% [12], and is characterized by chemotherapeutic drug resistance [13].

1.2 ALL: Etiology and risk factors

The etiology of ALL is complex and not yet fully understood; however, both genetic predispositions and environmental exposures have been implicated in increasing leukemia risk. Prior exposure to ionizing radiation, diagnostic x-rays and certain chemotherapeutic or immunosuppressive agents are associated with an elevated risk. In addition, several inherited genetic syndromes predispose to ALL, most notably trisomy 21 (Down syndrome), as well as immunodeficiency diseases (Wiskott-Aldrich syndrome, congenital hypogammaglobulinemia), and disorders of genomic instability and defective DNA repair, such as Bloom syndrome, Fanconi anemia, and ataxia-telangiectasia [14]. The development of certain ALL subtypes (ETV6::RUNX1–positive or hyperdiploid) has been linked to the immune system's maturation. Although the spectrum of genetic alterations in ALL varies with patient age, the molecular mechanisms driving leukemic transformation within specific genetic subtypes are largely conserved across age groups [15,16].

1.3 Clinical presentation and diagnosis

Patients with ALL present with a variety of nonspecific symptoms that correlate with the degree of bone marrow failure and the extent of extramedullary disease [2].

Common presenting symptoms reflect bone marrow infiltration and include fatigue, pallor, and anorexia (due to anemia); bleeding diathesis such as petechiae,

ecchymoses, or mucosal bleeding (due to thrombocytopenia); and fever (due to neutropenia and/or cytokine release). Bone pain is also frequent, and young children may present with a limp or refusal to walk due to leukemic infiltration of bones or joints. Less common systemic symptoms include night sweats and weight loss.

Extramedullary involvement can affect nearly any organ system:

- Central Nervous System (CNS): CNS involvement, typically restricted to the pia mater and arachnoid, may cause headaches, vomiting, lethargy, cranial nerve palsies, and visual complaints (e.g., papilledema, retinal hemorrhages). Epidural spinal cord compression is rare.
- Mediastinum: Approximately 55% of children with precursor T-ALL present with an anterior mediastinal mass [2]. This mass can compress the trachea or great vessels, leading to respiratory distress (cough, dyspnea, orthopnea, dysphagia) or superior vena cava syndrome, which manifests as facial edema, stridor, cyanosis, increased intracranial pressure, or syncope.
- Other Sites: Lymphadenopathy, hepatomegaly, and splenomegaly are among the most common extramedullary findings, which may be asymptomatic or cause abdominal fullness and early satiety. Other common sites of extramedullary disease include testis (usually a painless, asymmetric enlargement), tonsils, and adenoids. Less frequent involvement includes breast, gastrointestinal tract, salivary glands (Mikulicz syndrome), skin (leukemia cutis), and orbits [2].

1.3.1 Laboratory findings

Laboratory findings at diagnosis commonly reveal anemia and thrombocytopenia. Abnormalities in the complete blood count (CBC), with at least one hematologic parameter affected, are seen in more than 90% of ALL patients at the time of diagnosis; however, the percentage of blasts can range from 0 to 100%. Anemia is usually normochromic, normocytic, and accompanied by reticulocytopenia. The white blood cell (WBC) count may be low, normal or elevated: approximately 45% of children have a WBC count below 10 x 10^9/L, while 15% present with hyperleukocytosis (>100 x 10^9/L) [2]. Hyperleukocytosis is a medical emergency that can cause leukostasis, manifesting as dyspnea, chest pain, altered mental status, cranial nerve palsies, or priapism. It also increases the risk of tumor lysis syndrome (TLS). Neutropenia is

commonly present, and in contrast, eosinophilia is rare. Eosinophilia is seen in association with specific chromosomal abnormalities, including t(5;14)(q31;q32), or 8p11-associated ALL. The eosinophilia can mask the blast population in a subset of patients [2].

Other laboratory findings, especially in patients with a high leukemic burden, include elevated serum uric acid and lactate dehydrogenase. Tumor lysis syndrome can lead to hyperuricemia, hyperkalemia, hyperphosphatemia, and secondary hypocalcemia. Renal involvement or TLS can cause elevated creatinine and urea nitrogen. Hypercalcemia can also occur due to the release of parathyroid hormone-related protein by leukemic cells. Coagulopathy is usually mild. Finally, 10-20% of pediatric patients may present with liver dysfunction [2].

These clinical manifestations are illustrated in Figure 2.

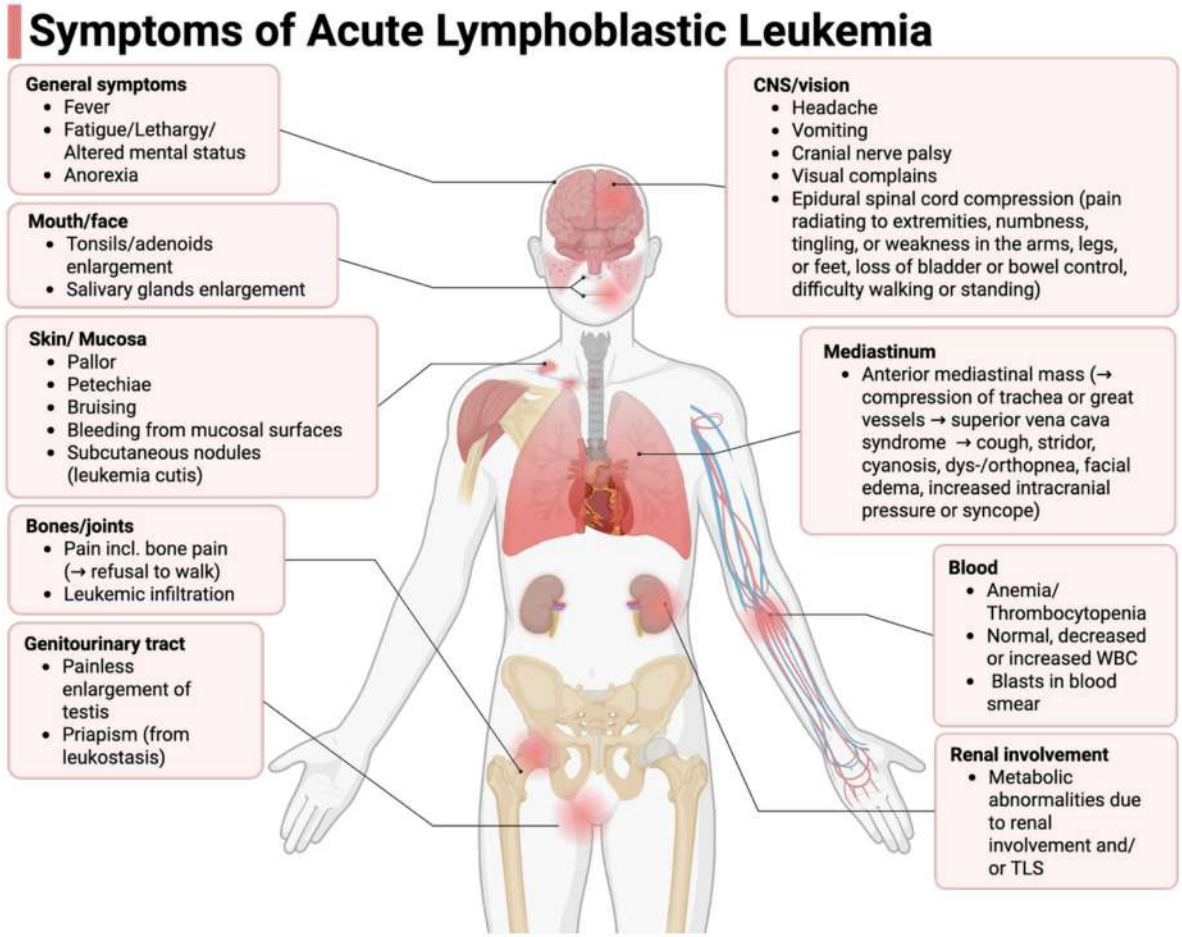

Figure 2. Common clinical manifestations of acute lymphoblastic leukemia. The primary symptoms of ALL arise from two main processes. (1) Bone marrow failure: The overproduction of lymphoblasts crowds out normal blood cell precursors, leading to anemia (causing fatigue, pallor, and weakness), thrombocytopenia (causing easy bruising, petechiae, and bleeding), and neutropenia (leading to frequent or severe infections). (2) Leukemic

infiltration: Lymphoblasts invade extramedullary sites, causing lymphadenopathy, hepatosplenomegaly, and bone pain (due to marrow expansion). Central Nervous System (CNS) involvement can lead to headaches, vomiting, or nerve palsies. Systemic symptoms (fever, night sweats, weight loss) and a high white blood cell (WBC) count are common. A high tumor burden can lead to Tumor Lysis Syndrome (TLS), a metabolic emergency.

Initial evaluation of a patient with suspected ALL, apart from detailed history and physical examination, should include CBC, comprehensive metabolic profile including liver function tests, LDH, uric acid, coagulation profile, bone marrow aspiration and biopsy (morphology, immunohistochemistry, flow cytometry, molecular and cytogenetic analysis), human leukocyte antigen (HLA) typing (if a patient is a potential candidate for allogenic stem cell transplantation (aSCT)), lumbar puncture, and chest radiography or computed tomography (CT) of the chest (Figure 3).

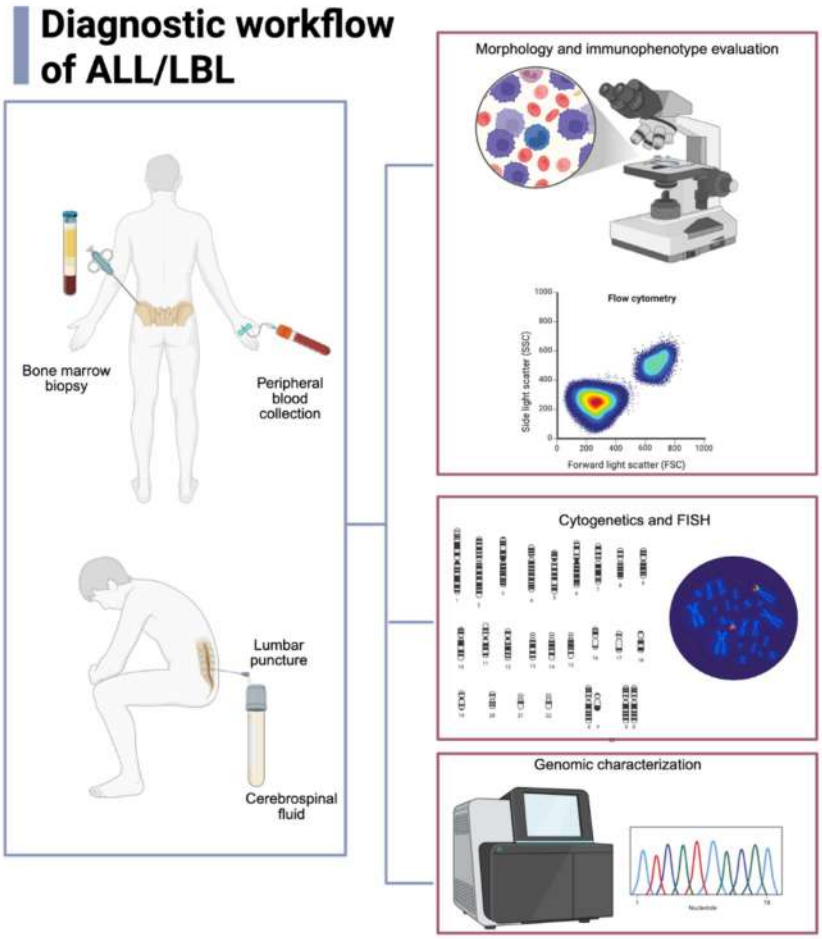

Figure 3. Diagnostic workflow for ALL/LBL. Initial suspicion arises from clinical symptoms and a complete blood count showing cytopenias or circulating blasts. A definitive diagnosis is made by bone marrow aspirate and biopsy, where morphology confirms >20% lymphoblasts and immunophenotyping by flow cytometry determines the B-cell or T-cell lineage. A lumbar puncture is performed to stage the central nervous system (CNS). Finally, genetic analyses (including cytogenetics, FISH, and molecular sequencing) are performed on the bone marrow to identify key structural variants (e.g., BCR-ABL1, KMT2Ar) and mutations (e.g., IKZF1) crucial for risk stratification and treatment planning. FISH, fluorescence in situ hybridization.

1.3.2 Morphology and immunophenotype evaluation

While evaluation of morphology and immunophenotype is sufficient for making the diagnosis, current risk stratification relies on additional cytogenetic and molecular genetic information. Morphologic evaluation was the first method known to distinguish leukemia types, and it relied on, currently partly outdated, French-American-British (FAB) classification [2]. It gives information about BM cellularity, and cell morphology and can already give first suspicion about the leukemia type (ALL or AML). For lineage distinction and the developmental stage at which the transformation occurred, extensive immunophenotypic characterization with multicolor flow cytometry is required, in which multiple antigens can be simultaneously detected on the lymphoblasts. No single antigen is specific for a given lineage, thus multiple antigens have to be evaluated to establish the correct diagnosis. The panel of antigens used for immunophenotyping of ALL is shown in Table 1.

	Commonly Positive	Variable Expression
B-ALL	*TdT*	*CD20*
	sCD22	*CD13*
	cCD22	*CD33*
	CD10	*CD34*
	Pax5	*CD38*
	cCD79a	*CD45*
	CD24	*CD58*
	CD19	*sIgM*
T-ALL	*TdT*	*CD1a*
	cCD3	*CD2*
	CD7	*sCD3*
		CD5
		CD8
		CD10
		CD13
		CD19
		CD33
		CD34
		CD56
		CD79a
		CD99
		CD117

Table 1. Antigens used in immunophenotyping characterization of ALL. B-ALL, B-acute lymphoblastic leukemia; T-ALL, T-acute lymphoblastic leukemia; c, cytoplasmic; s, surface.

1.3.3 Molecular alterations in ALL

Evidence for the prenatal origin of pediatric ALL is strongly supported by studies of monozygotic (identical) twins. The concordance rate for ALL is exceptionally high when the disease is diagnosed in infancy, approaching 100% for monochorionic twins who

share a single placenta. This high risk is attributed to the direct transfer of leukemic cells from one twin to the other via their shared placental circulation [17]. The concordance risk declines sharply with age, eventually reaching that of the general population by approximately age 7.

While this prenatal event establishes a pre-leukemic clone, the development of ALL is a multistep process that requires the acquisition of additional postnatal genomic alterations. Furthermore, ALL is not a single disease but a heterogeneous group of malignancies, with distinct subtypes defined by their unique molecular pathogenesis. This underlying genetic diversity is clinically critical, as it results in varying responses to therapy and forms the basis for modern risk stratification [2].

Advances from classical cytogenetic studies, complemented by fluorescence in situ hybridization (FISH) and targeted polymerase chain reaction (PCR), to whole-transcriptome sequencing have markedly increased the granularity of ALL classification. These technologies have enabled the identification of numerous molecular subclasses of ALL, facilitating the development of targeted therapies and more accurate risk stratification, which in turn allows the use of treatments with reduced toxicity.

Molecular alterations in B-cell Acute Lymphoblastic Leukemia (B-ALL)

B-ALL represents a genetically heterogeneous group of neoplasms derived from precursor B-lymphoblasts arrested at various stages of differentiation. Nearly all cases exhibit rearrangement of the immunoglobulin heavy chain (*IGH*) gene, although such rearrangements can also occur in T-ALL and AML, limiting their lineage specificity [1]. In contrast, immunoglobulin light chain (IGL) rearrangements are considered more specific for B-cell differentiation [1].

A. Quantitative chromosomal abnormalities

Chromosomal abnormalities can be detected in about 80% of B-ALL and 70% of T-ALL. Cytogenetic classification remains one of the most important prognostic factor for both pediatric and adult patients.

- **High hyperdiploidy**, defined by > 50 chromosomes, predicts an excellent prognosis and represents about ~25% of childhood B-ALL [18,19]. This favorable outcome is independent of age or white-blood-cell count [20].

Trisomies 4 and 10 are particularly favorable and are sometimes used as surrogates for hyperdiploidy in treatment assignment [21].

- **Moderate hyperdiploidy** (47–50 chromosomes) occurs in 10–15% of cases but does not confer the same favorable prognosis [19].
- **Hypodiploidy** (< 45 chromosomes) is associated with adverse outcome [22] and is now formally subdivided into low-hypodiploid B-ALL (32–39 chromosomes) and near-haploid B-ALL (24–31 chromosomes) [23–25]. Low-hypodiploid cases often harbor loss-of-function *TP53* and *RB1* mutations, with germline *TP53* alterations indicating a Li-Fraumeni–like predisposition [24]. Near-haploid cases instead show frequent *RAS* and receptor tyrosine kinase mutations [24,25].
- **Intrachromosomal amplification of chromosome 21 (iAMP21)**, characterized by ≥ 4 copies of *RUNX1* on an abnormal chromosome, defines another entity [26]. These patients (≈ 2% of childhood B-ALL) are typically older children with low WBC counts and *CRLF2* overexpression; the lesion predicts poor outcome without intensive therapy [26].

B. Recurrent translocations and gene fusions

ETV6::RUNX1 [t(12;21)(p13.2;q22.1)]

The *ETV6::RUNX1* fusion is the most common lesion in pediatric B-ALL (~25%) but rare in adults [27]. It encodes a hybrid transcription factor combining the HLH domain of ETV6 with the DNA-binding region of RUNX1 [28–30]. Because this cryptic translocation is balanced, detection typically requires FISH [31]. Immunophenotypically, these leukemias show CD34 +, partial CD20, dim or absent CD9, CD27 +, and CD44 low/negative [32,33]. *ETV6::RUNX1* conveys a favorable event-free survival [34], although late relapse has been reported [35]. Identical *ETV6::RUNX1* fusions found in monozygotic twins years apart support its role as an early leukemogenic event [36].

BCR::ABL1 and BCR::ABL1-like (Ph-like) B-ALL

The Philadelphia chromosome, t(9;22)(q34.1;q11.2), produces a constitutively active *BCR*::*ABL1* tyrosine kinase and occurs in ~ 25% of adult and up to 5% of childhood B-ALL [37,38]. The resultant 190 kDa fusion protein drives proliferation and survival

[38,39]. Historically conferring a poor prognosis [40–42], outcomes have improved with tyrosine kinase inhibitors (TKIs) [43]. The International Consensus Classification of Myeloid and Lymphoid Neoplasms (ICC) recognizes two subtypes: *BCR*::*ABL1*-positive ALL-L (lymphoid-restricted) and *BCR*::*ABL1*-positive ALL-M (multilineage involvement) [44]. The former originates in committed lymphoid progenitors; the latter resembles chronic myeloid leukemia (CML) in lymphoid blast phase but lacks prior CML history [44].

A related subgroup, BCR::ABL1-like (Ph-like) B-ALL, has a similar gene expression signature but lacks *BCR::ABL1*. It includes three molecular classes [45,46]:

1. **ABL1-class rearranged** – fusions of *ABL1, ABL2, PDGFRB,* or *CSF1R*, potentially responsive to ABL-directed TKIs [46];
2. **JAK–STAT-activated** – lesions involving *CRLF2* (*IGH*::*CRLF2* or *P2RY8*::*CRLF2*) and *JAK1/2* mutations, for which JAK inhibitors are in clinical trials [46];
3. **Not otherwise specified (NOS) subgroup** – heterogeneous kinase fusions (*FLT3, FGFR1, NTRK3, PTK2B*), often TKI-sensitive [46]. Overall, Ph-like B-ALL carries a poor prognosis [46].

KMT2A-rearranged B-ALL

Rearrangements of KMT2A (formerly MLL) at 11q23.3 are recurrent in infants and therapy-related B-ALL [47]. The most frequent fusion, *KMT2A::AFF1* [t(4;11)(q21;q23)], and variants with partners such as *MLLT1* (19p13) confer aggressive clinical behavior [47–49]. These leukemias typically show CD19+, CD10-, CD24-, and often co-express myeloid antigens (CD15, CD65) [48,49]. They frequently present with high leukocyte counts, organomegaly, and CNS involvement [47–49].

TCF3 fusions

The *TCF3::PBX1* [t(1;19)(q23.3;p13.3)] fusion defines ~5% of pediatric B-ALL [50]. The blasts are CD19+, CD10+, CD9 uniform, partially CD20+, and CD34- [50]. Once considered adverse, its prognosis is now comparable to other intermediate-risk groups under current regimens [51,52].The rare *TCF3::HLF* [t(17;19)(q22;p13.3)] fusion (<

1%) occurs mainly in adolescents with disseminated intravascular coagulation or hypercalcemia and has a very poor prognosis [53–55].

Other recurrent fusion subtypes

- **DUX4-rearranged B-ALL**, usually *IGH::DUX4*, occurs in 5–10% of adolescent and young-adult cases, with a favorable prognosis even in the presence of poor-risk lesions [33,56]. Detection may require RNA-seq because of the repetitive nature of *DUX4* and *IGH* loci [56].
- **ZNF384-rearranged B-ALL** (5–10%) affects children and young adults and shows variable outcome [57,58]. Frequent partners include *EP300*, *TCF3*, and *TAF15* [58].
- **MEF2D-rearranged** and **HLF-rearranged** B-ALLs are rare but associated with poor prognosis [59].
- **CDX2/UBTF** B-ALL carries a *UBTF::ATXN7L3* fusion and *CDX2* up-regulation, both required for leukemogenesis, this subtype also has poor prognosis.
- **NUTM1-rearranged B-ALL**, typically in infants, is paradoxically associated with a favorable outcome [59].
- **MYC-rearranged B-ALL**, although rare (~4% of adults), exhibits bone-marrow predominance rather than mass lesions and carries a poor prognosis [60].

C. Additional genetic lesions

Virtually all cases of B-ALL harbor additional genetic alterations beyond their defining driver lesions [61]. Recurrent events include *IKZF1*, *CDKN2A/B*, and *PAX5* deletions. The clinical impact of these secondary abnormalities depends on the primary subtype: for example, *IKZF1* loss is adverse in Ph-like B-ALL but not in DUX4-rearranged disease [61].

Molecular alterations in T-ALL

T-cell acute lymphoblastic leukemia arises from thymic T-cell precursors arrested at specific stages of differentiation and transformed by distinct genetic events. During normal thymic maturation, progenitor cells sequentially rearrange the T-cell receptor (TCR) loci, beginning with δ and γ concurrently, followed by β, and finally α. Each step of this process is tightly coordinated with transcriptional programs that guide lineage commitment and selection. Leukemic transformation often occurs through dysregulation of these developmental programs, leading to uncontrolled proliferation of immature T-lineage blasts [1].

A. TCR rearrangements and lineage definition

The majority of T-ALL cases harbor clonal rearrangements of TCR genes that reflect the differentiation stage at which transformation occurred. The most immature forms may retain a germline TCR configuration or show only TCR γ rearrangement, whereas more mature cases exhibit productive TCRβ and TCRα or δ rearrangements. Rearrangements of immunoglobulin loci, particularly IGH, are occasionally observed but less common, and IGL rearrangements are exceptional, consistent with T-lineage commitment during leukemogenesis [1].

B. Recurrent transcription factor activation

Unlike precursor B-ALL, which is typically defined by a limited number of canonical fusion genes, T-ALL exhibits extensive molecular heterogeneity. Many of its recurrent chromosomal abnormalities involve TCR loci on chromosomes 7q34 and 14q11, resulting in the juxtaposition of strong TCR enhancers to transcription factor genes such as *TAL1*, *TLX1 (HOX11)*, *TLX3 (HOX11L2)*, *LMO1*, *LMO2*, and *LYL1* [62]. These rearrangements lead to transcriptional activation of oncogenic programs that block differentiation and promote proliferation.

Gene expression profiling studies have further shown that T-ALL can be organized into molecular clusters defined by activation of specific transcriptional networks [63]. Each cluster includes cases driven by various mechanisms (chromosomal rearrangements, enhancer hijacking, or point mutations) that converge on the same transcription factor pathway. Unlike in B-ALL, a single structural event rarely defines an entire molecular subtype. Instead, T-ALL subgroups share downstream transcriptional profiles that reflect deregulation of core developmental regulators.

Because of this complexity, comprehensive genomic or transcriptomic profiling is often required to accurately assign a molecular subtype.

C. Early T-cell precursor (ETP) ALL and BCL11B activation

Among molecularly defined subtypes, early T-cell precursor (ETP) ALL represents one of the most distinctive. This entity, which accounts for approximately 10–15% of T-ALL, shows a gene expression profile closely resembling hematopoietic stem and myeloid progenitor cells [64]. ETP-ALL typically lacks *NOTCH1* mutations but is enriched for alterations in genes more commonly associated with myeloid malignancies, such as *FLT3* (ITD or D835), *DNMT3A*, *WT1*, and *RUNX1* [65]. These findings suggest that ETP-ALL originates from a very early progenitor with multilineage potential.

Within ETP-ALL, a subset of cases (~30%) shows aberrant activation of *BCL11B*, a key transcription factor required for T-cell commitment [66,67]. In most of these leukemias, *BCL11B* is upregulated through interchromosomal rearrangements or focal amplifications that create de novo enhancer regions, leading to sustained overexpression. Designated BCL11B-activated (BCL11B-a) ALL is now recognized as a distinct biological entity in the ICC, distinguishable by strong *BCL11B* immunoreactivity. However, *BCL11B* activation is not exclusive to T-lineage neoplasms and may also occur in AML, undifferentiated leukemia, and MPAL, consistent with its stem cell-related transcriptional signature [67,68].

D. Cooperating mutations and signaling pathway alterations

T-ALL frequently harbors secondary mutations that cooperate with transcription factor dysregulation to promote leukemic transformation. *NOTCH1* mutations, including point mutations, insertions, or deletions, are present in over half of T-ALL cases and cause constitutive activation of NOTCH signaling [69,70]. Because *NOTCH1* activation depends on γ-secretase activity, inhibition of γ-secretase has been proposed as a potential therapeutic approach [69]. *CDKN2A/B* deletions occur in approximately 70% of cases and are considered central to T-ALL pathogenesis, leading to loss of key cell-cycle regulators. Mutations in JAK–STAT or RAS–MAPK pathway genes (*JAK1*, *JAK3*, *NRAS*, *KRAS*) promote cytokine-independent growth and survival [70]. Loss or mutation of *PTEN* further enhances PI3K–AKT signaling and often coexists with *NOTCH1* alterations. In contrast, ETP-ALL typically lacks *NOTCH1* mutations and

displays a mutational spectrum dominated by *FLT3*, *DNMT3A*, and *RUNX1*, paralleling features of myeloid leukemias [64,65].

1.4 Therapeutic challenges and steroid resistance

1.4.1 The standard of care: A phased, risk-adapted approach

Treatment of acute lymphoblastic leukemia is a long-term, multi-modal process that typically spans 2-3 years. This therapy is guided by risk stratification, which varies by age group and protocol. It is divided into three main phases: remission induction, consolidation (or intensification), and maintenance (or continuation), as depicted in Figure 4.

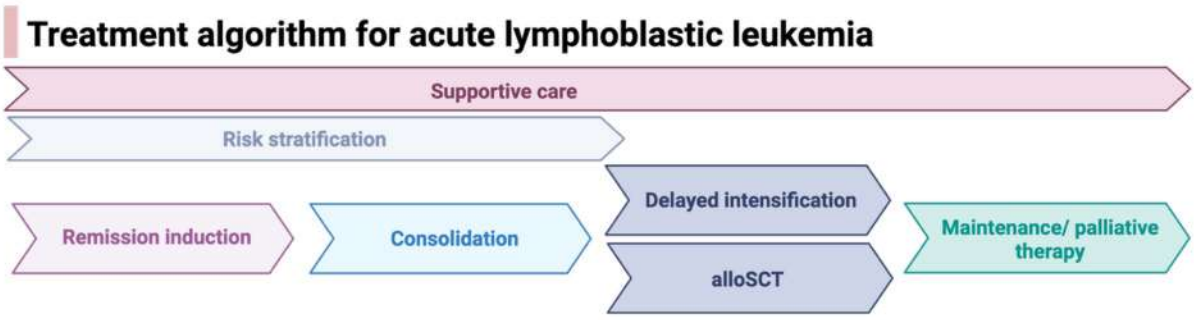

Figure 4. A generalized treatment algorithm for acute lymphoblastic leukemia. The diagram illustrates the major phases of ALL therapy. Treatment begins with remission induction to achieve a complete response, followed by a consolidation phase. Subsequent therapeutic decisions are guided by risk stratification (which includes genetic features, age, and initial response) and may include delayed intensification or allogeneic stem cell transplant (alloSCT). This is followed by a long-term maintenance or palliative therapy phase. Supportive care (e.g., transfusions, infection prophylaxis) is a critical component administered continuously throughout all treatment phases.

The treatment begins with a 4–6-week remission induction phase aimed at eradicating leukemia blasts and restoring normal hematopoiesis with minimal toxicity. This phase typically uses a four- or five-drug backbone consisting of an oral glucocorticoid (prednisone or dexamethasone), weekly vincristine, and at least one additional agent – most often asparaginase, anthracycline (doxorubicin, daunorubicin, or mitoxantrone), or both. Some groups also add cyclophosphamide [2]. Treatment intensity is risk-adapted: in most low-risk cases, a three-drug regimen is sufficient, while the four-drug regimen is used in most high-risk patients as it provides a benefit in long-term survival. Apart from systemic treatment, intrathecal chemotherapy is initiated to treat or prevent central nervous system disease. With current regimens, complete remission (CR) rates reach ~ 98% in children and 80-90% in adults [2].

However, despite this initial success, all patients would relapse if no further therapy were given [2].

The next step, consolidation, aims to eradicate residual leukemic cells. This phase often includes delayed intensification, using drugs similar to those in induction. Again, treatment is risk-adapted: intermediate-risk patients may benefit from a double-delayed intensification, while high-risk patients often receive additional doses of vincristine and asparaginase. Patients at the highest risk of relapse, even after achieving their first complete remission (CR1), are typically candidate for allogenic stem cell transplantation (alloSCT).

After completing induction and consolidation, patients receive maintenance therapy for up to 2.5 years. This low-intensity chemotherapy, designed to eradicate any residual leukemic cells, consists of weekly low-dose methotrexate and daily oral mercaptopurine. Some protocols also involve pulses of vincristine and corticosteroids. The treatment goal is to maintain a white cell count between 2 and 3 x 10^9/L.

1.4.2 The challenges of chemoresistance

While this risk-adapted, multi-phase approach has dramatically improved outcomes, significant therapeutic challenges remain. Risk stratification itself is a complex process, with criteria differing between cooperative consortia [2,71]. Key factors include patient age, initial WBC count, CNS involvement, immunophenotype, and specific genetic alterations (Table 2) [2,72,73].

Risk group	***Features***	***Recommended therapy***	***Projected five-year event-free survival***
Low	**ALL** of the following: 1. NCI standard risk group[a] 2. Lesser risk cytogenetics: - Trisomies 4 and 10 **or** ETV-RUNX1 (United States) **or** Hyperdiploid (Europe) 3. Rapid response to therapy[b]	Conventional antimetabolite-based therapy	>95%
Average	**EITHER** of the following:	Intensified antimetabolite therapy	60 to 95%

	1. NCI standard risk group[a] **and** Rapid response to therapy[b] 2. NCI standard risk group[a] **and** Lesser risk cytogenetics **and** Slow response to therapy[e]		
High	**ANY** of the following: 1. NCI high risk group[e] **and** Rapid response to therapy[b] 2. NCI standard risk group[a] **and** Slow response to therapy[cd] 3. CNS-positive leukemia 4. Testicular leukemia	Intensive multiagent chemotherapy	88-90%
Very high	**ANY** of the following: 1. MRD+ at day 29[d] 2. Induction failures 3. MLL rearrangements **or** iAMP21 amplification 4. Age <1 year (or >13 years if treated on a COG protocol)	Consider allogeneic hematopoietic cell transplantation in first remission Allogenic transplant not recommended for infants	<80%
Special groups	T cell ALL	Intensive multiagent chemotherapy	66-80%
	Philadelphia chromosome [t(9;22)]	Intensive multiagent chemotherapy containing a BCR-ABL tyrosine kinase inhibitor	70%

Table 2. Clinical risk assignment and suggested therapies in childhood acute lymphoblastic leukemia. WBC: white blood cell count; NCI: National Cancer Institute; MRD: measurable residual disease; CNS: central nervous system; MLL: mixed lineage leukemia gene; iAMP21: intrachromosomal amplification of chromosome 21; COG: Children's Oncology Group; ALL: acute lymphoblastic leukemia.

[a] *NCI standard risk group: WBC <50,000/μL AND age one to <10 years.*

[b] *MRD negative at days 8 and 29 (rapid response to therapy).*

[c] *MRD positive at day 8 and negative at day 29 (slow response to therapy).*

[d] *With some exceptions.*

[e] *NCI high risk group: WBC ≥50,000 μL OR age ≥10 years (up to 13 years if treated on a COG protocol).*

Crucially, one of the most powerful prognostic factors is the patient's response to therapy. A patient's response is no longer measured just by achieving morphological remission but by the detection of measurable residual disease (MRD, previously termed minimal residual disease) [74]. Patients who are late responders, fail to achieve MRD negativity after induction, or who relapse have a significantly worse prognosis, highlighting the core challenge of chemoresistance [13,74,75].

This resistance is often evident from the very beginning of treatment. A cornerstone of the induction phase is the glucocorticoid backbone (prednisone or dexamethasone) [2]. A poor initial response to steroids, including approximately 10% of children with ALL [76], is a major negative prognostic factor and a key indicator of underlying resistance [77–84].

Glucocorticoids (GCs) were among the first drugs to demonstrate therapeutic activity in patients with B-cell malignancies, based on the early discovery that they induce a unique mechanism of cell death in lymphoid, but not myeloid, cells [85]. This effect is mediated by the glucocorticoid receptor (GR), encoded by *NR3C1* gene [86]. Upon GC binding, the activated GR translocates from the cytosol to the nucleus, where it binds to specific DNA recognition motifs known as glucocorticoid response elements. Because chromatin accessibility and the expression of GR cofactors vary by cell type, GCs have different effects in different tissues.

GR binding initiates a transcriptional shift characterized by induction of pro-apoptotic genes (e.g. *BCL2L11*) and repression of anti-apoptotic genes (e.g. *BCL2*, BCL-XL) [87,88], leading cells to apoptosis [89]. However, the exact mechanism is not fully understood, and other effects, such as reduced glucose metabolism [90], metabolic reprogramming [91], or suppression of B-cell development genes, have also been suggested as key drivers of cell death [92].

Crucially, *ex vivo* sensitivity of ALL cells to glucocorticoids directly correlates with treatment outcome and the persistence of MRD [93]. This link confirms that steroid resistance is a fundamental driver of treatment failure. Because curative regimens rely on combinations of agents, and since current regimens are insufficient for patients with resistant disease, new synergistic drug combinations that can overcome this resistance are urgently needed.

1.5 CDK12 and CDK13 as therapeutic targets

The previous sections have established that resistance to glucocorticoids is a fundamental driver of treatment failure in ALL, rooted in the leukemic cell's failure to execute a lethal transcriptional program. This "transcriptional addiction" to a pro-survival state represents a core vulnerability. A logical therapeutic strategy, therefore,

is to target the kinases that govern and maintain this aberrant transcriptional machinery.

CDK12 and CDK13 are central coordinators of gene expression. They are transcriptional kinases that, in complex with cyclin K, phosphorylate the C-terminal domain (CTD) of RNA polymerase II (Pol II). This action is critical, as it couples transcription elongation with RNA processing, DNA repair, and replication stress responses. Understanding the biology of these kinases is the next essential step in building the rationale for their inhibition as a strategy to overcome glucocorticoid resistance.

1.5.1 Physiological roles of CDK12 and CDK13

Adaptation to intrinsic and extrinsic stimuli is critical for the survival of all cells, both healthy and cancerous. Upon exposure to stimuli, cells initiate transcriptional and translational processes, leading to dynamic changes in RNA and protein expression, ultimately modulating cellular signaling pathways [94]. Among essential regulators coordinating these adaptive responses are cyclin-dependent kinase 12 and cyclin-dependent kinase 13, two transcriptional kinases involved in various aspects of gene expression.

Cyclin-dependent kinase 13 (CDK13, also known as CHED, CDC2L, CDC2L5, hCDK13; located on chromosome 7p14) and its paralog cyclin-dependent kinase 12 (CDK12, also termed CRKRS, CRKR or CRK7; located on chromosome 17q12) were initially identified through cDNA screens seeking cell-cycle regulators related to CDK1 (CDC2) [95,96]. Both kinases belong to the serine/threonine kinase (STK) subgroup within the eukaryotic protein kinase family [97]. STKs play crucial roles in relaying and modulating signals derived from the local cellular environment [98]. CDK12 and CDK13 are evolutionarily and structurally related, displaying substantial sequence homology (~43%) and high conserved kinase domain with >93% sequence identity, crucial for their catalytic activity [95].

Functionally, CDK12 and CDK13 are classified into the transcription-regulating kinase subgroup [99]. Both kinases phosphorylate the C-terminal domain of RNA polymerase II [100,101]. They associate with cyclin K, forming distinct complexes that differentially modulate kinase activity and substrate specificity [102]. These complexes regulate critical aspects of transcription, including promoter-proximal pause release, elongation

rate, Pol II processivity, and 3' mRNA processing events, enabling proper mRNA maturation [101,103–106]. Alongside their CTD kinase activity, they effectively couple transcription with RNA splicing. CDK12 and CDK13 contain arginine/serine-rich motifs in their N-terminal regions, which serve as docking sites for splicing factors localized within nuclear speckles, specialized subnuclear compartments enriched in splicing regulators [95]. Furthermore, CDK12 and CDK13 regulate the translation of key proteins, such as DNA repair factors, ribosome and translation factors, and structural components essential for chromosome segregation, including centromere and kinetochore proteins [107]. Additionally, the CDK12-cyclin K complex critically influences cell cycle progression by phosphorylating cyclin E1; disruption of this complex leads to G1-phase arrest and mitotic abnormalities [106,108,109].

CDKs have established roles in various pathological conditions, including cancer. CDK12 mutations are among the most frequently observed CDK alterations, identified in approximately 5% of diverse cancer types [110] . CDK12 and CDK13 regulate critical signaling cascades, including NF-kB, MAPK, WNT/β-catenin, and PI3K-AKT underscoring their multifaceted roles in cancer biology [106,111–117].

The following sections will explore these critical functions in detail, beginning with their roles in the transcription and co-transcriptional processing, as illustrated in Figure 5.

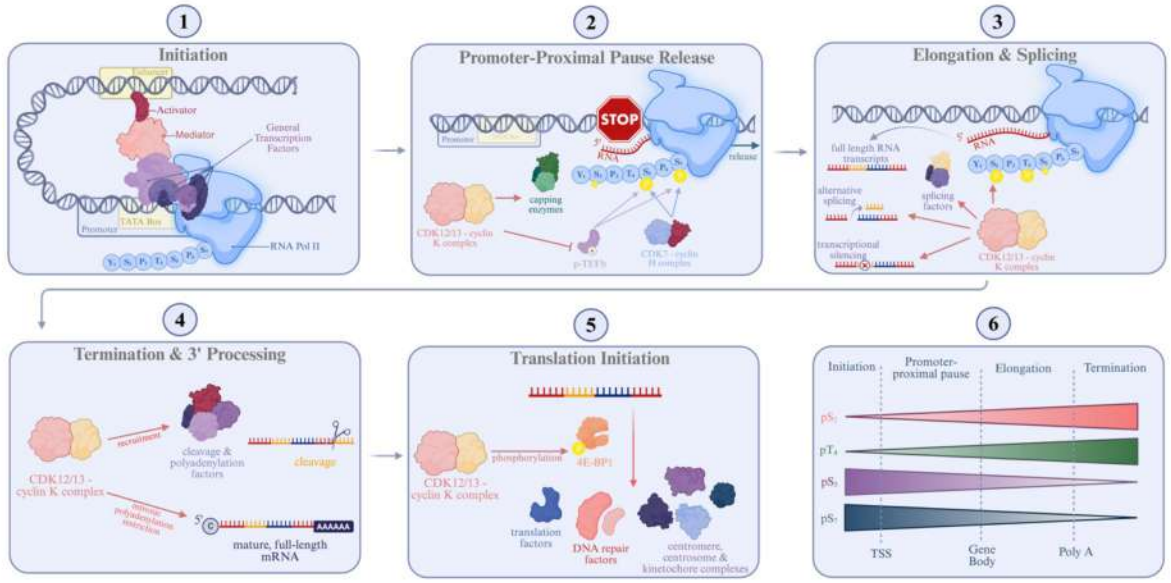

Figure 5. The CDK12/13 complexes regulate multiple stages of transcription and translation. 1. Initiation: RNA polymerase II, together with general transcription factors, activators, and the mediator complex, assembles into the pre-initiation complex (PIC). Following PIC formation, Pol II transcribes a short RNA before pausing at the promoter-proximal pause site, allowing for quality control prior to elongation. 2. Promoter-Proximal Pause Release: The

CDK7-cyclin H complex and p-TEFb (CDK9-cyclin T complex) promote pause release and productive elongation. CDK12/13-cyclin K complex represses p-TEFb. 3. Elongation and Splicing: During productive elongation, CDK12/13 phosphorylate Ser2 of Pol II CTD, enhancing elongation rate and processivity to ensure efficient synthesis of full-length transcripts. CDK12/13 also regulate the activity and expression of splicing factors. Modulation of Pol II elongation rate influences alternative splicing outcomes. 4. Termination and 3' Processing: CDK12 promotes recruitment of cleavage and polyadenylation factors, ensuring proper 3' mRNA processing. CDK12/13 prevent premature transcription termination, maintaining transcriptional fidelity. 5. Regulation of translation initiation: CDK12/13 promote translation by phosphorylating and displacing 4E-BP1 from mRNA targets, which facilitates recruitment of translation factors to the 5' cap. 6. Pol II CTD phosphorylation dynamics: As transcription progresses, phosphorylation of Ser5 and Ser7 decreases, whereas phosphorylation on Ser2 and Thr4 increases. Adapted from "Eukaryotic Gene Regulation - Transcriptional Initiation", by BioRender.com (2025).

Transcription

A. C-Terminal Domain - A key regulatory point of RNA polymerase II

Transcription is a critical regulatory step in gene expression involving precise interactions among Pol II, transcription factors, regulatory cofactors, chromatin remodelers, and enzymes responsible for post-translational modifications (Figure 5) [118]. A distinctive feature of Pol II is the carboxy-terminal heptapeptide repeat domain, located within its largest subunit, RPB1 [119]. Multiple residues within these repeats undergo various post-translational modifications, including phosphorylation, glycosylation, methylation, ubiquitination, acetylation, and cis/trans isomerization. These modifications dynamically regulate interactions crucial for each transcriptional phase and coordinate co-transcriptional RNA processing and histone modifications, collectively forming the "transcription cycle" [119,120]. Both CDK12 and CDK13 possess Pol II CTD kinase activity, specifically regulating Pol II elongation, processivity, and alternative polyadenylation in a gene-specific manner [101,121].

B. Transcription initiation & promoter-proximal pausing

Transcription begins with the recruitment of Pol II to gene promoters (Figure 5). RNA polymerase II, along with general transcription factors, assembles into the pre-initiation complex (PIC). A critical mediator of this process is the unphosphorylated CTD of Pol II, which strongly interacts with transcription initiation factors and chromatin regulators. Additionally, it coordinates the recruitment of the mediator complex - a bridge between transcription factors bound at enhancers and the transcriptional machinery assembled at gene promoters [103,122,123]. After PIC formation and promoter clearance, Pol II synthesizes a short RNA (~25-50 bp) before pausing at the promoter-proximal pause region due to phosphorylation events at CTD residues. This regulated pause allows cells to respond to regulatory cues and ensures transcription quality control before elongation proceeds [104].

C. Promoter-proximal pause release, elongation, and pre-mRNA maturation: key roles of CDK12/13

Transcription initiation and promoter-proximal pause release rely on phosphorylation of Pol II CTD residues, mainly Ser5 and Ser7, by CDK7/cyclin H and CDK9/cyclin T complexes (Figure 5) [105,121]. The CDK9-cyclin T complex, also known as P-TEFb, promotes pause release and productive elongation. CDK12/cyclin K maintains repression of P-TEFb through stabilization of the 7SK snRNP complex. Inhibition of CDK12 disrupts this repression, leading to P-TEFb activation and accelerated pause release at thousands of genes, even those not previously dependent on P-TEFb [112]. The exact mechanism of this regulation has still not been discovered. Once Pol II clears the pause and enters elongation, a new Pol II complex is rapidly recruited and pauses at the same site. This continual replenishment maintains a pool of paused Pol II at promoters, allowing for efficient re-initiation and rapid transcriptional responses [105]. Similar pauses occur throughout elongation as a regulatory checkpoint [124,125].

CDK12 may regulate 5' cap assembly by phosphorylating translation factors, such as 4E-BP1 [106]. Ser5 phosphorylation peaks early in transcription, then gradually declines toward the 3' end of genes (Figure 5) [126,127].

During productive elongation, CDK12 and CDK13 are actively recruited to gene bodies, independently regulating Pol II elongation rates (Figure 5) [128,129]. Both kinases phosphorylate Ser2 residues on the CTD, enhancing elongation [115,121]. Ser2 phosphorylation increases throughout gene bodies, sharply declining after polyadenylation sites (Figure 5) [115]. CDK12/13 also enhance Pol II processivity, preventing premature dissociation and ensuring efficient synthesis of full-length RNA transcripts.

Additionally, CDK12 and CDK13 mediate transcriptional silencing at damaged genes, protecting genome integrity by preventing faulty mRNA synthesis [130]. Following DNA damage, CDK12 recruitment suppresses gene expression independently of DNA damage response (DDR) signaling, yet dependent on PARP activity. Loss or inhibition of CDK12 leads to transcription of damaged genes resistant to DDR mechanisms, causing accumulation of DNA double-strand breaks at these loci [130].

D. Splicing regulation and transcriptional coupling

CDK12 and CDK13 integrate transcription with RNA processing, including splicing (Figure 5) [97,131]. Approximately 50% of introns are spliced co-transcriptionally as they emerge from RNA polymerase II. Synchronization between Pol II elongation and spliceosome assembly is crucial, as disruptions in either process may delay splicing [131]. Slower Pol II elongation promotes alternative splicing by enabling recognition of weaker splice sites [132]. Since CDK12 and CDK13 modulate Pol II activity, they directly affect splicing dynamics [121].

Both CDK12 and CDK13 contain arginine/serine-rich motifs in their N-terminal regions, serving as docking sites for splicing factors within nuclear speckles [95,133]. These kinases regulate activity and expression of splicing factors, with their depletion disrupting RNA processing [116,134–136]. Therefore, CDK12 and CDK13 integrate transcription and splicing through Pol II control and splicing factors regulation [95,133,137].

Pol II pausing further contributes to splicing regulation by allowing additional time for spliceosome function [138]. Paused Pol II is characterized by Ser5 hyperphosphorylation, while subsequent release is marked by increased Ser2 phosphorylation, facilitating exon progression [138]. Simultaneous CDK12/13 inhibition decreases Ser2 and Thr4 phosphorylation, disrupting transcriptional regulation [121]. Given CDK12/13's role in Ser2 phosphorylation, their exact contribution to Pol II pausing and splicing coordination requires further exploration.

E. 3' End processing - polyadenylation and cleavage

CDK12 critically regulates mRNA polyadenylation, a crucial step in transcript maturation. CDK12-mediated Ser2 phosphorylation recruits cleavage and polyadenylation factors to nascent RNA 3' ends, as shown for MYC mRNA (Figure 5) [139]. This is particularly relevant for long genes with cryptic intronic polyadenylation (IPA) sites, notably DDR genes, relevant in ovarian and prostate cancer [140]. CDK12 restricts intronic polyadenylation, ensuring full-length transcript production. Loss of CDK12 globally increases IPA usage, generating shorter mRNA isoforms [135]. Genes with abundant IPA sites are particularly sensitive to CDK12 depletion [115].

CDK12's regulatory role in DDR genes is well-documented across various cancers [116]. Recent studies show that CDK13 also contributes to transcript integrity by

suppressing IPA, a process that leads to premature transcription termination. Loss of CDK13 results in increased production of truncated RNA isoforms from cryptic intronic polyA sites, indicating its role in preventing aberrant RNA processing [141]. Furthermore, CDK12/13 regulate alternative polyadenylation (APA), affecting polyadenylation site selection [116,121,140]. APA controls alternative last exon (ALE) splicing, leading to diverse mRNA isoforms varying at their 3' ends [142].

Therefore, CDK12 and CDK13 enable the maturation of long transcripts and proper transcription termination. They also regulate alternative splicing and polyadenylation [97,121,139].

Translation and cell cycle

CDK12 plays a critical role in regulating translation of specific target mRNAs (Figure 5). Genome-wide analysis identified over 200 genes whose translation is controlled by CDK12 [107]. A key phosphorylation target uncovered by Choi et al. was 4E-BP1, a translation repressor [107]. By phosphorylation of 4E-BP1 at residues S65 and T70, similarly as mTORC1, CDK12 facilitates recruitment of additional translation factors to the 5' mRNA cap. This process controls translation of mRNAs encoding DNA repair and translation factors, centromere, centrosome and kinetochore complexes, essential for chromosome segregation during mitosis and meiosis [107]. Additionally, the CDK12-cyclin K complex critically regulates cell cycle by phosphorylating cyclin E1 at Ser366, thereby blocking its interaction with CDK2. CDK2-cyclin E and CDK2-cyclin A complexes are essential for G1/S phase transition and S/G2 progression. These complexes activate the pre- replicative complex (pre-RC), ensuring that DNA replication occurs precisely once per cycle, preventing DNA re-duplication [143]. Consequently, inhibition of CDK12, CDK13 or cyclin K disrupts pre-RC assembly and results in G1-phase arrest [108,109,115], and persistent DNA damage triggers apoptosis [104,121].

Disruption of translational network and mitotic defects underscore importance of CDK12, CDK13 and cyclin K in maintaining genomic stability and proper cell cycle progression [107,144].

CDK12/13 in embryonic cells and human development

CDK12 maintains pluripotency in embryonic stem cells [145]. Cdk12−/− blastocysts fail to develop due to increased DNA damage, reduced expression of DNA damage

response genes, and apoptosis. Consequently, CDK12 mutations are embryonically lethal in mice [145]. When CDK12 depletion was induced starting from day 10.5, the mice either died shortly after birth or by postnatal day 1 [146]. Moreover, CDK12 or CDK13 knockdown in mouse embryonic stem cells results in loss of self-renewal [147]. In humans, heterozygous mutations within the kinase catalytic domain of CDK13 are associated with a syndromic form of intellectual disability, characterized by feeding difficulties, structural cardiac anomalies, seizures, corpus callosum abnormalities, craniofacial dysmorphism, and autism spectrum disorder [148].

CDK12 and CDK13 play critical roles in neurogenesis, regulating proliferation and differentiation of neuronal precursor cells, DDR gene expression, splicing of blood-brain barrier proteins, and axonal extension [149]. Inhibition of CDK12 disrupts neurogenesis, reducing cerebral cortex size, causing microcephaly, and shrinking the olfactory bulb and cerebellum. Axons fail to cross properly within corpus callosum, leading to abnormalities, alongside reductions in the anterior commissure, internal capsule and posterior commissure [146]. During corticogenesis, CDK12 and CDK13 regulate axonal extension and neuronal migration to the cortical plate [146]. In adult Drosophila, CDK12 loss causes age-dependent neurodegeneration, disrupted actin remodeling, mitochondrial fragmentation, and axonal swelling [150]. Moreover, CDK12 ablation impairs learning in Drosophila melanogaster [151], and is also critical for splicing of Neurexin IV, essential for blood-brain barrier formation [152].

1.5.2 The dual role of CDK12 and CDK13 in cancer

Gene expression dysregulation is a defining hallmark of tumorigenesis [153]. The transcriptional kinases CDK12 and CDK13 are central players in this process, but their influence is highly context-dependent, acting as oncogenic drivers in some tumors and tumor suppressors in others. Figure 6 summarizes the principal types of genomic alterations affecting the CDK12/13-cyclin K complex and the tumor contexts in which they are most frequently observed. These include gene amplifications, deletions, truncating mutations, and fusion events that can either enhance oncogenic transcriptional output or compromise DDR fidelity. Such diversity in alteration type underlies the dual functional spectrum of CDK12/13 across human cancers, discussed in the following sections.

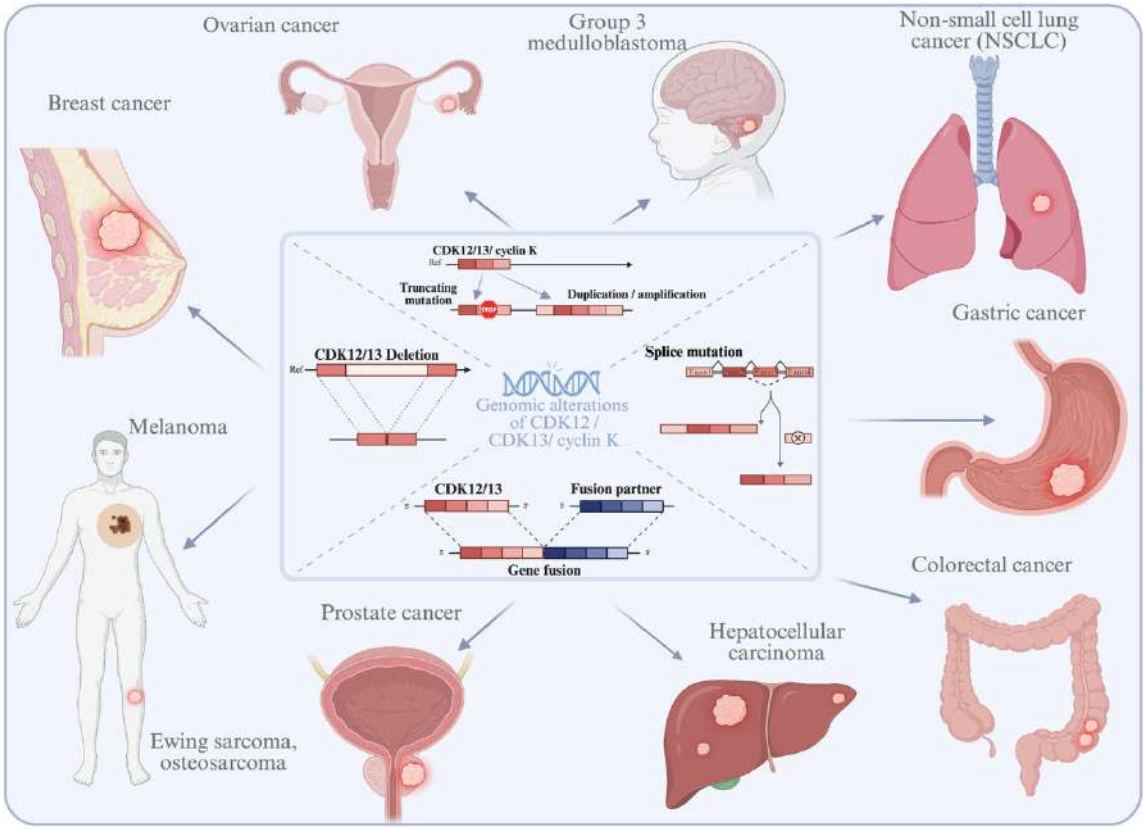

Figure 6. Diverse genomic alterations of CDK12/13/CCNK in cancer. These alterations can either drive oncogenic activity (e.g., amplifications) or lead to a tumor suppressor phenotype (e.g., deletions and truncating mutations). Representative alteration frequencies observed in key malignancies include: CDK12 truncation/loss-of-function in approximately 6% of metastatic prostate cancers, 2-3% of high-grade serous ovarian cancers [154], and CDK12 recurrent somatic alterations (bi-allelic deletions, genomic amplifications and mutations) in 13% of breast cancers [116]. Created with BioRender.com.

To fully appreciate the diverse roles of CDK12 and CDK13 in oncology, it is essential to contextualize their alterations within the broader pan-cancer landscape. The selective pressure for tumors to co-opt these kinases is not uniform; rather, it manifests through distinct genomic, transcriptomic, and dependency patterns that vary by malignancy. Integration of large-scale, multi-omic datasets from the DepMap project and cBioPortal reveals a comprehensive overview of this landscape (Figure 7).

This analysis reveals several key trends. First, a striking functional dependency on both CCNK and CDK12 is evident across most cancer cell lines, as demonstrated by pan-cancer negative CRISPR scores. This dependency co-exists with widespread transcriptional upregulation. While this overexpression is a general feature, specific genomic events are concentrated in particular tumor types. For instance, CDK12 alterations are notably frequent in breast, colorectal, pancreatic and prostate carcinomas. Interestingly, very few cancer cell lines harbor CDK12/13 mutations or deletions, which points to a possible reduced fitness of such clones when cultured in

vitro. This is consistent with the idea that complete loss of CDK12/13 function is poorly tolerated outside specific genetic backgrounds.

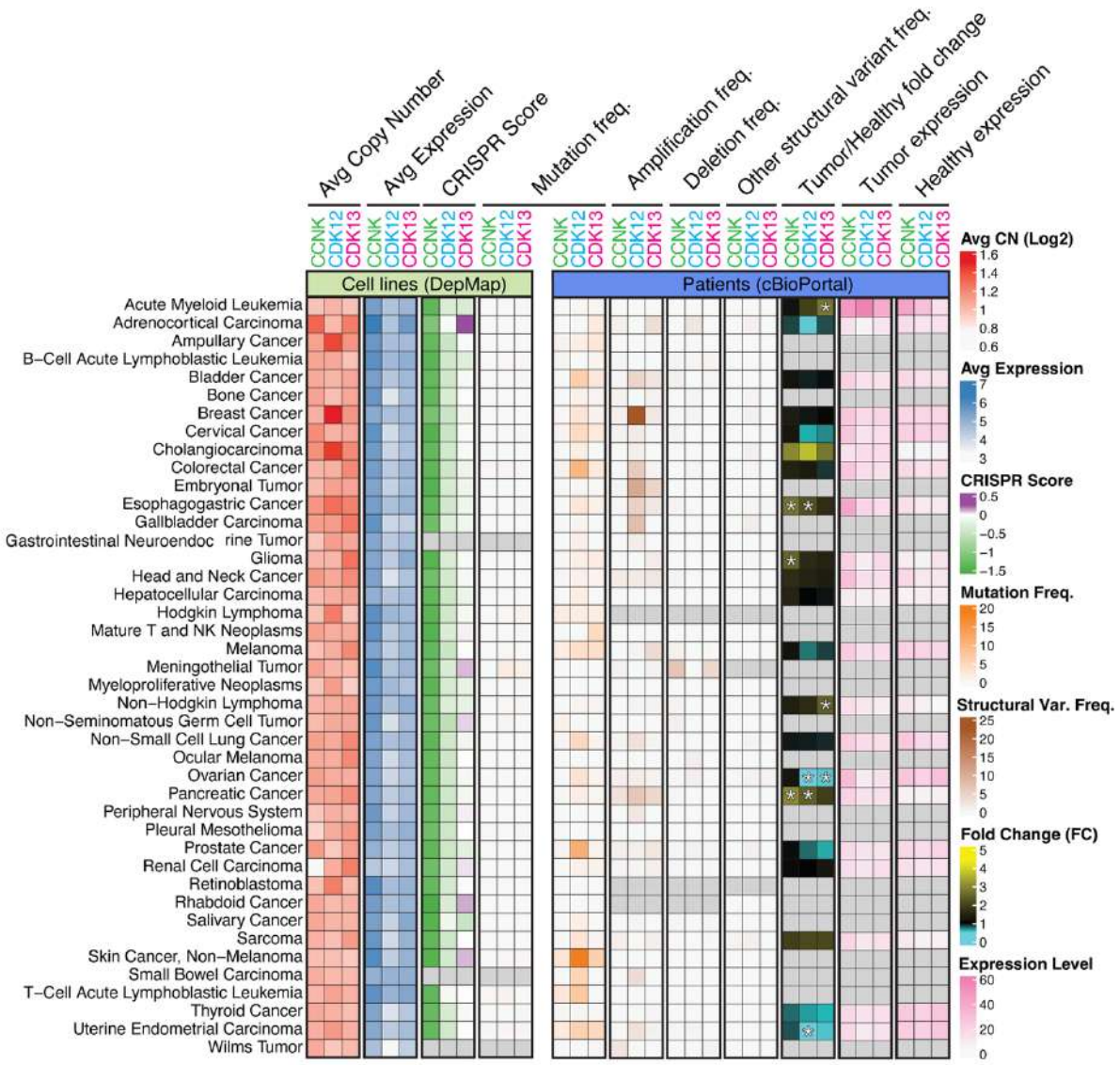

Figure 7. Genomic and transcriptomic features of CCNK, CDK12, CDK13 across human cancers. This figure integrates multi-omic data from cell line models (left panel) and patients (right panel) to provide a comprehensive pan-cancer landscape. Data was integrated from publicly available datasets (DepMap 24Q4 and cBioPortal, 231 studies) and harmonized using a standardized ontology to map disparate histological subtypes to unified cancer lineages (rows). We aggregated lineage-specific means for WGS copy number, gene expression, and CRISPR Chronos scores, alongside mutation frequencies (mutated/total cell lines). Additionally, tumor versus normal expression comparisons were integrated from GEPIA, utilizing its standard one-way ANOVA on $log_2(TPM + 1)$ values, where TMP is Transcripts Per Million. Asterisks (*) denote statistically significant tumor-to-normal expression differences ($p < 0.05$), and grey squares indicate missing data values. These multi-omics metrics for CCNK, CDK12, and CDK13 were merged and visualized using the ComplexHeatmap R package.

A. The oncogenic roles of CDK12/13

In many cancers, elevated CDK12/13 activity is a key driver of tumor progression. This is frequently achieved through gene amplification or transcriptional upregulation (Figure 7) [155]. Analysis of tumor versus normal tissue shows that CDK12 and CDK13

are frequently upregulated across multiple cancer types (Figure 7) [110]. Enhanced CDK12/13 activity drives oncogenic transcriptional programs, sustaining higher expression levels of replication and stress-response genes and supporting tolerance to replication stress [107,113]. In breast cancer, overexpression of CDK12 activates the WNT/β-catenin and PI3K–AKT pathways [107], while in gastric cancer CDK12 cooperates with PAK2 to sustain MAPK signaling [113].

Large-scale CRISPR dependency screens confirm that numerous tumor cell lines display strong dependence on CDK12/13 [156] (Figure 7). These data position CDK12/13 among key transcriptional kinases that maintain oncogenic gene-expression networks and indicate that their inhibition may disrupt the transcriptional addiction characteristic of numerous cancers [153].

B. Tumor suppressor functions, genomic instability, and adaptive responses to CDK12/13 loss

In contrast to their oncogenic roles, CDK12 and CDK13 can also function as tumor suppressors in specific contexts, particularly in ovarian and metastatic castration-resistant prostate cancers [144,157]. In these tumors, CDK12 is frequently inactivated by truncating mutations, deletions, or gene fusions (Figure 7). Loss of CDK12 disrupts transcription of key DDR genes, such as *BRCA1, ATR*, and *FANCI*, and leads to defective HR. The resulting “BRCAness” phenotype manifests as tandem duplications and widespread genomic instability [100,140]. Mechanistically, CDK12 loss promotes transcription-replication conflicts, causing polymerase collisions and DNA double-strand breaks [130]. This triggers a dependency on compensatory repair pathways and sensitizes cells to PARP inhibitors, representing a prototypical synthetic-lethal interaction [158,159].

However, the biological consequences of CDK12 inactivation differ between acute pharmacologic inhibition and chronic genomic loss. In tumors chronically adapted to CDK12 deficiency, HR genes can become transcriptionally restored through compensatory mechanisms, including partial redundancy with CDK13, while specific loci such as ATM remain truncated and downregulated. As a result, these tumors often retain functional HR capacity and lack the genomic scars typical of HR-deficient cancers [160]. This adaptive equilibrium may explain the limited clinical efficacy of PARP inhibitor monotherapy in certain CDK12-mutant malignancies and underscores

the importance of co-targeting CDK13 or other transcriptional dependencies to overcome resistance.

C. CDK12 and tumor immunogenicity

The loss of CDK12 function impacts tumor immunogenicity through multiple, interconnected mechanisms. Primarily, the resulting genomic instability leads to the accumulation of tandem duplications, which generate a high burden of fusion-derived neoantigens [144,157]. This enhanced neoantigen load increases the tumor's visibility to the immune system, often fostering a T-cell-inflamed microenvironment characterized by elevated expression of interferon-stimulated genes and pro-inflammatory cytokines [161].

Beyond increasing antigen presentation, CDK12 directly shapes immune evasion pathways. It has been shown to regulate the alternative splicing of *CD274* (encoding PD-L1), thereby controlling the abundance of specific immunomodulatory isoforms at the cell surface [162].

Furthermore, the impaired DDR inherent to CDK12 loss can lead to the accumulation of DNA breaks. This damage can trigger the release of cytoplasmic DNA, activating the cGAS/STING innate immunity pathway and further influencing the tumor-immune landscape [163]. Bao et al. reported that CDK12/13 inactivation causes transcription-replication conflicts, cytosolic DNA release, and activation of STING and TBK1, which promoted CD8+ T cell anti-tumor response [164].

These findings establish CDK12/13 as regulators of tumor-immune interactions, whose genetic or functional status may serve as a predictive biomarker for response to immune checkpoint blockade [161].

D. Role of CDK12/13 in hematologic neoplasms

CDK13 plays an important role in regulating the myeloid lineage. Analysis of Cancer Dependency Map (DepMap) identified cyclin K - the cognate cyclin for CDK12/13 - as essential across 62 hematological cancer cell lines [165]. Upregulation of CDK13 was identified in patients with myelodysplastic/myeloproliferative neoplasm with ringed sideroblasts and thrombocytosis (MDS/MPN-RS-T) [166]. Approximately 80-90% of these patients harbor mutations in *SF3B1*, a key splicing factor regulated by CDK12/13 [137,167]. CDK12/13 enhances splicing by facilitating interaction between RNA polymerase II and SF3B1, thus reinforcing its role in transcription-coupled splicing.

CDK12 inhibition with THZ531 was shown to suppress SF3B1-Pol II interaction [137]. *SF3B1* mutations are also linked to increased thrombotic risk [167]. CDK13 is also essential for megakaryocyte development in bone marrow cultures [168].

Aberrant transcription is a hallmark of acute myeloid leukemia (AML) [169]. Inhibition of CDK12/13 using THZ531 or CRISPR KO significantly reduces RNA polymerase II elongation rate and processivity by roughly 50%, with the strongest effect observed in long genes. Combined CDK12/13 inhibition decreases Ser2 and Thr4 phosphorylation, resulting in premature transcription termination. In AML MV4;11 cells, CDK12/13 inhibition also alters mRNA processing, notably affecting alternative last exon selection, generating diverse mRNA isoforms [165].

CDK12 and CDK13 knockout or knockdown cause growth disadvantage in various myeloid leukemia cell lines as evidenced by multiple CRISPR and siRNA screens. Most AML cell lines treated with THZ531 exhibit IC50 values within the therapeutic range of 34-116 nM, with the FAB M4/M5 subtypes demonstrating higher sensitivity. Moreover, venetoclax-resistant cell lines and primary patient samples resistant to venetoclax/azacitidine treatment remain sensitive to SR4835 and THZ531. Notably, cord blood-derived hematopoietic stem and progenitor cells (HSPCs) were unaffected by SR4835 and THZ531 at effective therapeutic doses [169]. However, despite its emerging importance in myeloid malignancies, the role of the CDK12/13 transcriptional axis in acute lymphoblastic leukemia remained unexplored.

1.6 Need for further research

Building on the mechanisms established in the previous chapters, two central concepts define the challenge and opportunity in treating glucocorticoid-resistant ALL.

1. Glucocorticoid resistance, a primary driver of treatment failure, stems from the failure of GR-mediated transcription of pro-apoptotic program.
2. CDK12 and CDK13 are master transcriptional kinases, essential for phosphorylating the Pol II CTD, coordinating transcription-coupled splicing, and maintaining the expression of long, complex genes, including those involved in the DNA damage response pathway. These kinases are critical for maintaining the oncogenic "transcriptional addiction" seen in acute leukemias.

These observations lead to the hypothesis that the pro-survival, glucocorticoid-resistant state of ALL cells is actively maintained by CDK12/13-dependent transcription.

This study proposes that targeting CDK12/13 disrupts the survival machinery of leukemic cells from two angles: first, by disrupting oncogenic transcription and pro-survival networks, and second, by inhibiting the DDR pathway, leading to overwhelming genomic stress. This disruption will "re-wire" the resistant transcriptional state, lowering the threshold for apoptosis and synergizing with the pro-apoptotic signaling induced by dexamethasone.

The following chapter outlines the specific aims designed to test this hypothesis.

1.7 Objectives of this thesis

This thesis aims to investigate the synergistic anti-leukemic effects of targeting CDK12 and CDK13 in combination with glucocorticoids in both B-cell and T-cell acute lymphoblastic leukemia. While the dual pro- and anti-oncogenic functions of CDK12 and CDK13 have been well documented in solid tumors such as prostate, ovarian, and breast cancer, their specific biological roles in acute leukemias remain poorly understood. Furthermore, the potential therapeutic interaction between CDK12/13 inhibition and glucocorticoid signaling has not yet been explored. To address these gaps, this work integrates bioinformatic, pharmacologic, and molecular approaches to delineate how transcriptional CDK inhibition modulates glucocorticoid sensitivity and resistance mechanisms in ALL.

The core objectives of this thesis are as follows:

1. **To characterize the expression of CDK12, CDK13, and Cyclin K across normal hematopoietic lineages and distinct molecular ALL subtypes using publicly available transcriptomic datasets.**
2. **To assess the genetic dependency of ALL cells on CDK12/13 using public CRISPR screens, and to correlate this dependency with glucocorticoid sensitivity, to identify a genetic rationale for combinatorial targeting.**

3. **To evaluate the cytotoxicity and potential selectivity of CDK12/13 inhibition in ALL by screening a representative panel of B-ALL and T-ALL**

cell lines, as well as primary patient-derived samples, with selective small-molecule inhibitors.

4. **To determine whether CDK12/13 inhibitors act synergistically with glucocorticoids by conducting combinatorial drug studies and evaluating the outcomes through quantitative synergy models.**
5. **To define the transcriptional programs underlying glucocorticoid–CDK12/13 inhibitor interactions by performing RNA sequencing to identify differential gene expression and pathway rewiring induced by single-agent and combination treatments.**
6. **To investigate the downstream cellular and molecular consequences of CDK12/13 inhibition, alone and in combination with glucocorticoids, through the evaluation of apoptosis, cell-cycle dynamics, and Western blot validation of key protein markers.**

Chapter 2: Materials and Methods

2.1. Materials

2.1.1 Cell lines

Cell line	*Disease type*	*Mutational burden*	*Sex*	*Age*	*Ancestry*	*Source*
SEMK2	*B-ALL*	*KMT2A-AFF1* *CDKN2A* *TP53*	*F*	*5Y*	*Caucasian*	*DSMZ (Braunschweig, Germany)*
SEM	*B-ALL*	*KMT2A-AFF1* *CDKN2A* *TP53*	*F*	*5Y*	*Caucasian*	*DSMZ (Braunschweig, Germany)*
RS4;11	*B-ALL*	*KMT2A-AFF1* *NSD2* *PIK3CD*	*F*	*32Y*	*Caucasian*	*DSMZ (Braunschweig, Germany)*
NALM-6	*B-ALL*	*IGH-DUX4* *EGFR* *NRAS* *RARA* *MSH2 (LoF)*	*M*	*19Y*	*Caucasian*	*DSMZ (Braunschweig, Germany)*
NALM-16	B-ALL	CDKN2A (LoF) MTAP (LoF) NF1 (LoF) TP53 (LoF)	F	12Y	Caucasian	DSMZ (Braunschweig, Germany)
SUP-B15	B-ALL	BCR-ABL1	M	9Y	Caucasian	DSMZ (Braunschweig, Germany)
SD-1	B-ALL	BCR-ABL1	F	Adult	-	DSMZ (Braunschweig, Germany)
REH	B-ALL	ETV6-RUNX1 NR3C1 PTEN	F	15Y	Caucasian	DSMZ (Braunschweig, Germany)

		TP53				
697	B-ALL	TCF3-PBX1	M	12Y	Caucasian	DSMZ (Braunschweig, Germany)
MHH-CALL4	B-ALL	KRAS	M	10Y	Caucasian	DSMZ (Braunschweig, Germany)
MUTZ-5	B-ALL	IGH-CRLF2 JAK2	M	26Y	-	DSMZ (Braunschweig, Germany)
MOLT-4	T-ALL	TP53 NOTCH1 PTEN NRAS STK11	M	19Y	Caucasian	DSMZ (Braunschweig, Germany)
JURKAT	T-ALL	PTEN INPP5D TP53 MSH2 BAX	M	14Y	Caucasian	DSMZ (Braunschweig, Germany)

Table 3. Characteristics of the acute lymphoblastic leukemia cell line panel used in thesis. The table summarizes the disease type, key genetic alterations, and patient demographics for each cell line used in this study. B-ALL, B-cell acute lymphoblastic leukemia; T-ALL, T-cell acute lymphoblastic leukemia; LoF, loss of function; F, Female; M, Male; Y, Year(s); -, data not available; DSMZ, German Collection of Microorganisms and Cell Cultures.

2.1.2 Primary cells

Cell type	*Origin*
ALL patient bone marrow cells	Department of Hematology, Institute of Hematology and Transfusion Medicine, Warsaw, Poland (IRB approval 43/2016)

Table 4. Primary cells used in this thesis. ALL, Acute Lymphoblastic Leukemia; IRB, Institutional Review Board.

2.1.3 Chemicals, reagents, and cell culture media

Name	*Manufacturer*
BSA (bovine serum albumin), heat shock fraction, protease free (A3294)	Sigma-Aldrich (St. Louis, MO, USA)
CytoFlex Isoflow Sheath Fluid	Beckman Coulter (Brea, CA, USA)
DMSO	Sigma-Aldrich (St. Louis, MO, USA)
Ethanol	Sigma-Aldrich (St. Louis, MO, USA)
Fetal Bovine Serum (Chile origin)	Sigma-Aldrich (St. Louis, MO, USA)
GeneRuler 1 kb DNA ladder	Thermo Fisher Scientific (Waltham, MA, USA)
HEPES (1M)	Thermo Fisher Scientific (Waltham, MA, USA)
Hoechst 34580	BD (Franklin Lakes, NJ, USA)
L-Glutamine (200 mM)	Thermo Fisher Scientific (Waltham, MA, USA)
NuPAGE™ Bis-Tris Mini Protein Gels, 4–12%	Thermo Fisher Scientific (Waltham, MA, USA)
Penicillin/Streptomycin (10,000 U/mL)	Thermo Fisher Scientific (Waltham, MA, USA)
Ponceau S	Sigma-Aldrich (St. Louis, MO, USA)
Propidium iodide	BD (Franklin Lakes, NJ, USA)
PVDF membrane	Merck Millipore (Burlington, MA, USA)
RPMI-1640	Sigma-Aldrich (St. Louis, MO, USA)
SR4835	MedChemexpress (Shanghai, China)
THZ531	MedChemexpress (Shanghai, China)
Trypan blue	Thermo Fisher Scientific (Waltham, MA, USA)
Western Lightning Pro, Chemiluminescent Substrate	PerkinElmer (Shelton, CT, USA)
Western Lightning Ultra, Chemiluminescent Substrate	PerkinElmer (Shelton, CT, USA)
β-mercaptoethanol	Sigma-Aldrich (St. Louis, MO, USA)

Table 5. Reagents and consumables used in this study. All reagents were of analytical or molecular biology grade and used according to standard laboratory procedures.

2.1.4 Kits

Name	*Manufacturer*	*Catalog number*
CometAssay Single Cell Gel Electrophoresis Assay	Trevigen (Gaithersburg, MD, USA)	4250-050-K
FITC Annexin V Apoptosis Detection Kit	BD Biosciences (San Jose, CA, USA)	556547
MycoAlert Mycoplasma Detection Kit	Lonza (Walkersville, MD, USA)	LT07-318
Pierce BCA Protein Assay Kit	Thermo Fisher Scientific (Waltham, MA, USA)	23225

Table 6. Commercial kits and reagents used in this study. Summary of assay kits and detection reagents applied for functional and biochemical analyses. The table lists the full product names, manufacturers with locations, and catalog numbers to facilitate reproducibility. All kits were used according to the manufacturers' instructions

2.1.5 Buffers, solutions, and cell culture media

Name	*Composition/ Manufacturer*
Laemmli Buffer (4x)	12.5 mL 1 M Tris-HCl, pH 6.8 2.5 g SDS (5%) 20 mL Glycerol (40%) Add a trace of Bromophenol Blue Bring to 50 mL with ddH_2O
Medium Stripping Buffer	15 g Glycine 1 g SDS 10 ml Tween 20 Adjust pH to 2.2 with conc. HCl (37%) Bring to 1 L with ddH_2O
MOPS Running Buffer (10x)	41.86 g MOPS free acid 4.1 g Sodium acetate 3.72 g Disodium EDTA Add ddH_2O to ~800 mL Adjust pH to 7.0 with NaOH Bring to 1L
PBS (10x)	400 g NaCl 10 g KCl 72 g $Na_2HPO_4.2H_2O$ 12 g KH_2PO_4 Dissolve in 4.5 L ddH_2O, adjust pH (7.4), bring to 5 L total
RIPA (2x)	3 mL 5 M NaCl 1 mL NP-40 (100%) 0.5 g Sodium deoxycholate 1 mL 10% SDS 5 mL 1 M Tris 1 mL 0.5 M EDTA Bring to 50 mL with ddH_2O
TBS (10x)	30 g Tris base (250 mM) 80 g NaCl (1.5 M) 2 g KCl Add ddH_2O to ~800ml, adjust pH to 7.4 with HCl, bring to 1L
Transfer Buffer (10x)	60.6 g Tris (0.25 M) 288.8 g Glycine (1.92 M) Bring to 2 L with ddH_2O

Table 7. Composition of buffers and solutions used in this study. All solutions were prepared with ultrapure ddH_2O, adjusted to the indicated pH at room temperature, and stored at 4 °C unless stated otherwise.

2.1.6 Antibodies

Antibody Name	*Cat. No.*	*Dilution*	*Species*	*Source*

pPol2	#14958t	1:1000	rabbit	Cell Signaling Technology (Danvers, MA, USA)
pSer2	#13499t	1:1000	rabbit	Cell Signaling Technology (Danvers, MA, USA)
pSer5	#13523t	1:1000	rabbit	Cell Signaling Technology (Danvers, MA, USA)
Anti-Cyclin K	#ab316203	1:1000 (WB) 1:400 (IHC)	rabbit	Abcam (Waltham, MA, USA)
Anti-CDK12	#ab317746	1:1000 (WB) 1:100 (IHC)	rabbit	Abcam (Waltham, MA, USA)
Anti-CDK13	#ab323865	1:1000 (WB) 1:100 (IHC)	rabbit	Abcam (Waltham, MA, USA)
GR	#12041s	1:1000	rabbit	Cell Signaling Technology (Danvers, MA, USA)
GAPDH	#5174	1:1000	rabbit	Cell Signaling Technology (Danvers, MA, USA)
cPARP	#9542	1:1000	rabbit	Cell Signaling Technology (Danvers, MA, USA)
B-actin	#4970	1:2000	rabbit	Cell Signaling Technology (Danvers, MA, USA)
Anti-Rabbit IgG	#7074	1:2000	goat	Cell Signaling Technology (Danvers, MA, USA)

Table 8. List of antibodies used in this study. All antibodies were diluted in 5% BSA in TBST and incubated according to the manufacturer's recommendations.

2.1.7 Software

Name	*Manufacturer*	*Version*
Benchling	Benchling (San Francisco, CA, USA)	Online
BioRender	BioRender (Toronto, Canada)	Online
DESeq2	Bioconductor (Boston, MA, USA)	1.48.1
Excel	Microsoft (Redmond, WA, USA)	365
FlowJo	BD Biosciences (Franklin Lakes, NJ, USA)	10.10
Illustrator	Adobe (San Jose, CA, USA)	CC
ImageJ	NIH (Bethesda, MD, USA)	1.53
Prism	GraphPad (Boston, MA, USA)	10.0
R	R Core Team (Vienna, Austria)	4.4.3
R Studio	Posit (Boston, MA, USA)	2025.05.0
Sciugo	Jonah Librah (Toronto, Canada)	Online
SynergyFinder	FIMM (Helsinki, Finland)	Online

Table 9. Software, databases, and analytical tools used in this study. Online tools were accessed through their official web interfaces during 2024–2025.

2.2 Methods

2.2.1 Culture of mammalian cell lines

Human leukemia cell lines were obtained from authenticated commercial repositories (DSMZ, Braunschweig, Germany; listed in Table 3). Cells were maintained under standard conditions at 37 °C in a humidified atmosphere containing 5 % CO_2. Cultures were grown in RPMI-1640 medium supplemented with 10–20 % fetal bovine serum (FBS), 100 U/mL penicillin, 100 µg/mL streptomycin, 2 mM L-glutamine, and 10 mM HEPES. Mycoplasma testing was routinely performed using the MycoAlert Mycoplasma Detection Kit (Lonza). Suspension cell lines were sub-cultured 24 h before experiments to achieve a density of 0.5 × 10^6 cells/mL, and new media were

used for experimental seeding at the same density. Cultures were passaged two to three times weekly to prevent overgrowth, and fresh vials were thawed and expanded approximately every three months to maintain line stability.

2.2.2 Isolation of mononuclear cells from bone marrow aspirates

Bone marrow aspirates were collected directly into sodium heparin–coated tubes. Samples were diluted 1:1 with complete RPMI-1640 medium, and 6 mL of the mixture was carefully layered over 3 mL of Histopaque-1077 at room temperature in a 15 mL conical tube. Density-gradient centrifugation was carried out at 400 × g for 20 min with acceleration = 3 and deceleration = 0 (brake off). The mononuclear cell layer was aspirated, transferred to a new tube, and washed once with RPMI-1640. Red blood cell lysis was omitted to preserve viability. Cell counts and viability were assessed using a hemocytometer and trypan blue exclusion. Freshly isolated cells were used immediately for downstream applications such as flow cytometry or drug-response assays.

2.2.3 Proliferation and viability assays by flow cytometry

To evaluate drug effects on viability and proliferation, primary patient cells were plated one day before treatment at 20 000 cells per well in 96-well flat-bottom plates (50µL of complete medium). After overnight incubation at 37°C, drug solutions were added in an equal volume (50µL per well) using serial dilutions; DMSO concentration in control wells was kept below 0.02%. Plates were incubated for 72h. On day 3, cells were gently resuspended by pipetting, and 50µL of suspension was transferred into microtubes containing 50µL PBS with propidium iodide (PI, 1µg/mL final). Samples were immediately analyzed on a CytoFLEX S flow cytometer. Debris and doublets were excluded by forward/side scatter gating. Viable cells were identified as PI^-, and dead cells as PI^+. The fraction of PI^- cells was used to compute IC_{50} values by fitting a four-parameter logistic (4PL) curve.

2.2.4 MTS cell proliferation assay

For proliferation and drug-synergy testing, cell viability was assessed using the CellTiter 96 AQueous One Solution (MTS) assay according to the manufacturer's protocol. The assay measures metabolic activity through the NAD(P)H-dependent bioreduction of MTS in the presence of phenazine methosulfate, producing a soluble

formazan dye. Cells were seeded in 96-well plates at 20 000 cells per well in 50µL medium. Then, 25µL of each drug (4× concentrated) was added in a checkerboard layout to reach 100µL total volume per well. Serial dilutions produced concentration gradients for both agents. Control wells received DMSO only, and blank wells with medium + MTS reagent were used for background subtraction. Plates were incubated for 2h at 37°C, and absorbance was read at 490nm using a microplate reader. Absorbance values, proportional to the number of metabolically active cells, were analyzed in Excel and SynergyFinder to calculate dose-response relationships.

2.2.5 Annexin V-based apoptosis detection

Apoptotic and necrotic cells were quantified with the PE Annexin V Apoptosis Detection Kit following the manufacturer's instructions. After harvesting, cells were washed twice with cold PBS and resuspended in 1× Annexin V Binding Buffer at 1 × 10^6 cells/mL. An aliquot (100µL, 1 × 10^5 cells) was transferred into a 5mL polystyrene tube, and 5µL PE Annexin V and 5µL 7-AAD were added. Samples were gently mixed and incubated for 15min at room temperature in the dark, followed by addition of 400µL Binding Buffer. Flow cytometry was performed within 1h to distinguish live, early apoptotic, late apoptotic, and necrotic populations.

2.2.6 Comet assay

DNA strand breaks were analyzed using the alkaline CometAssay Silver Kit with slight modifications. Cells were washed with cold Ca^{2+}/Mg^{2+}-free PBS and resuspended at 1 × 10^5 cells/mL. Low-melting-point Comet LMAgarose (pre-melted at 80°C, equilibrated to 37°C) was mixed with cells at a 10:1 ratio (500µL agarose: 50µL cells). Immediately, 50µL of this mixture was pipetted onto CometSlides and evenly spread. Slides were placed flat at 4°C for 10min in the dark to solidify. They were then incubated in chilled Lysis Solution for 1h, followed by 20min alkaline unwinding at room temperature (dark). Electrophoresis was conducted at 33V (1 V/cm) for 30min in cold alkaline buffer. Slides were rinsed twice in deionized water (5min each) and once in 70 % ethanol (5min), then air-dried at 37°C for 15min. DNA was stained with SYBR Gold, and comets were visualized by epifluorescence microscopy using a fluorescein filter. DNA damage was quantified in ImageJ as the tail-to-head DNA ratio.

2.2.7 Cell cycle analysis

Cells were incubated with Hoechst 34580 (10µg/mL final) for 30min at 37°C. After staining, samples were analyzed on a CytoFLEX flow cytometer using the PB-450 channel. Histogram peaks were assigned as follows: the first fluorescence peak represented G_1 phase, the second (approximately twice the intensity) corresponded to G_2/M, and intermediate signals denoted S phase cells undergoing DNA synthesis. Events below the G_1 peak were classified as sub-G_1 (apoptotic), and those exceeding the G_2/M peak were identified as polyploid populations.

2.2.8 BCA protein quantification

Protein concentrations were determined with the Pierce BCA Protein Assay Kit according to the microplate procedure. Samples and BSA standards (125–2000 µg/mL) were pipetted into clear 96-well plates. Freshly prepared working reagent was made by combining Reagent A and B in a 50:1 ratio. 200µL working reagent was added to 2µL of sample or standard, and plates were incubated at 37°C for 30min protected from light. Absorbance was read at 562nm. Protein concentrations were derived from the standard curve using linear regression. All samples were assayed in triplicate.

2.2.9 SDS–polyacrylamide gel electrophoresis (SDS-PAGE) and western blotting

Equal protein amounts (10–40 µg/lane) were loaded onto NuPAGE gels along with molecular-weight markers. Electrophoresis was performed in 1× MOPS buffer, starting at 90V (stacking) and increased to 125V for resolving, continuing until the dye front reached the gel bottom (~60–90min). Proteins were transferred to PVDF membranes (pre-wet in methanol ≥ 1min) using a wet-transfer system at 30V for 1 h 20 min at 4°C. Membranes were stained with Ponceau S to verify transfer, washed with water, and blocked for 1 h at room temperature in 5 % BSA in TBST. Primary antibodies diluted in 5% BSA/TBST were applied overnight at 4°C. Membranes were washed three times (15min each) in TBST, then incubated for 1h at room temperature with HRP-conjugated secondary antibodies (in 5% BSA/TBST). After three additional washes (10min each), signals were developed using ECL chemiluminescence and imaged on a Chemidoc system. For reprobing, membranes were treated with Medium Stripping

Buffer for 10min, washed, re-blocked for 1h, and re-incubated with the next antibody. Fully processed membranes were air-dried and archived.

2.2.10 Immunochemistry

Immunohistochemical staining was performed on a tissue microarray (TMA) constructed from formalin-fixed paraffin-embedded (FFPE) bone marrow trephine biopsies. The specimens, representing both patients with acute lymphoblastic leukemia and healthy donors, were retrieved anonymously from the Department of Pathology, Brigham and Women's Hospital (Boston, MA, USA). For processing, 4µm sections were cut, mounted onto charged glass slides, and dried. Following deparaffinization and rehydration, slides underwent heat-induced epitope retrieval (HIER) using either citrate buffer (pH 6.0) or Tris-EDTA buffer (pH 9.0), depending on the target antigen. Endogenous peroxidase activity was blocked with 3% hydrogen peroxide, and nonspecific binding was minimized through the application of an appropriate blocking buffer. The following primary antibodies included: Anti-CDK12, Anti-CDK13, Anti-CCNK. Slides were incubated with these primary antibodies for one hour at room temperature, followed by detection using an HRP-conjugated secondary antibody. Visualization was performed using a DAB chromogen substrate. Slides were lightly counterstained with hematoxylin, dehydrated, and mounted. Staining was evaluated using a Leica DM2000 microscope. Microphotographs were taken during a single session, using standardized parameters for light intensity, magnification, brightness and exposure settings.

2.2.11 RNA-seq data processing and analysis

RNA-seq library preparation and sequencing

B-ALL cells were treated for 24h with DMSO (vehicle control), the CDK12/13 inhibitors SR4835 (SR) or THZ531 (THZ), 130nM each, dexamethasone (DEXA) 2.5uM, or their combinations (SR+DEXA, THZ+DEXA). All conditions were evaluated in biological triplicate (n = 3 per condition, yielding 18 samples total). Total RNA was extracted using TRIzol reagent, and RNA integrity and quality were assessed using an Agilent Bioanalyzer. Poly(A)-enriched RNA-seq libraries were subsequently prepared using a NEBNext poly(A) kit (New England Biolabs). Sequencing was performed by CeGaT (CTS Classic pipeline) on an Illumina platform. Libraries were sequenced as 2 x 100 bp paired-end reads to a targeted depth of 30 million clusters (approximately 6 Gb)

per sample, ensuring sufficient depth for robust differential expression and alternative splicing analyses.

Read alignment and quantification

Sequencing reads were aligned to the human reference genome (GRCh38) using STAR (version 2.7.x) with the GENCODE v44 primary assembly annotation. Alignment files were sorted and indexed using samtools. Gene-level read counts were generated using featureCounts (Subread package) with default parameters for stranded paired-end data. Reads mapping to multiple features were excluded.

Differential expression analysis

Differential gene expression was performed using DESeq2 (version 1.38) in R (version 4.3). A single DESeq2 model was fitted on all 18 samples simultaneously using the design formula ~ *condition*, with DMSO set as the reference level. Genes with fewer than 10 total counts across all samples were excluded prior to model fitting. The following contrasts were extracted: each treatment versus DMSO (SR, THZ, DEXA, SR+DEXA, THZ+DEXA), each combination versus its single-agent components (SR+DEXA vs SR, SR+DEXA vs DEXA, THZ+DEXA vs THZ, THZ+DEXA vs DEXA), and pooled comparisons (Pooled Combo vs Pooled Single, Pooled Combo vs DMSO, Pooled Single vs DMSO). Pooled contrasts were constructed using numeric contrast vectors that averaged the relevant coefficients from the fitted model. Genes were classified as differentially expressed using a threshold of Benjamini–Hochberg adjusted $p < 0.05$ and $|\log_2(\text{fold change})| \geq 1$. Variance-stabilizing transformation (VST) was applied for visualization purposes, including principal component analysis and heatmaps.

Gene set enrichment analysis

Gene set enrichment analysis (GSEA) was performed using the clusterProfiler package with gene sets obtained from the Molecular Signatures Database (MSigDB) via the msigdbr R package. For each contrast, genes were ranked by the Wald test statistic from DESeq2. Gene set sizes were constrained between 15 and 500 genes. *p*-values were adjusted using the Benjamini–Hochberg method with a significance threshold of 0.05. For the TF_Targets_Legacy collection, gene sets corresponding to microRNA targets (identified by the presence of “MIR” in the gene set name or motif sequences without a known transcription factor annotation) were excluded to retain

only bona fide transcription factor–target associations. Results were visualized as dot plots with pathways ordered by normalized enrichment score (NES), with dot size proportional to $-\log_{10}$(FDR) and color indicating the direction and magnitude of enrichment.

Read distribution and intronic content analysis

The genomic distribution of mapped reads was assessed using the read_distribution.py module from the RSeQC package. For each sample, the fraction of reads mapping to CDS exons, 5′ UTR, 3′ UTR, introns, and flanking regions (TSS ±1 kb, TES ±1 kb) was calculated. To test whether CDK12/13 inhibition altered intronic read content, the percentage of reads mapping to introns was compared between DMSO and each CDK12/13 inhibitor (SR, THZ) using paired *t*-tests with samples matched by biological replicate.

Alternative splicing analysis

Alternative splicing events were quantified using rMATS (replicate Multivariate Analysis of Transcript Splicing) with junction counts (JC) mode. Five event types were analyzed: skipped exons (SE), mutually exclusive exons (MXE), retained introns (RI), alternative 3′ splice sites (A3SS), and alternative 5′ splice sites (A5SS). Events were required to have a mean of at least 10 junction-spanning reads across samples in both conditions. Significant splicing changes were defined as FDR < 0.05 and |inclusion level difference (ΔΨ)| > 0.05. To assess the concordance of splicing changes between SR4835 and THZ531, the ΔΨ values for events detected in both contrasts were compared using Spearman rank correlation.

Chapter 3: Results

3.1 Experimental overview and study workflow

This chapter presents the experimental results addressing the objectives defined in Section 1.7. The research strategy combined in silico and in vitro approaches to investigate the role of CDK12 and CDK13 in acute lymphoblastic leukemia and their interaction with glucocorticoids. The study progressed from bioinformatic analyses of CDK12/13 expression and genetic dependency, through cytotoxicity and combination assays using selective CDK12/13 inhibitors, to transcriptomic and molecular characterization of the resulting cellular responses (Figure 8).

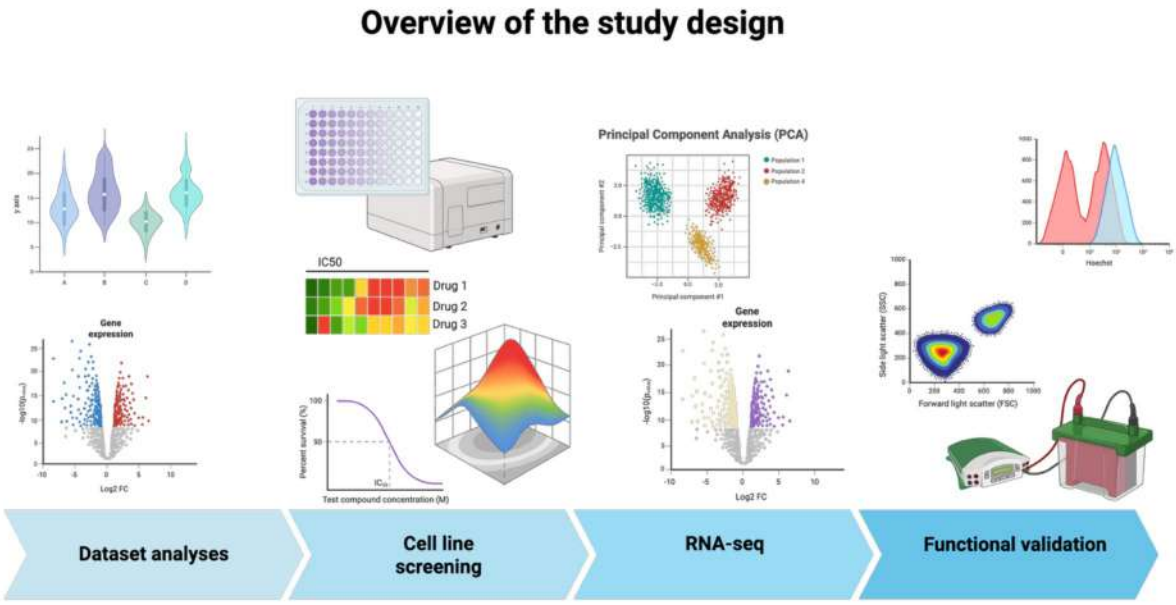

Figure 8. Schematic representation of the overall study workflow integrating bioinformatic analyses, drug sensitivity assays, combination testing, and transcriptomic profiling.

3.2 Multimodal expression profiling of the CDK12/13/CCNK axis

3.2.1 Transcriptomic landscape in healthy and malignant hematopoiesis

As transcriptomic data capture both the functional state and heterogeneity of hematopoietic cells, the initial step of this study involved assessing the expression of *CDK12, CDK13*, and their cyclin partner *CCNK* in healthy and malignant cells. Expression data were obtained from the MILE study (GSE13159) via BloodSpot 3.0, a public database integrating transcriptomic and proteomic profiles of normal hematopoietic populations and various hematologic malignancies in both mice and human patient samples [170].

Figures 9-11 summarize the expression patterns of *CDK12, CDK13*, and *CCNK* across normal and malignant hematopoiesis. The hierarchical tree illustrates their expression within hematopoietic origin, while the strip plots show median $\log_2$ expression values across healthy bone marrow and hematologic malignancy subtypes, including acute lymphoblastic leukemia, acute myeloid leukemia, chronic lymphocytic leukemia (CLL), chronic myeloid leukemia (CML), and myelodysplastic syndromes (MDS). Statistical significance between groups was assessed using pairwise t-tests implemented in BloodSpot, with only significant comparisons indicated.

Across these datasets, the three genes displayed context-dependent elevation in specific leukemic subtypes. *CDK12* showed increased expression in AML with normal karyotype, CLL, and AML t(8;21) (Figure 9). *CDK13* expression was elevated in ETV6-RUNX1 (t(12;21)), TCF3-PBX1 (t(1;19)), hyperdiploid ALL, pro-B-ALL with KMT2A (t(1;11)), CLL, pre-B-ALL with or without t(9;22), T-ALL, and APL (t(15;17)) (Figure 10). *CCNK* showed higher expression observed in CLL, and in AML with complex karyotype (Figure 11).

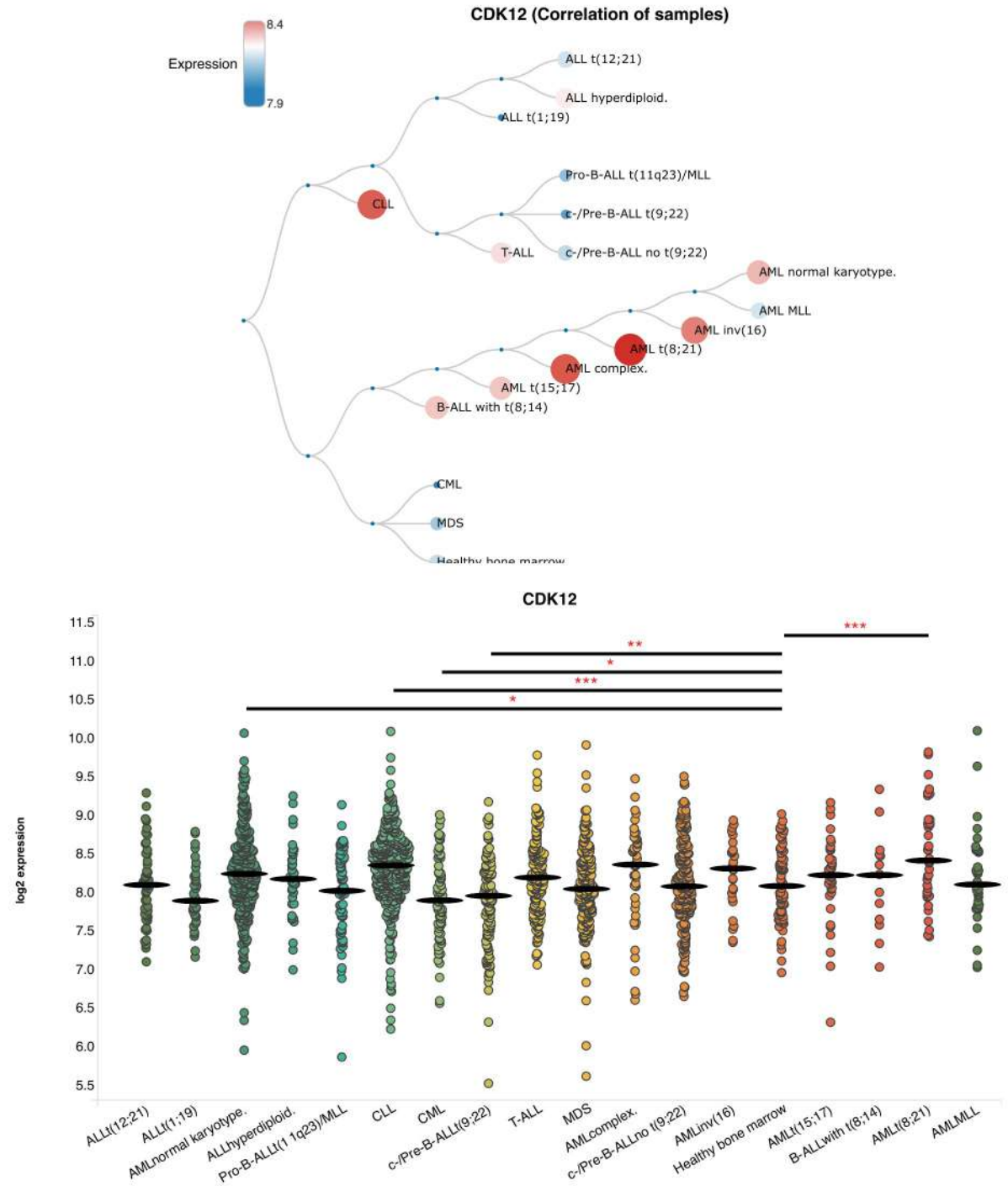

Figure 9. Expression of CDK12 in normal and malignant hematopoiesis. Gene-expression data for human AML, ALL, and preleukemic cell populations were obtained from the MILE study (GSE13159) and visualized using the BloodSpot 3.0 database. The tree diagram (A) illustrates CDK12 expression across hematopoietic differentiation, while the strip plots (B) present median log_2 expression levels in healthy bone marrow and hematologic malignancies. Dataset abbreviations: ALL hyperdiploid – ALL with hyperdiploid karyotype; ALL t(12;21) – ALL with ETV6-RUNX1; ALL t(1;19) – ALL with TCF3-PBX1; AML complex – AML with complex/aberrant karyotype; AML inv(16) – AML with inv(16)/t(16;16); AML normal karyotype – AML with normal karyotype or other abnormalities; AML MLL – AML with t(11q23)/KMT2A; AML t(15;17) – APL; AML t(8;21) – AML with RUNX1-RUNX1T1; CLL – chronic lymphocytic leukemia; CML – chronic myeloid leukemia; MDS – myelodysplastic syndromes; Pro-B-ALL t(11q23)/MLL – pro-B-ALL with KMT2A rearrangement; T-ALL – T-cell ALL; c-/Pre-B-ALL t(9;22) – BCR-ABL1-positive common/pre-B-ALL; c-/Pre-B-ALL no t(9;22) – BCR-ABL1-negative common/pre-B-ALL; B-ALL with t(8;14) – mature B-ALL with MYC translocation.

*Statistical testing: pairwise two-tailed t-tests as implemented in BloodSpot. Only statistically significant differences are indicated: *, p < 0.05; **, p < 0.01; ***, p < 0.001.*

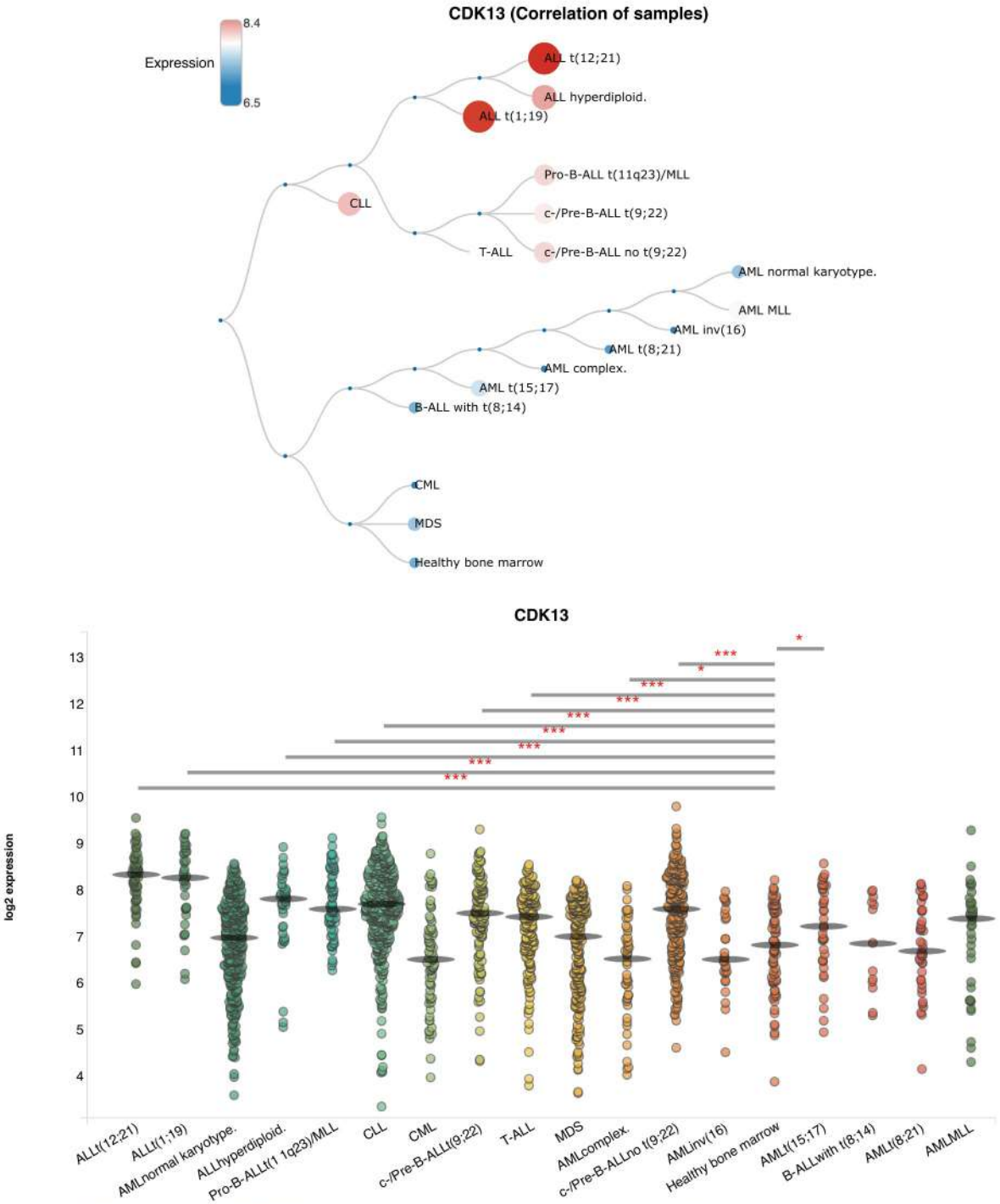

Figure 10. Expression of CDK13 in normal and malignant hematopoiesis. Gene expression data, panel layout, dataset abbreviations, and statistical testing are as described for Figure 9.

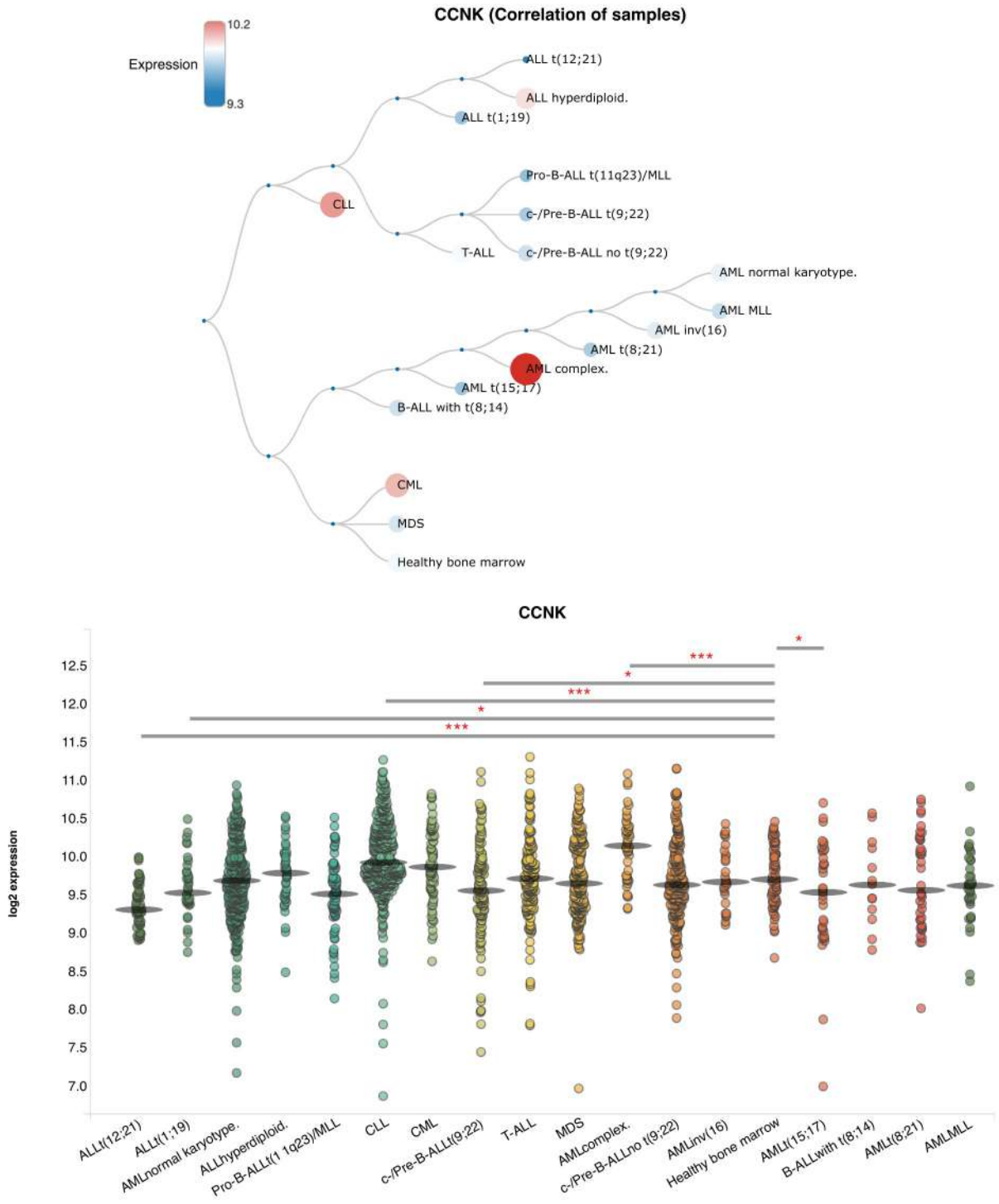

Figure 11. Expression of CCNK in normal and malignant hematopoiesis. Gene expression data, panel layout, dataset abbreviations, and statistical testing are as described for Figure 9.

Overexpression of *CDK12, CDK13,* and *CCNK* across ALL and AML subtypes supports the hypothesis that the CDK12/13–Cyclin K transcriptional module is broadly relevant in hematologic malignancies. Although these genes demonstrated partially overlapping expression profiles, CDK13 was notably elevated across multiple B-ALL subtypes as well as within the T-ALL cohort.

3.2.2 Immunohistochemical characterization of the CDK12/CDK13/CCNK in primary B-ALL blasts and healthy bone marrow

To validate the transcriptomic analysis, immunohistochemical (IHC) staining was performed on a tissue microarray containing patient-derived bone marrow trephine biopsies (Figure 12). This validation aimed to determine whether the mRNA elevations observed in the MILE dataset translated into detectable protein signatures in malignant B-ALL cells compared to healthy hematopoiesis.

The IHC analysis of B-ALL revealed that CDK13 exhibited the most robust and consistent staining pattern (Figure 12A, C). Its expression profile in ALL cases demonstrated high sensitivity and specificity, concordant with PAX5, a B-lineage specific transcription factor included as a positive control for leukemic blast identification. In contrast, while CDK12 and CCNK protein expression was also detected in the leukemic blasts, these markers exhibited a more heterogeneous staining profile, with several cases showing relatively light or dim immunoreactivity.

Critically, all three markers were notably absent in healthy bone marrow specimens, which remained consistently negative across the cohort (Figure 12D). These data suggest that while the intensity of CDK12 and CCNK may vary across ALL subtypes, the overexpression of CDK12, CDK13, and CCNK is a specific feature of the malignant state. However, this patterns alone do not establish functional dependence. Consequently, the analysis was extended to genetic essentiality and pharmacologic inhibition to determine whether ALL rely on CDK12/13 activity and whether targeting these kinases modulates glucocorticoid responsiveness.

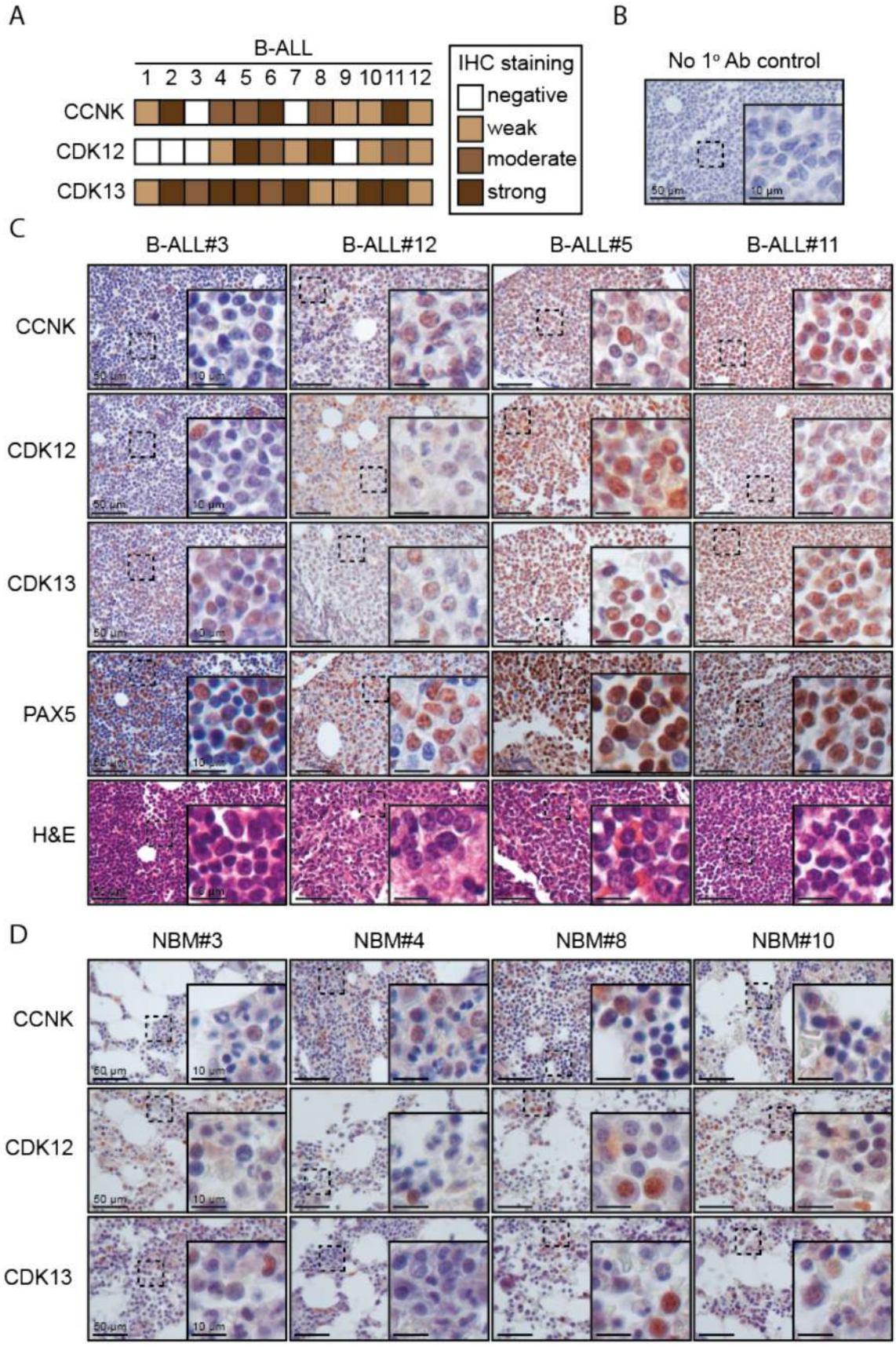

Figure 12. Protein expression of CDK12, CDK13, and CCNK in B-ALL and healthy bone marrow. (A) IHC staining intensity across 12 B-ALL patient samples, categorized by staining intensity (white: negative; light brown: weak; medium brown: moderate; dark brown: strong). (B) Representative negative control using no primary antibody. (C) Representative IHC images of four B-ALL patient samples stained for CCNK, CDK12, CDK13. PAX5

(a B-lineage specific transcription factor) is included as a positive diagnostic control for leukemic blast identification. H&E staining provides morphological context. (D) IHC staining of four representative healthy bone marrow specimens, showing absence of target kinase expression.

3.3 Functional dependency on CDK12 and CDK13 in ALL

Genome-scale CRISPR/Cas9 loss-of-function screening provides a quantitative, comparative framework to assess whether a gene is required for proliferation and survival in a given cell line [171,172]. Publicly available cancer dependency data was used to evaluate whether *CDK12, CDK13*, and their cyclin partner *CCNK* show evidence of functional essentiality in B- and T-cell lymphoblastic leukemia/lymphoma cell line models.

3.3.1 Analysis of CRISPR/Cas9 essentiality datasets

CRISPR essentiality scores were obtained from the DepMap portal 25Q3 release using the Chronos processing framework, which infers gene knockout fitness effects using a model of cell population dynamics and corrects for systematic biases observed in pooled CRISPR screens. In Chronos, more negative scores indicate stronger fitness defects upon knockout, meaning higher functional dependency of the cell line on that gene [171].

To focus on acute lymphoblastic leukemia, cell lines were subsetted using DepMap metadata for primary disease, restricting the analysis to B-cell acute lymphoblastic leukemia and T-lymphoblastic leukemia/lymphoma. For each ALL cell line, Chronos dependency scores were extracted for *CDK12, CDK13*, and *CCNK*. Results are summarized in the accompanying forest plots (Figure 13), stratified by ALL subtype. For each gene, points represent Chronos dependency values, with a dashed reference line at 0 (no growth effect), and the x-axis scaled to capture the observed range in ALL models.

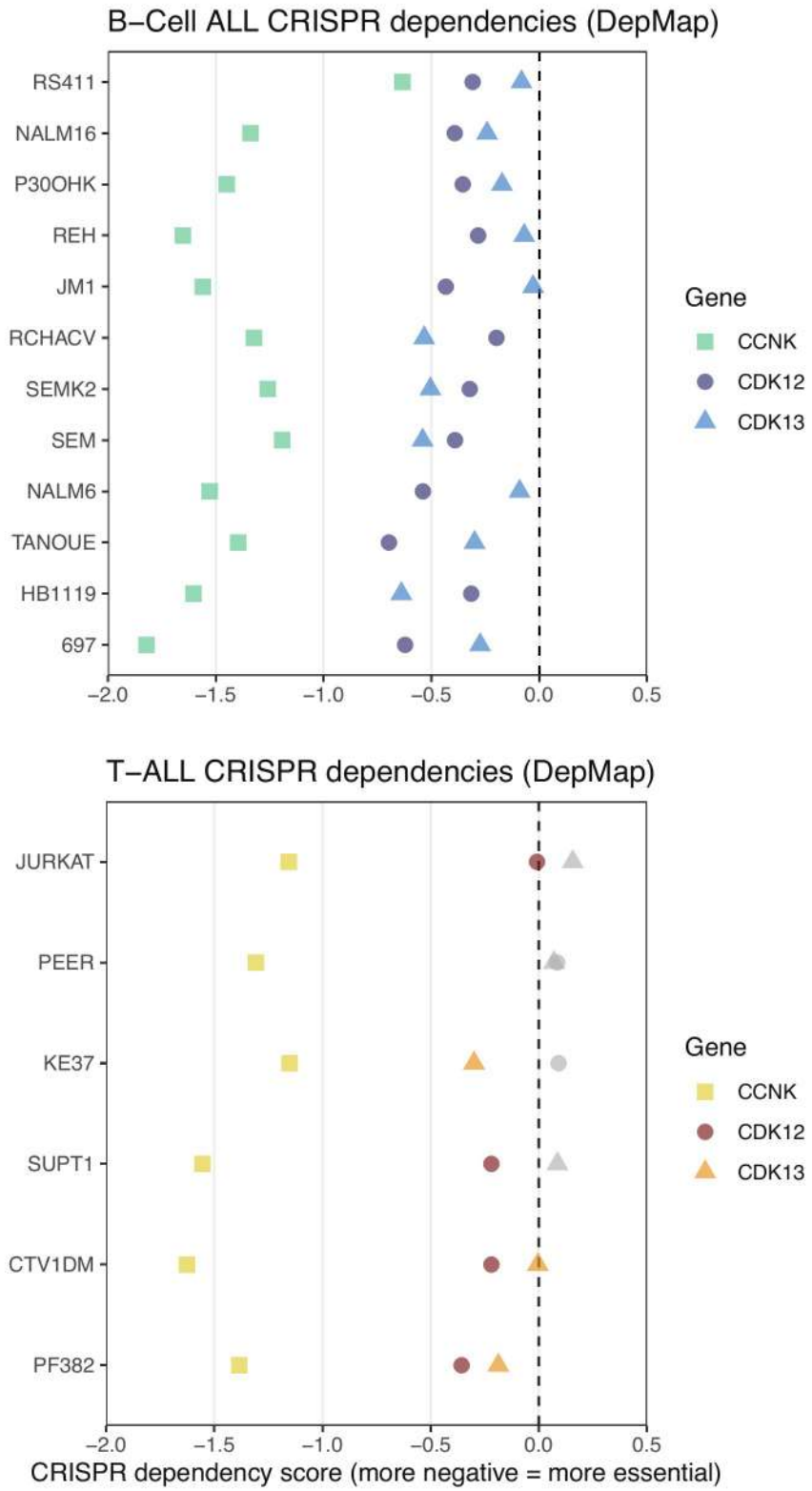

Figure 13. CRISPR dependency profiles of CDK12, CDK13, and CCNK in ALL cell lines (DepMap). Forest plots show Chronos CRISPR knockout dependency scores for CDK12, CDK13, and CCNK across acute lymphoblastic leukemia cell lines, grouped by primary disease (B-ALL vs. T-ALL). Each point corresponds to one cell line. The vertical dashed line denotes a score of 0 (no growth defect), and more negative values indicate higher dependency/essentiality. Chronos scores were derived using the DepMap Chronos processing pipeline. Coloring highlights negative dependency values (gene-specific color) and positive values (grey), as specified in the plotting code. Data visualized with ggplot2 R package.

Across both B-ALL and T-ALL models, most cell lines showed negative Chronos dependency scores for *CDK12, CDK13*, and *CCNK*, indicating that loss of these genes imposes a measurable fitness cost and that this transcriptional kinase complex is broadly required for optimal proliferation or survival in ALL cell lines. The dependency pattern was strongest for *CCNK*, which displayed the most negative scores in both disease groups. This is consistent with CCNK acting as an obligate cyclin partner for CDK12/13, such that CCNK loss functionally disrupts the same pathway and may produce a more penetrant phenotype than loss of either kinase alone. In contrast, CDK12 and CDK13 showed more heterogeneous dependency, with variation in magnitude across cell lines and between B-ALL and T-ALL. This spread suggests that although the pathway is commonly important, the degree of reliance on CDK12 versus CDK13 may be context-dependent, potentially reflecting differences in transcriptional programs, DNA damage response capacity, or lineage-specific wiring. Overall, these data support that ALL cell lines exhibit recurrent functional dependency on the CDK12/13–CCNK complex, and they motivate follow-up experimental validation in ALL context.

3.3.2 Correlation with glucocorticoid sensitivity

To test whether CDK12/CDK13 dependency relates specifically to glucocorticoid response, rather than reflecting baseline ALL cell fitness, we reanalyzed a published functional screening dataset from Poulard et al., who used the B-ALL cell line NALM6 as a model of glucocorticoid response [173]. The authors performed a genome-wide pooled lentiviral shRNA screen and quantified the abundance of integrated shRNA cassettes after selection to infer gene-level phenotypes. Two primary readouts were reported: a growth score (γ), capturing the effect of gene depletion on baseline proliferation and survival, and a dexamethasone sensitivity score (ρ), capturing the effect of gene depletion on survival under dexamethasone selection relative to the growth control condition. Each score is accompanied by a statistical confidence estimate obtained by comparing shRNAs targeting a given gene to control shRNAs, reported as a raw p value and an FDR-adjusted q value.

Figures 14 and 15 summarize baseline fitness effects using volcano plots with γ on the x-axis and -log10(q) or -log10(p) on the y-axis. Figure 14 uses -log10(p) to display raw statistical support, whereas Figure 15 uses -log10(q) to account for multiple testing

across the genome and enable FDR-controlled hit calling. The vertical line at γ = 0 indicates no net effect on growth. Genes on the left (negative γ) represent cases where gene depletion impairs growth, while genes on the right (positive γ) represent cases where gene depletion increases growth. In this analysis, *CDK12, CDK13*, and *CCNK* fall on the negative γ side, together with leukemia-relevant genes including *NRAS, KMT2A, MCL1, BCL2*, and *NR3C1*, indicating that depletion of these genes reduces baseline NALM6 fitness.

To assess drug-specific effects, Figure 16 displays a volcano plot of ρ (x-axis) versus -log10(q) (y-axis), where q denotes the FDR-adjusted significance. Among the *CDK12/CDK13/CCNK*, *CDK13* depletion shows an FDR-significant ρ effect consistent with increased dexamethasone sensitivity, whereas *CDK12* and *CCNK* do not meet the same significance criterion in this dataset. Together, these results support a role of the *CDK12/CDK13/CCNK* axis in baseline ALL cell fitness and identify *CDK13* as the component most clearly linked to modulation of glucocorticoid response in NALM6 cells in this screen.

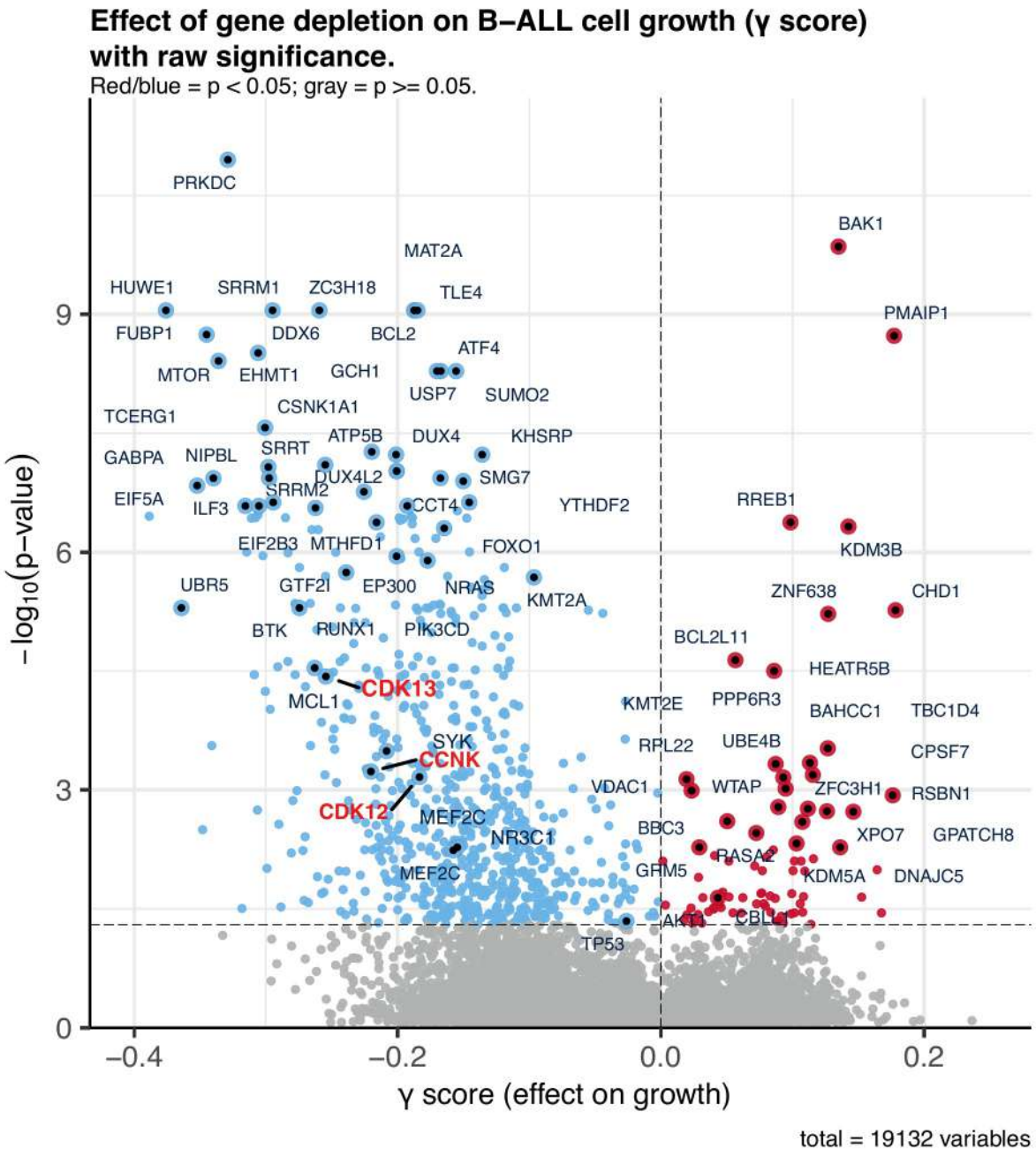

Figure 14. Baseline growth dependencies in NALM6 using raw significance. Volcano plot of γ score (x-axis) versus -log10(p-value) (y-axis) generated using dataset from genome-wide pooled shRNA screen in NALM6 cells [173]. Each point represents a gene. Significant genes ($p < 0.05$) are colored by effect direction: blue, negative γ (growth inhibition upon depletion); red, positive γ (increased growth upon depletion). Grey indicates non-significant genes ($p \geq 0.05$).

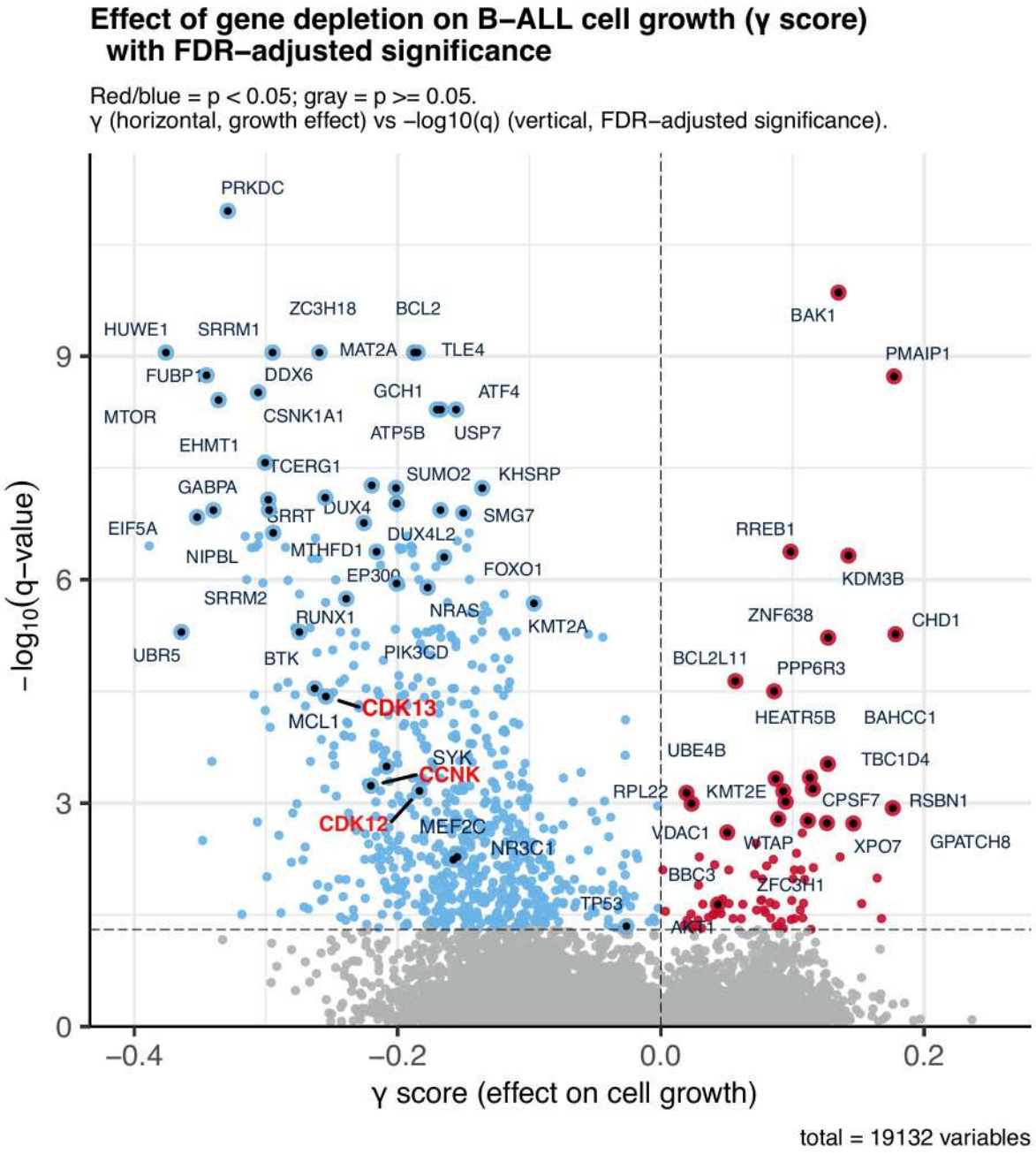

Figure 15. Baseline growth dependencies in NALM6 using FDR-adjusted significance. Volcano plot of the growth score γ (x-axis) versus -log10(q-value) (y-axis) generated using the published genome-wide pooled shRNA screening dataset in NALM6 cells [173]. The source table used for reanalysis was prefiltered to genes with q ≤ 0.1 (as reported in the original screen), and in this figure significance was defined more stringently as q < 0.05. Each point represents a gene. Blue indicates significant genes with negative γ (growth inhibition upon depletion), red indicates significant genes with positive γ (increased growth upon depletion), and grey indicates q ≥ 0.05.

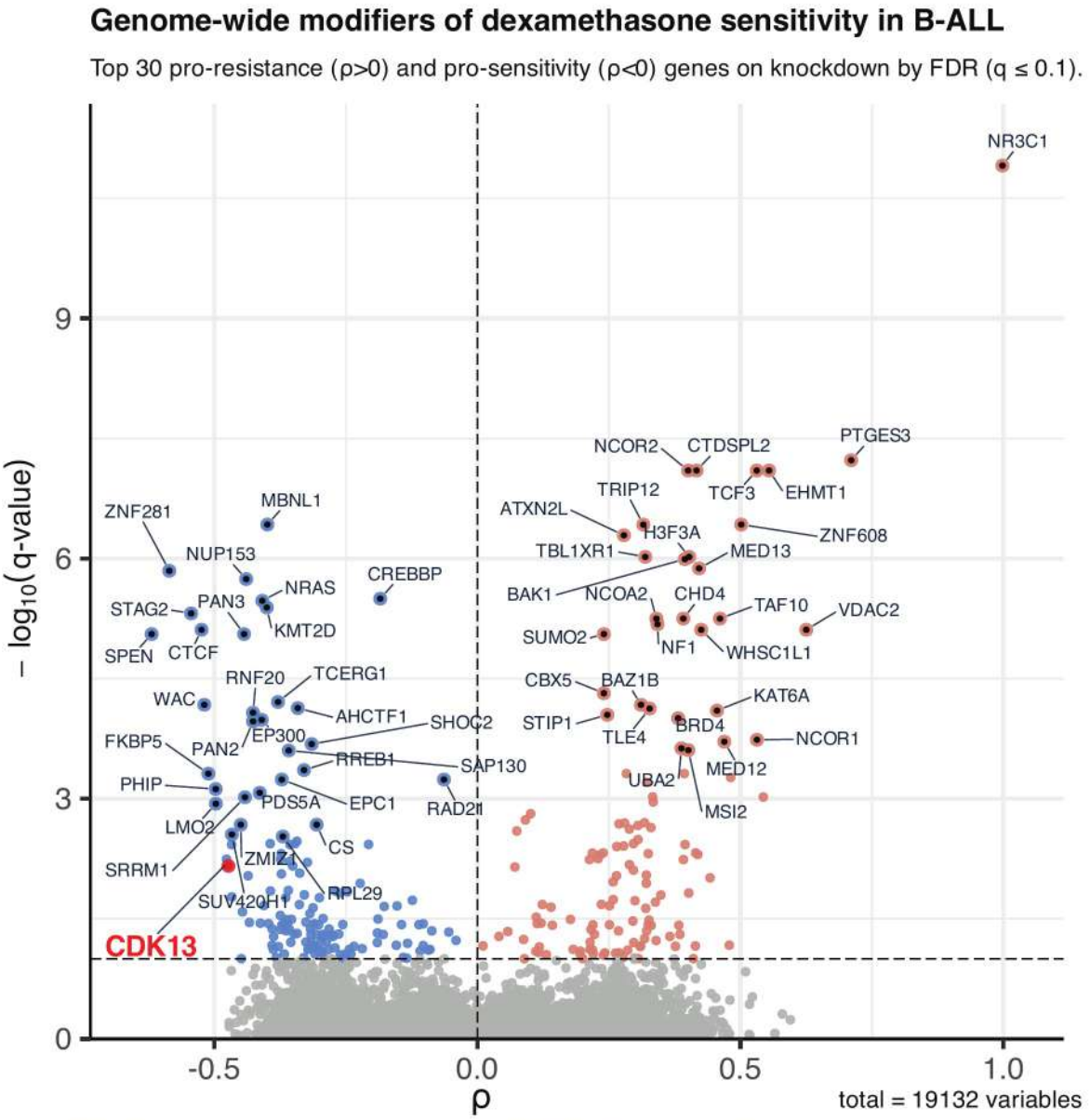

Figure 16. Modifiers of dexamethasone sensitivity in NALM6. Volcano plot of the dexamethasone sensitivity score ρ (x-axis) versus -log10(q-value) (y-axis) generated using the published genome-wide pooled shRNA screening dataset in NALM6 cells [173]. The source table used for reanalysis was prefiltered to genes with q ≤ 0.1, and significance in this figure was defined as q < 0.05. Each point represents a gene. Blue indicates significant genes whose depletion sensitizes cells to dexamethasone (ρ direction as defined in the dataset), pink indicates significant genes whose depletion is protective (reduced dexamethasone sensitivity), and grey indicates q ≥ 0.05.

3.4 Cytotoxicity and selectivity of CDK12/13 inhibition

3.4.1 Single-agent sensitivity of ALL cell lines and primary samples to glucocorticoids and CDK12/13 inhibitors

To establish the baseline sensitivity of acute lymphoblastic leukemia models to glucocorticoids and transcriptional CDK12/13 inhibition, a panel of B-cell and T-cell ALL cell lines, together with two primary B-ALL patient samples, was screened with dexamethasone and two selective CDK12/13 inhibitors – SR4835 and THZ531. Drug

response was quantified using dose response assays, and half-maximal inhibitory concentrations (IC_{50}) were calculated for each condition.

B-ALL cell lines and patient-derived samples exhibited marked heterogeneity in their sensitivity to dexamethasone (Figure 17). While several B-ALL cell lines exhibited robust responses to glucocorticoid treatment, a subset of models demonstrated limited or overt resistance. In particular, SEM, SEMK2, SD1 (B-ALL), CCRF-CEM, MOLT-4, and JURKAT (T-ALL) cells displayed reduced sensitivity to dexamethasone, with IC_{50} values substantially higher than those observed in glucocorticoid-responsive lines. Both primary patient-derived samples similarly showed reduced dexamethasone responsiveness, indicating partial intrinsic glucocorticoid resistance.

In contrast, treatment with CDK12/13 inhibitors resulted in broad cytotoxic activity across both B-ALL and T-ALL cell lines, with most models exhibiting low micromolar to nanomolar IC_{50} values, especially in B-ALL (Figures 18-19). Notably, no consistent difference in single-agent sensitivity to CDK12/13 inhibition was observed between B-ALL and T-ALL cell lines. Sensitivity to CDK12/13 inhibitors was retained in cell lines that were poorly responsive to dexamethasone, indicating non-overlapping resistance mechanisms.

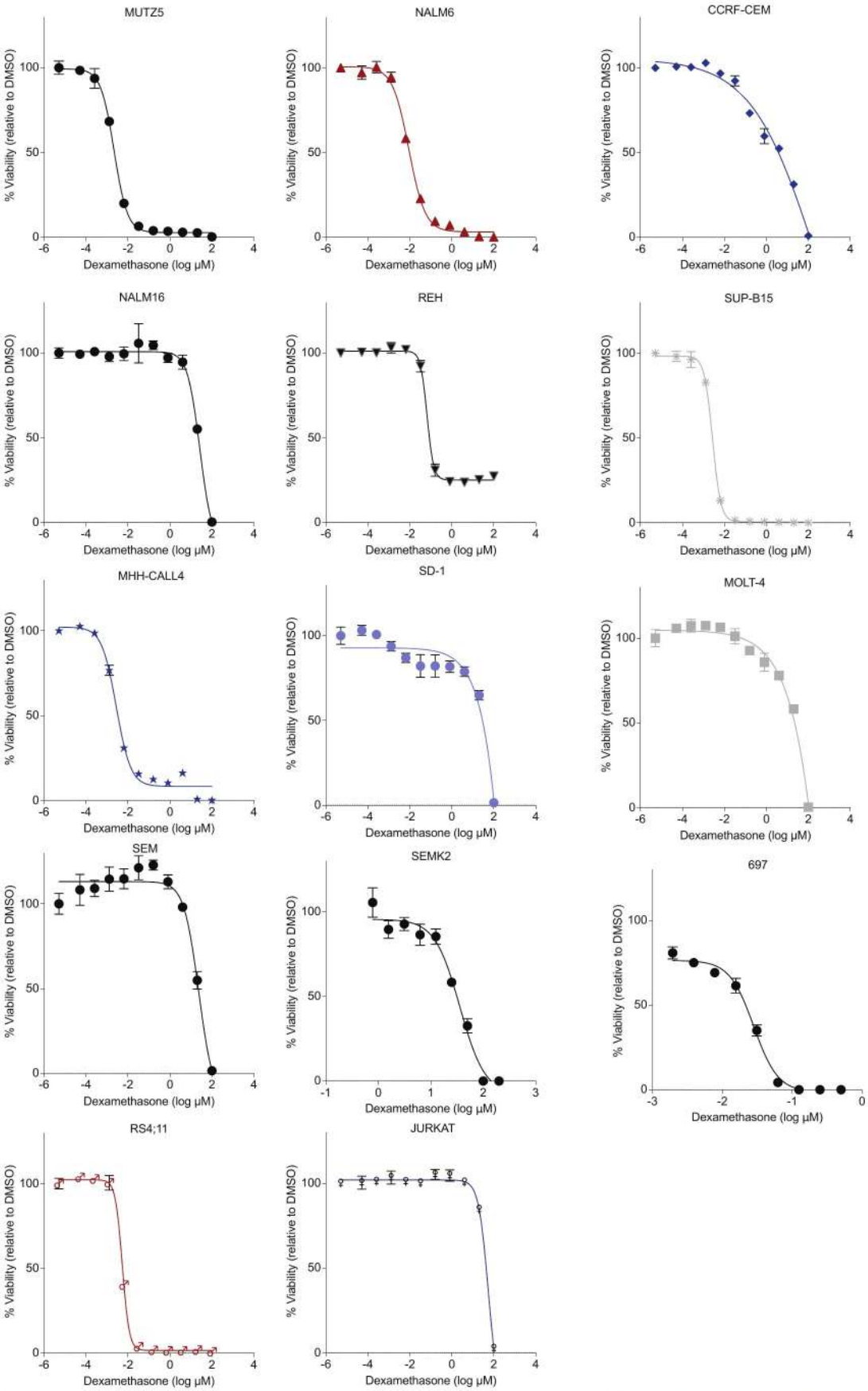

Figure 17. Dose-response curves for dexamethasone in B-ALL and T-ALL cell lines. Conditions for Figures 17–19: 72h treatment, MTS viability assay; IC_{50} from nonlinear regression.

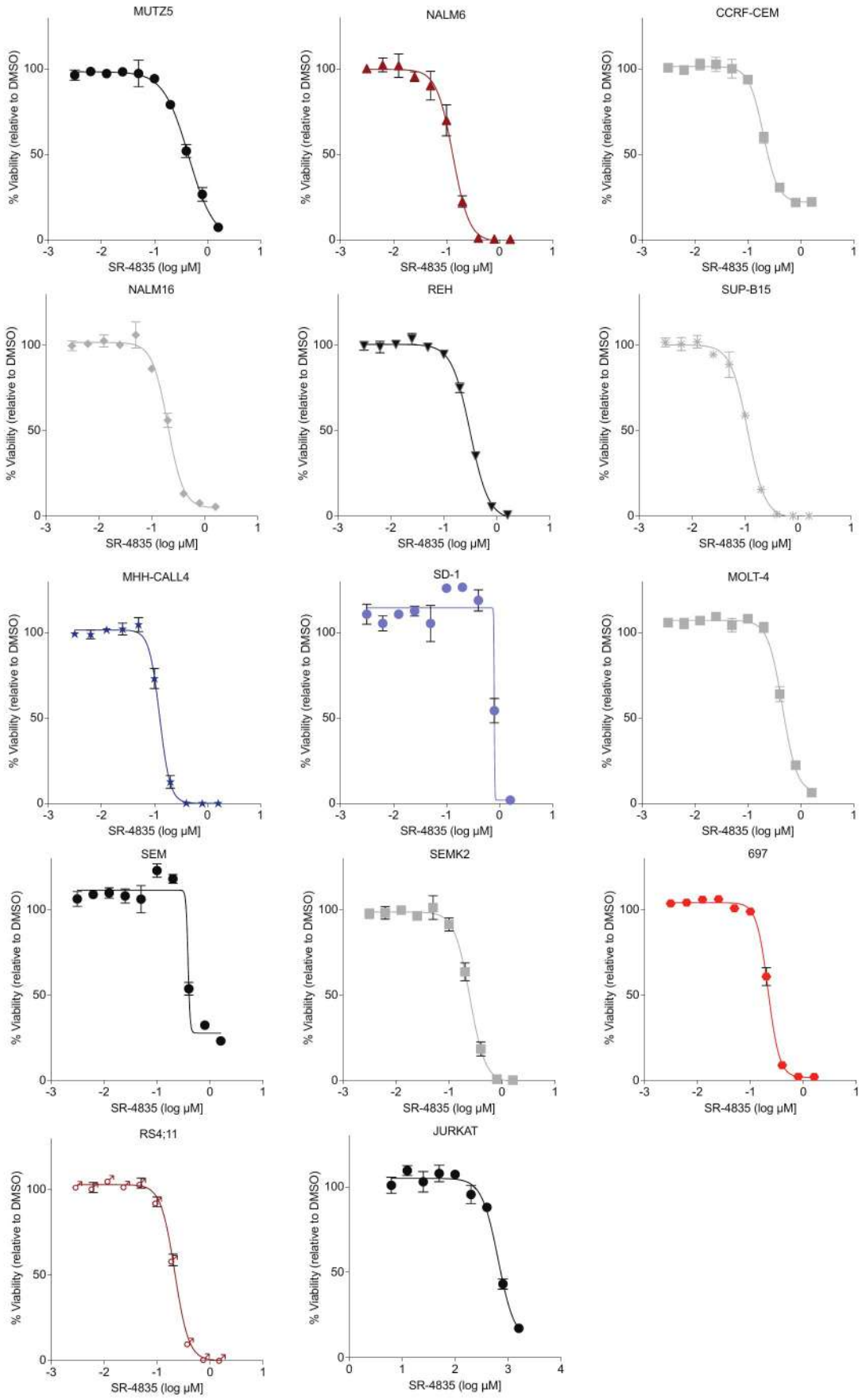

Figure 18. Dose-response curves for SR-4835 in B-ALL and T-ALL cell lines.

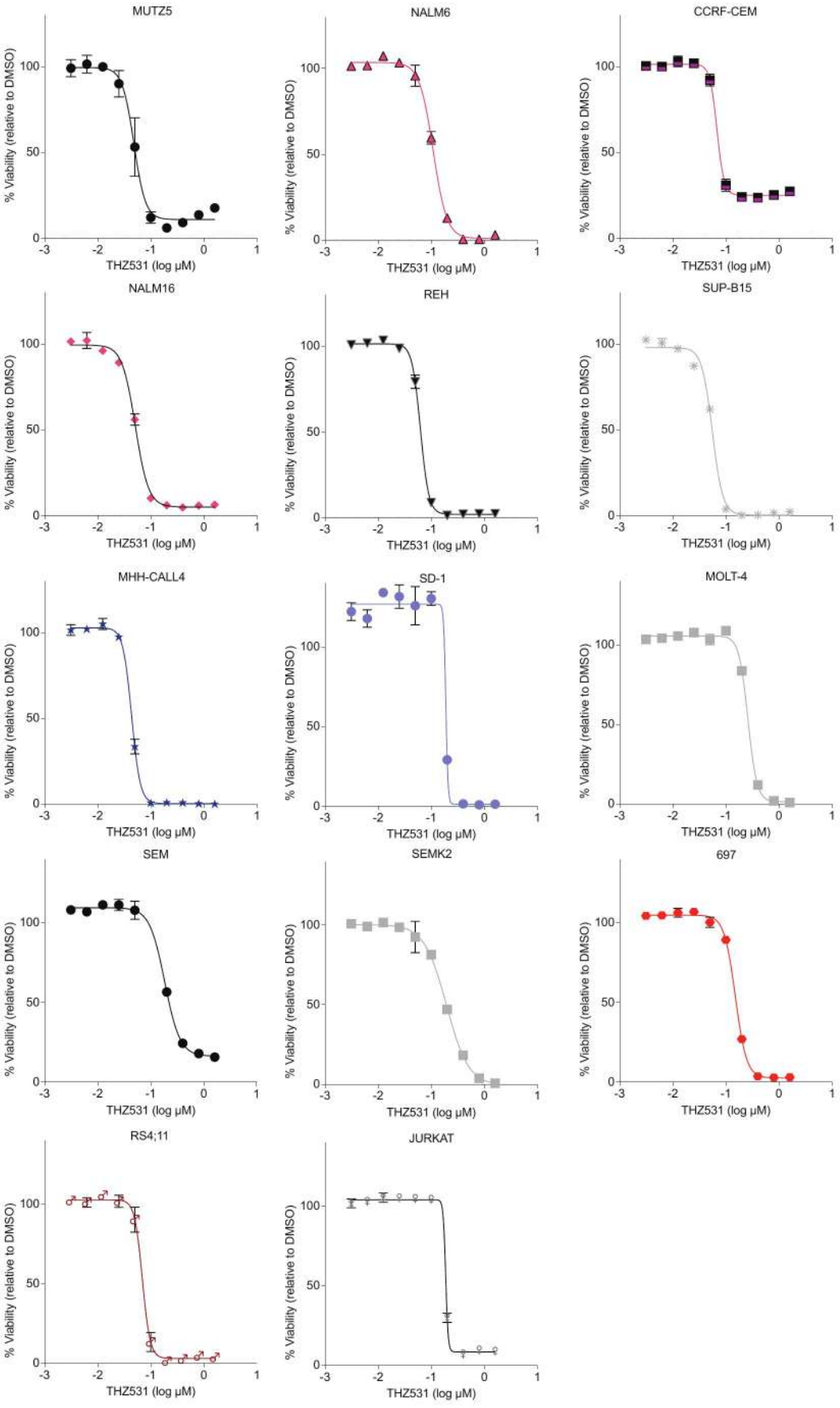

Figure 19. Dose-response curves for THZ531 in B-ALL and T-ALL cell lines.

To compare drug responses across all models, IC_{50} values were visualized as a heatmap (Figure 20). While glucocorticoid sensitivity varied significantly across ALL models, the response to CDK12/13 inhibition remained more uniform.

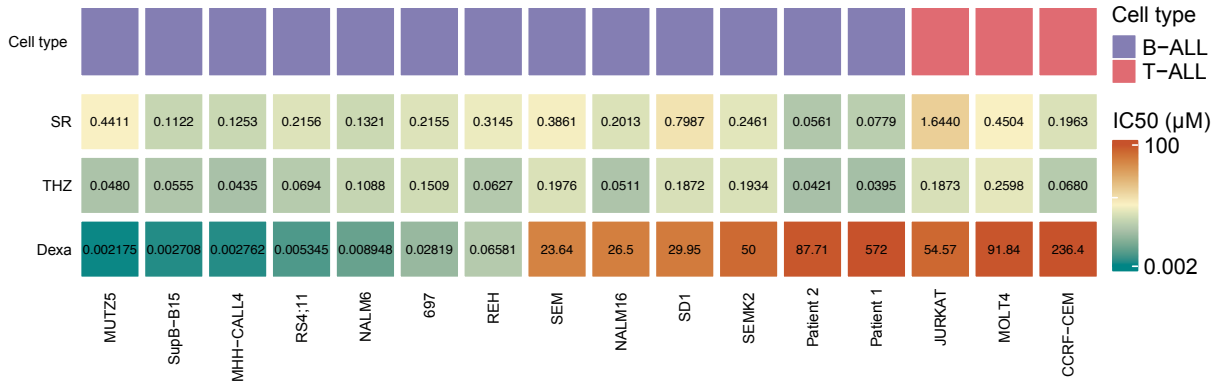

Figure 20. Comparative drug sensitivity across ALL models. Heatmap illustrating IC_{50} values for dexamethasone (Dexa), SR4835 (SR), and THZ531 (THZ) in B-ALL and T-ALL cell lines and primary B-ALL patient samples following 72h of treatment. Cell line viability was determined via MTS assay, while primary sample viability was defined as the propidium iodide (PI)-negative fraction measured by flow cytometry. IC_{50} values were derived from four-parameter logistic (4PL) regression. Data visualization was performed using the ComplexHeatmap R package.

Given that dexamethasone-resistant models remained highly sensitive to CDK12/13 inhibitors, I sought to determine if combining these agents would result in synergistic anti-leukemic effects.

3.5 Synergistic interaction between CDK12/13 inhibitors and glucocorticoids

To determine whether inhibition of CDK12/13 enhances glucocorticoid efficacy, combinatorial effects of dexamethasone with either SR4835 or THZ531 were evaluated across a panel of B-cell and T-cell acute lymphoblastic leukemia cell lines, healthy donor peripheral blood mononuclear cells (PBMCs), and primary patient samples. Drug interactions were assessed after 72 h treatment using dose–response matrices, and synergy was quantified using the Zero Interaction Potency (ZIP) synergy score model. ZIP scores quantify the deviation of the observed combination effect from the expected effect under the assumption of no interaction, integrating concepts from both Bliss independence and Loewe additivity. ZIP scores greater than zero indicate synergistic interactions, scores near zero indicate additive effects, and negative scores indicate antagonism.

3.5.1 Synergistic responses in ALL cell lines

Combinations of SR4835 plus dexamethasone and THZ531 plus dexamethasone resulted in synergistic anti-leukemic effects across most of the tested leukemia cell lines, as reflected by positive ZIP synergy scores (Figures 21 and 22). Overall, B-ALL cell lines demonstrated stronger and more consistent synergy compared with T-ALL models. In contrast, the T-ALL cell lines MOLT-4 and JURKAT exhibited weaker or absent synergistic responses to both combinations.

Despite the overall trend toward synergy in B-ALL, heterogeneity in combination responses was observed within this lineage. Several B-ALL cell lines, including REH, SUP-B15, and MHH-CALL4, displayed limited or inconsistent synergy. This variability likely reflects molecular and transcriptional heterogeneity within B-ALL, including differences in baseline glucocorticoid responsiveness, transcriptional dependencies, and survival pathway engagement.

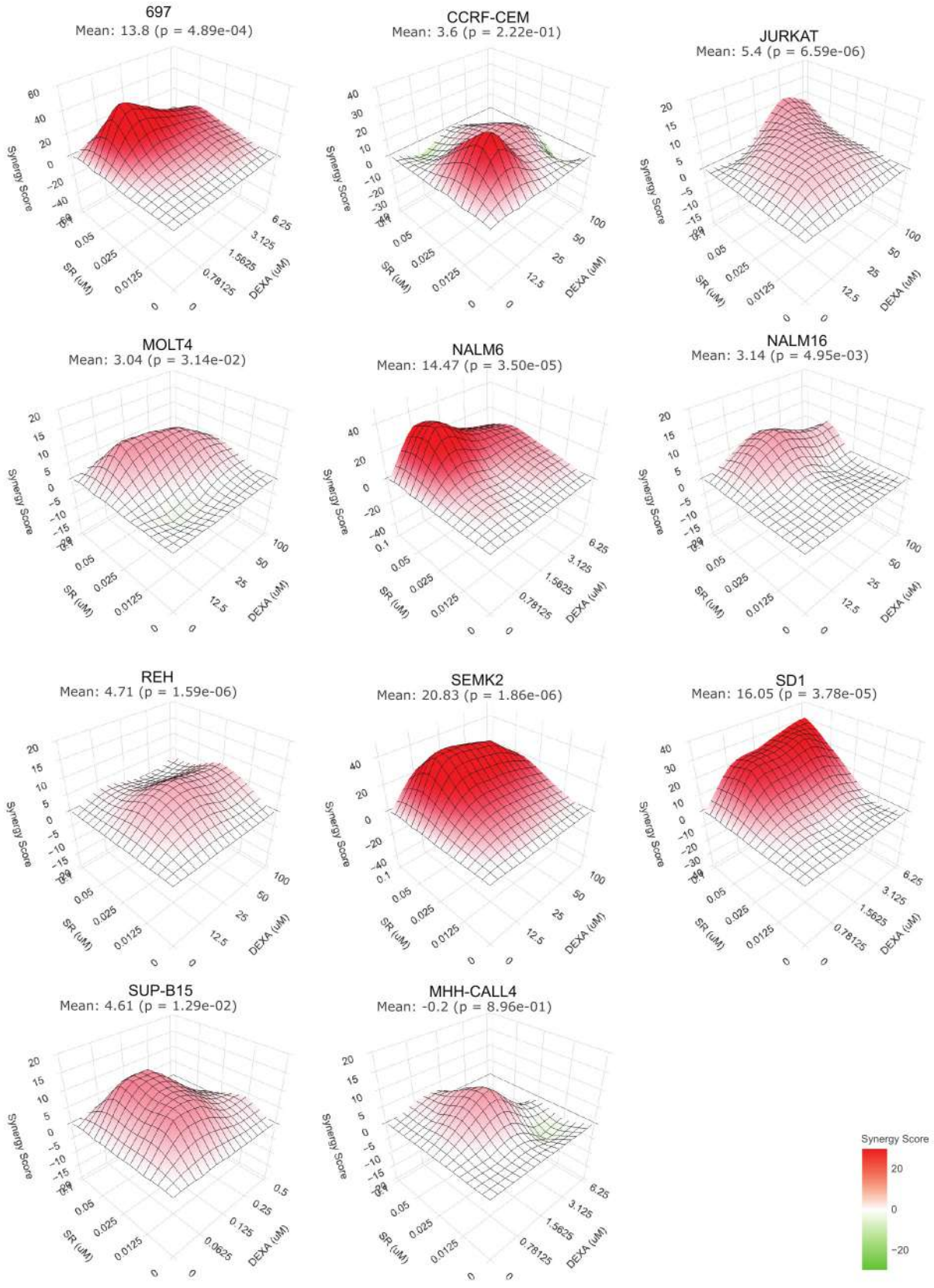

Figure 21. Synergy between SR-4835 and dexamethasone in ALL cell lines. Representative dose response interaction matrices for SR-4835 plus dexamethasone in B-ALL and T-ALL cell lines after 72 h treatment. Drug interactions were quantified using the ZIP synergy model. Created with SynergyFinder [174].

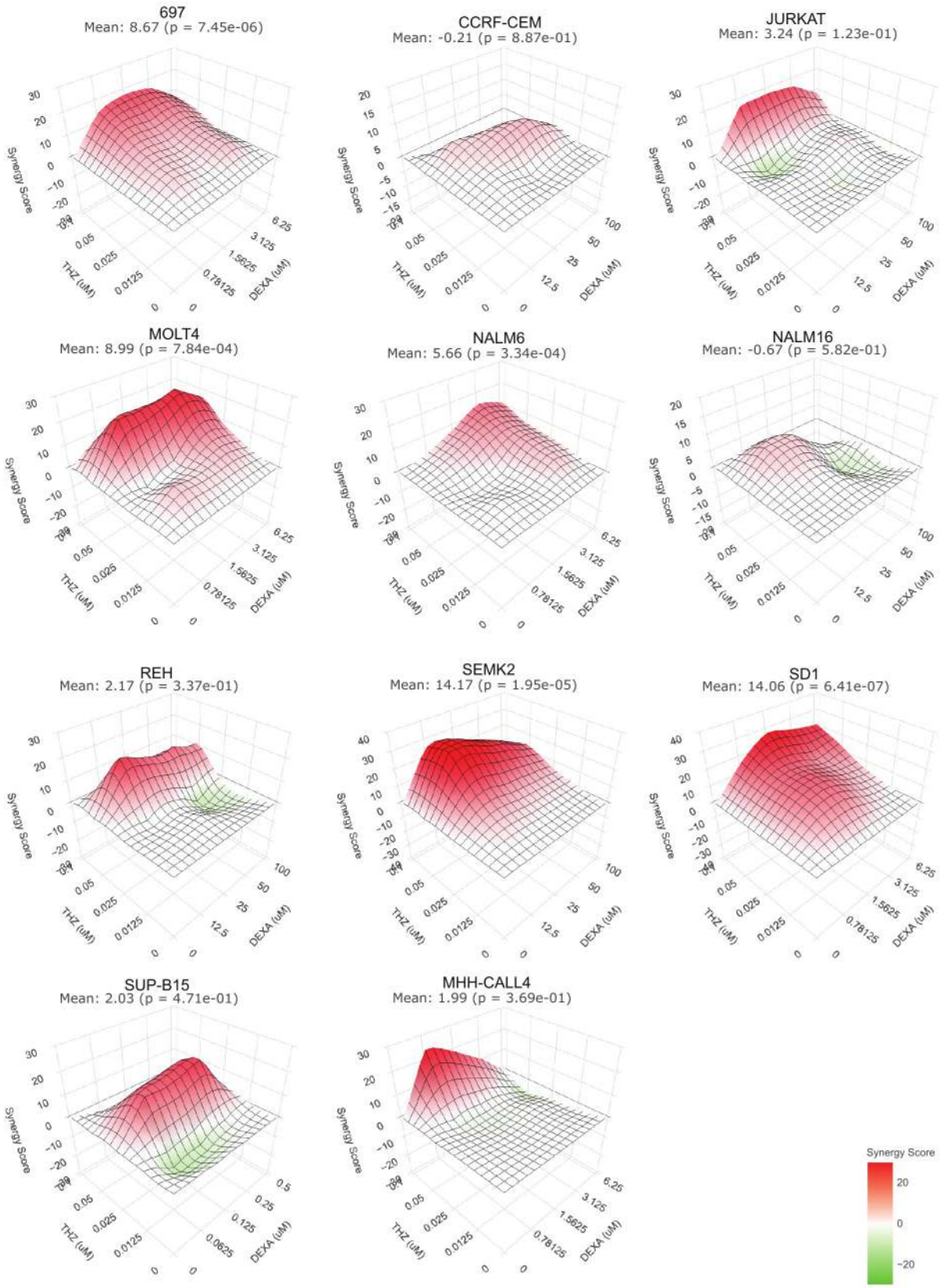

Figure 22. Synergy between THZ531 and dexamethasone in ALL cell lines. Representative dose response interaction matrices for THZ531 plus dexamethasone in B-ALL and T-ALL cell lines after 72 h treatment. ZIP synergy scores indicate the degree of interaction. Created with SynergyFinder [174].

3.5.2 Combination effects in healthy donor PBMCs

To assess whether synergistic interactions were selective for malignant cells, combination treatments were evaluated in PBMCs from four healthy donors. In contrast to leukemia cell lines, both SR4835–dexamethasone and THZ531–dexamethasone combinations generally resulted in negative ZIP synergy scores in PBMCs (Figure 23), indicating a lack of synergy and, in some cases, antagonistic interactions. These findings suggest that the synergistic effects observed in ALL models are not recapitulated in non-malignant hematopoietic cells.

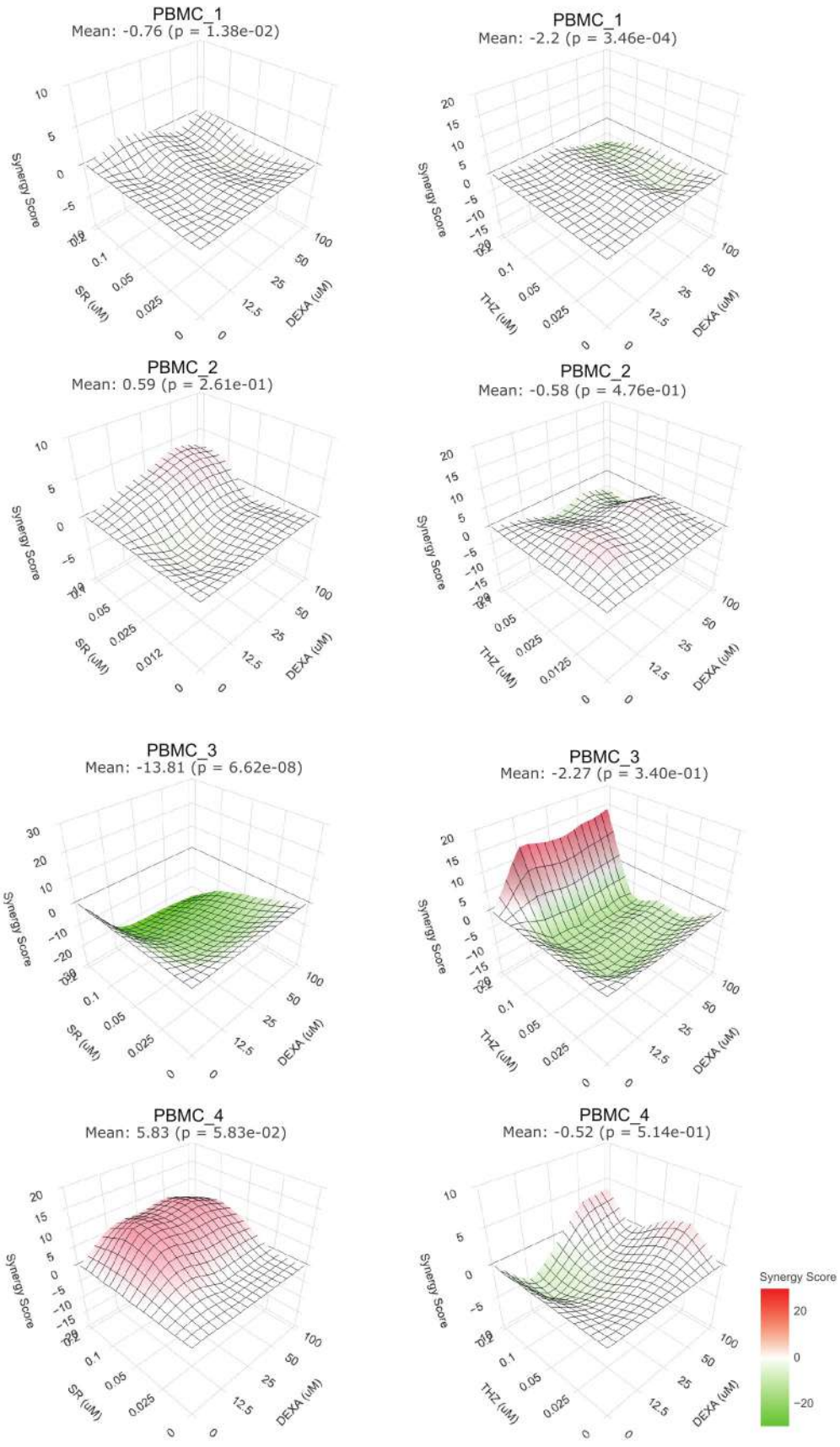

Figure 23. Combination responses in healthy donor PBMCs. ZIP synergy scores for SR-4835 plus dexamethasone and THZ531 plus dexamethasone in PBMCs from four healthy donors after 72 h treatment. Created with SynergyFinder [174].

3.5.3 Combination responses in primary patient samples

Combinatorial effects were additionally tested in two primary ALL patient samples. One patient sample exhibited mild synergistic interaction, as reflected by a modestly positive ZIP synergy score, whereas the second sample showed no evidence of synergy under the same conditions (Figure 24). Given the limited number of primary samples analyzed and the variability observed, these findings should be interpreted cautiously. Larger patient cohorts will be required to determine the prevalence and clinical relevance of CDK12/13 inhibitor–glucocorticoid synergy in primary ALL.

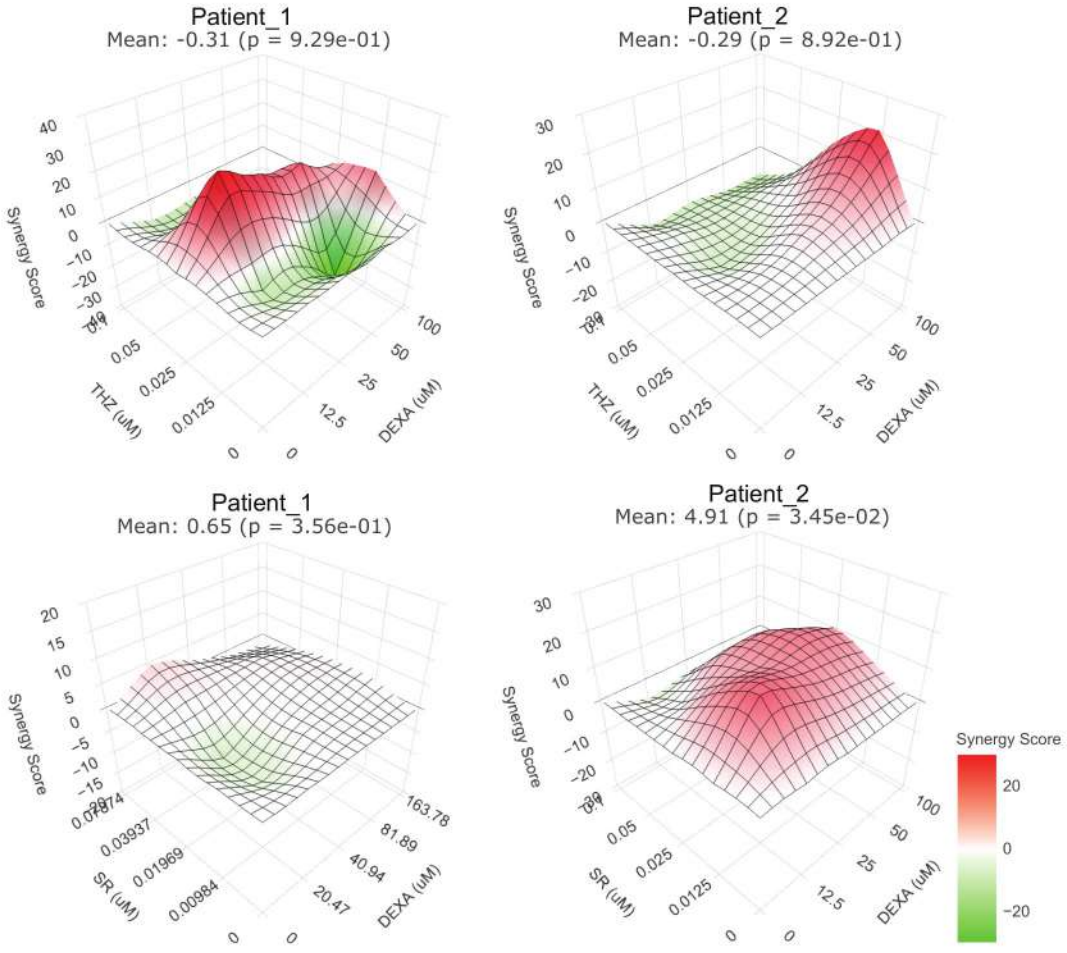

Figure 24. Combination responses in primary ALL samples. Representative dose response interaction matrices and ZIP synergy scores for CDK12/13 inhibitor–dexamethasone combinations in two primary ALL patient samples after 72 h treatment. Created with SynergyFinder [174].

3.5.4 Summary of synergistic interactions across models

A summary heatmap of ZIP synergy scores across all tested models is shown in Figure 25. This analysis highlights a clear distinction between frequent synergistic

interactions in ALL cell lines, particularly B-ALL models, and the predominantly non-synergistic or antagonistic responses observed in healthy PBMCs. Together, these data indicate that combined CDK12/13 inhibition and glucocorticoid treatment can elicit synergistic anti-leukemic effects in a substantial subset of ALL models, while sparing non-malignant cells.

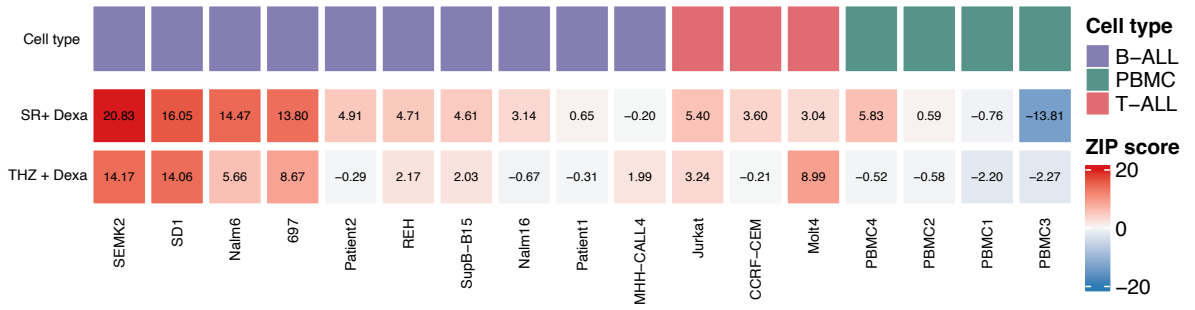

Figure 25. Summary of drug combination synergy across ALL models. Heatmap summarizing ZIP synergy scores for SR4835 plus dexamethasone and THZ531 plus dexamethasone across ALL cell lines, healthy donor PBMCs, and primary patient samples. Visualized using the ComplexHeatmap R package.

Among the tested leukemia models, SEMK2 consistently exhibited one of the most pronounced and reproducible synergistic responses to both SR4835–dexamethasone and THZ531–dexamethasone combinations. Based on these results, SEMK2 was selected as a representative model for subsequent mechanistic studies aimed at elucidating the transcriptional and cellular basis of CDK12/13 inhibitor–glucocorticoid synergy.

3.6 Transcriptional programs modulated by CDK12/13 inhibitors and glucocorticoids

3.6.1 CDK12/13 inhibitors induce a shared transcriptional program in B-ALL

To characterize the transcriptomic landscape associated with CDK12/13 inhibition, we performed RNA-seq on SEMK2 cells treated for 24h with SR4835, THZ531, dexamethasone, their combinations, or vehicle control. Principal component analysis (PCA) of variance-stabilized counts demonstrated that the primary source of variation (PC1; 82.4%) separated CDK12/13 inhibitor-treated samples from both DMSO and DEXA controls (Figure 26A). Notably, SR4835- and THZ531-treated cells clustered in proximity along PC1, suggesting a shared transcriptional response to these inhibitors.

The second principal component (PC2) further resolved the variance by separating dexamethasone-treated cells from non-treated populations.

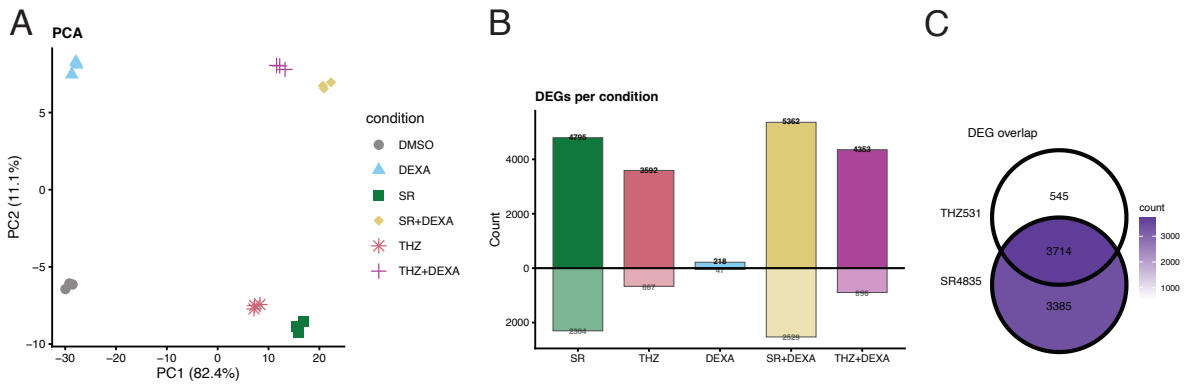

Figure 26. CDK12/13 inhibition induces a convergent transcriptional program in B-ALL cells. (A) Principal component analysis (PCA) of variance-stabilized counts. (B) Differential expression analysis of genes significantly altered by SR4835 and THZ531 (adjusted $p < 0.05$, $|\log_2 FC| \geq 1$). (C) Venn diagram illustrating the overlap of differentially expressed genes (DEGs) between SR4835 and THZ531 treatments.

Differential expression analysis identified 7,099 and 4,259 genes significantly altered by SR4835 and THZ531, respectively (Figure 26B). In both conditions, upregulated genes outnumbered downregulated genes, with 4,786 genes induced by SR4835 and 3,145 by THZ531. A Venn analysis revealed that 3,714 differentially expressed genes (52% of the SR4835 set, 87% of the THZ531 set) were shared between the two inhibitors (Figure 26C), demonstrating a high degree of similarity.

3.6.2 CDK12/13 inhibition suppresses biosynthetic and mitochondrial programs while activating stress-response pathways

To define the functional consequences of CDK12/13 inhibition, we compared the transcriptional profiles elicited by SR4835 and THZ531. Volcano plots confirmed a high level of concordance between the two inhibitors, with the most significantly modulated genes being shared (Figure 27A). Among the top differentially expressed genes were *HEXIM1* (a negative regulator of P-TEFb-mediated transcription elongation), the pro-apoptotic member *BMF*, and the transcriptional repressor *ID2*.

To characterize the broader biological programs affected, we performed Gene Set Enrichment Analysis (GSEA) across MSigDB. Hallmark analysis identified a significant negative enrichment of MYC Targets (V1/V2), Oxidative Phosphorylation, mTORC1 Signaling, and E2F Targets in both inhibitor conditions, indicating a broad suppression of growth-associated and biosynthetic transcriptional programs (Figure 27B).

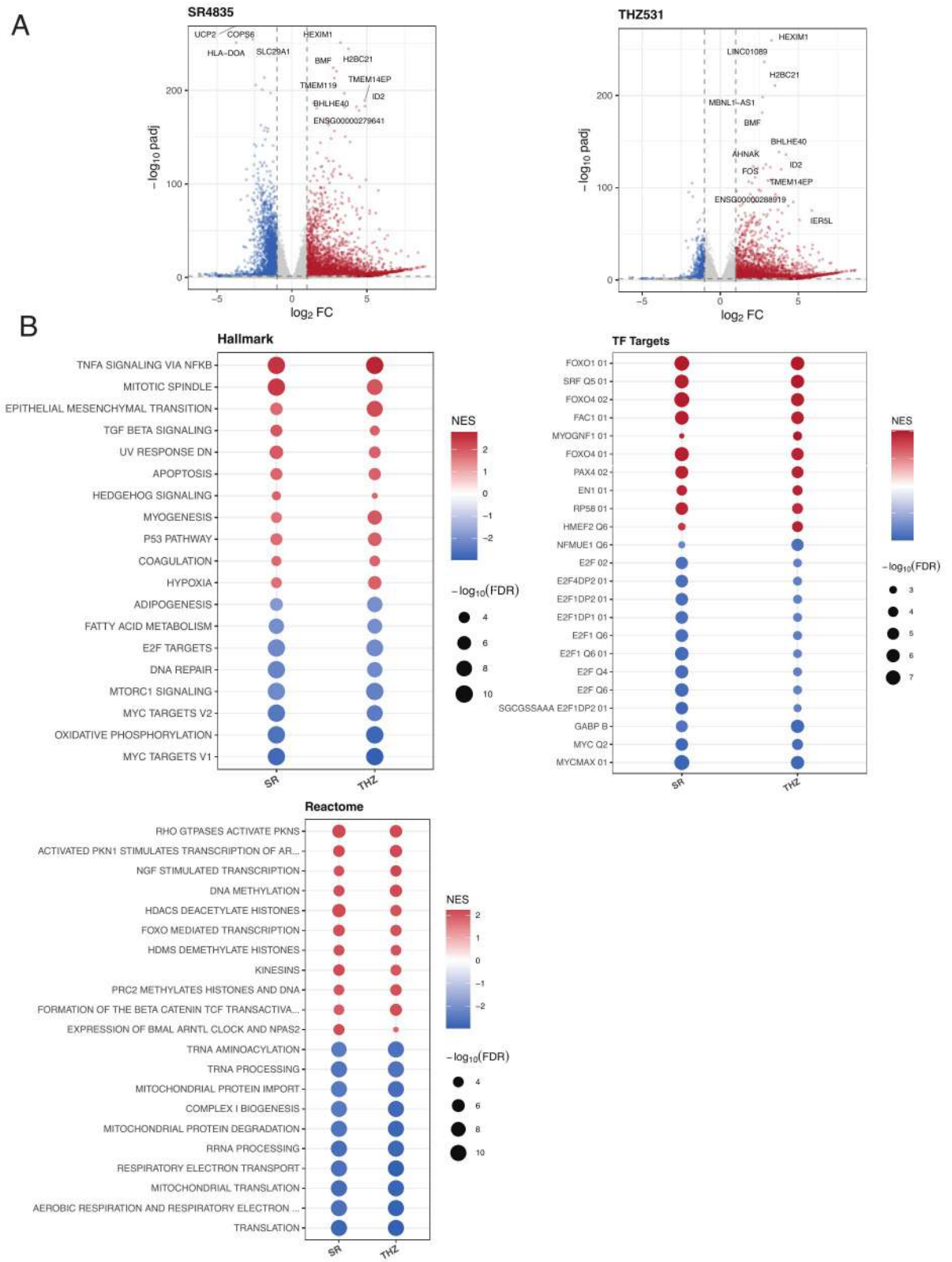

Figure 27. CDK12/13 inhibition suppresses biosynthetic and mitochondrial programs while activating stress-response pathways. A) Volcano plots of differentially expressed genes in SEMK2 cells following 24h treatment with SR4835 (left) or THZ531 (right) relative to DMSO control. Significantly upregulated genes are indicated in red, and downregulated genes in blue (adjusted $p < 0.05$, $|log_2FC| \geq 1$). Selected genes involved in transcriptional regulation and apoptosis are highlighted. (B) Gene Set Enrichment Analysis (GSEA) of differentially expressed genes after SR4835 or THZ531 treatment. Dotplots illustrate significant enrichment in Hallmark (top), TF Target (middle), and Reactome (bottom). The size of the dots represents the statistical significance (-log_{10}FDR), and the color indicates

the Normalized Enrichment Scores (NES), where red denotes positive enrichment (activation), and blue negative enrichment (suppression).

Reactome pathway analysis confirmed this pattern, with the most strongly suppressed pathways including Translation, Mitochondrial Translation, Respiratory Electron Transport, and rRNA Processing. Conversely, TNFα Signaling via NF-κB, p53 Pathway, Apoptosis, and TGF-β Signaling were positively enriched, indicating activation of stress and adaptive response. This shift toward a pro-apoptotic state was further corroborated by transcription factor (TF, filtered to exclude microRNA target sets) target enrichment analysis, which identified a significant suppression of MYC/MAX, E2F1, and GABPα target gene sets, alongside a notable induction of FOXO1 target genes (Figure 27B). Given the established role of FOXO1 in mediating glucocorticoid-induced apoptosis in lymphoid cells, and its target gene overlap with the glucocorticoid receptor (GR) transcriptional program, its activation suggests a potential mechanistic intersection between CDK12/13 inhibition and the dexamethasone response.

The transcriptional landscape remains stable under combinatorial treatment

We next investigated how the addition of dexamethasone modulated these programs. GSEA of the combination-treated cells (SR4835+DEXA and THZ531+DEXA) revealed a pathway profile that largely recapitulated the effects of the single agents. The negative enrichment of MYC Targets and E2F Targets persisted (Figure 28A), as did the suppression of Translation and Mitochondrial Respiratory pathways (Figure 28C). Furthermore, the induction of FOXO1-driven programs was maintained in the presence of DEXA (Figure 28B). Collectively, these data indicate that the combinatorial treatment does not deviate from the fundamental mechanism of action established by CDK12/13 inhibition.

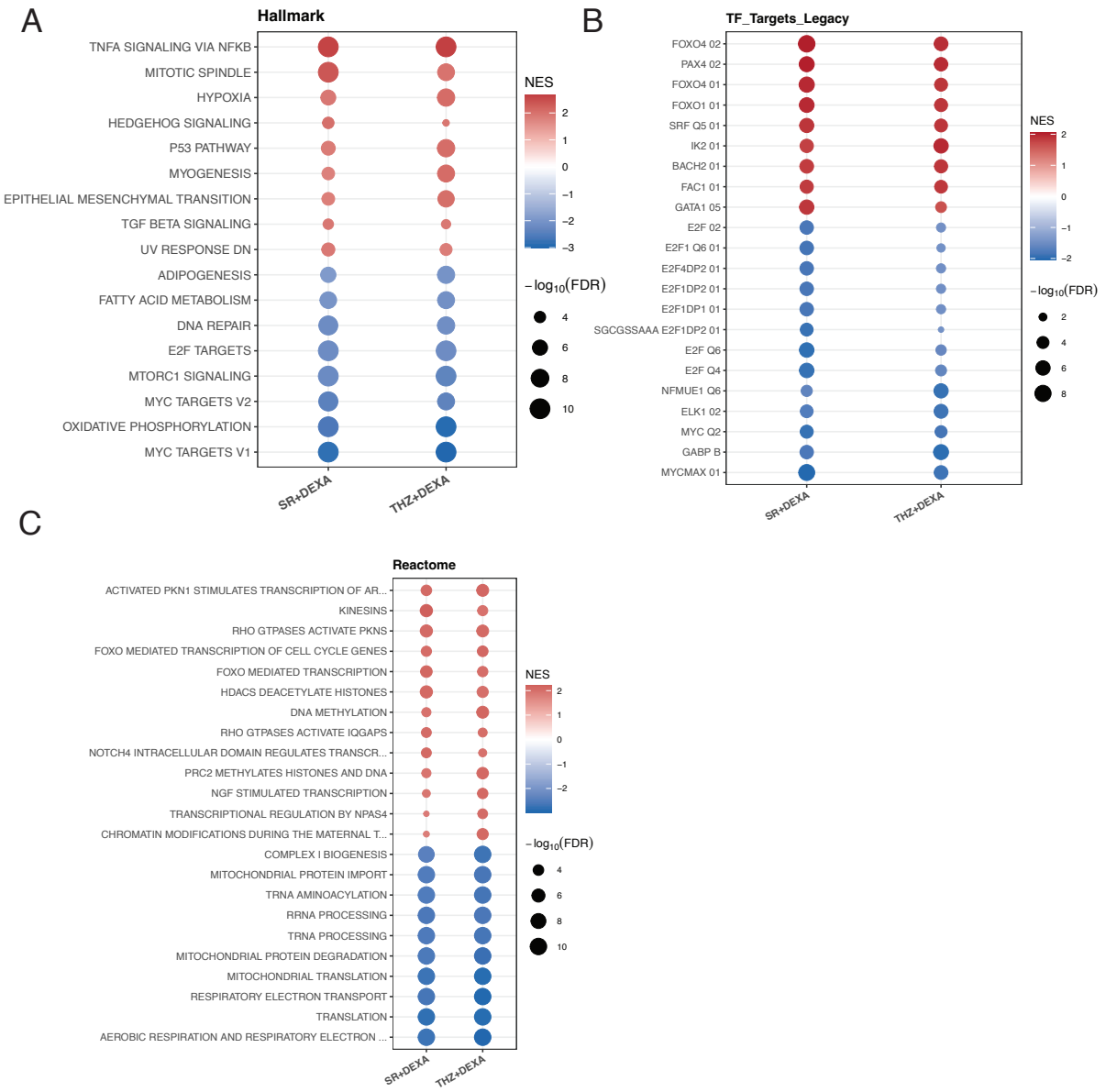

Figure 28. Combinatorial treatment with CDK12/13 inhibitors and dexamethasone maintains core transcriptional programs. (A) Dotplot illustrating GSEA results for the Hallmark collection. (B) Dotplot for the TF Target collection. (C) Dotplot for the Reactome collection. In all panels, SEMK2 cells were treated with the indicated inhibitor+dexamethasone (DEXA) combinations for 24h. The size of the dots represents the statistical significance (-log$_{10}$FDR), and the color indicates the Normalized Enrichment Score (NES), where red denotes positive enrichment (activation) and blue denotes negative enrichment (suppression).

CDK12/13 inhibition impairs the DNA damage response and DNA repair machinery

In addition to the broad repression of growth-associated signatures, we observed a coordinated downregulation of the DNA damage response and DNA repair machinery. Gene sets associated with these processes were among significantly depleted signatures under both CDK12/13 inhibitor conditions (Figure 27B). Focused analysis of Gene Ontology (GO) Biological Process terms revealed a downregulation of Recombinational Repair, Double-Strand Break Repair, Mismatch Repair, and Nucleotide Excision Repair pathways (Figure 29A). These results are consistent with

the established role of CDK12 in sustaining the expression of core DDR genes through its regulation of RNA polymerase II processivity, suggesting that CDK12/13 inhibition may render B-ALL cells vulnerable to the accumulation of genomic instability.

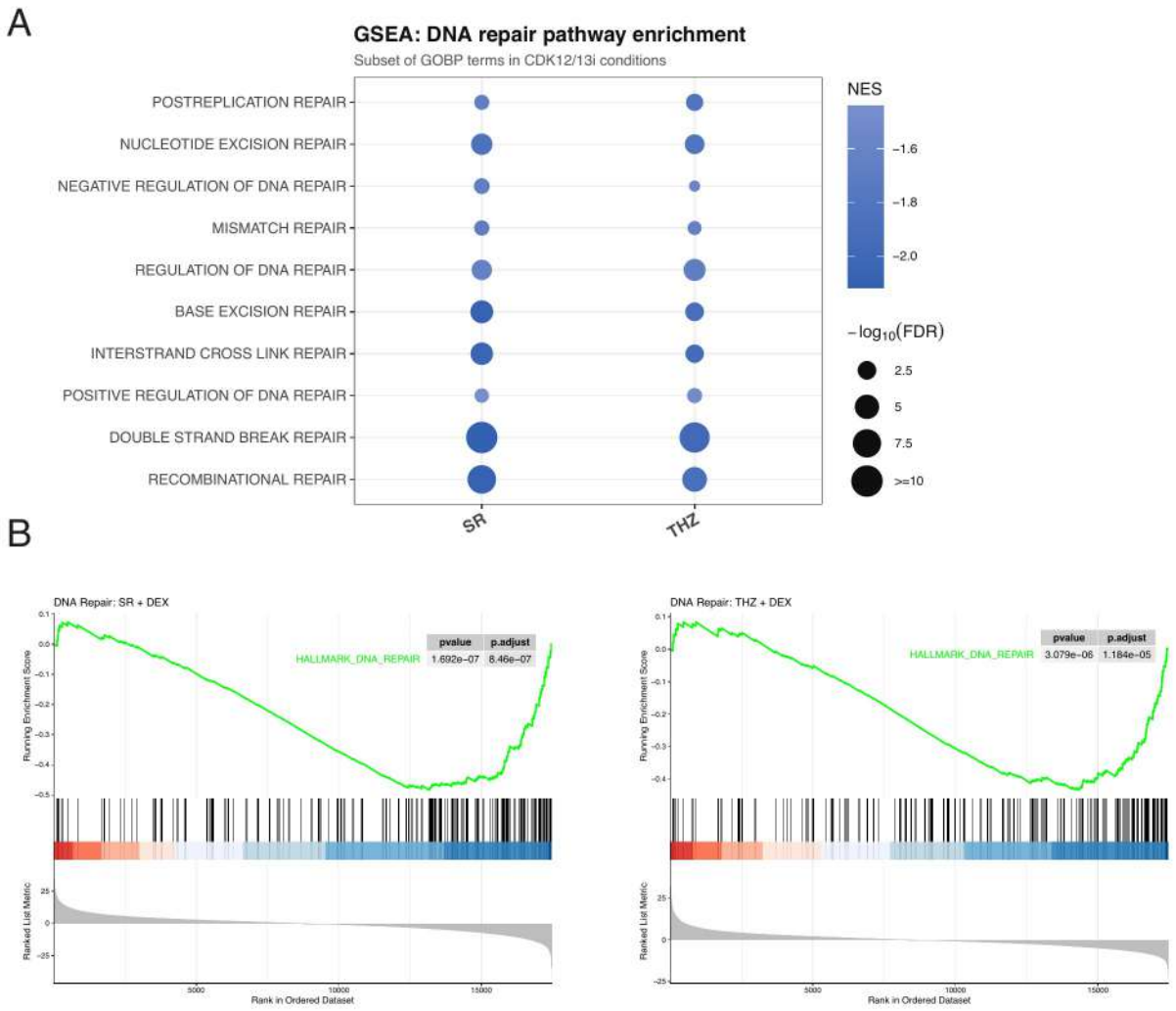

Figure 29. CDK12/13 inhibition targets genomic integrity pathways. (A) Negative enrichment analysis of DNA repair pathway in single-agent inhibitor conditions. Size indicates -log$_{10}$FDR; color indicates Normalized Enrichment Score (NES). (B) GSEA barcode plots for the Hallmark DNA Repair gene set in cells after the combinatorial treatments. The vertical black lines (barcodes) represent individual genes in the set, ranked by their differential expression from upregulated (left) to downregulated (right). The green line tracks the running enrichment score, and the NES and FDR are indicated. FDR, False Discovery Rate

This impairment was preserved in the combinatorial setting. GSEA analysis of cells treated with the SR4835+DEXA or THZ531+DEXA combinations confirmed the sustained suppression of the Hallmark DNA Repair signature (Figure 28A, 29B). Barcode plots for these conditions illustrate a strong enrichment of DNA repair genes, reinforcing the observation that the transcriptional impact of CDK12/13 inhibition on DNA damage genes remains the dominant feature of the combinatorial response.

3.6.3 CDK12/13 inhibition perturbs RNA processing leading to alternative splicing events

Given the established roles of CDK12 and CDK13 in regulating RNA polymerase II processivity and co-transcriptional RNA processing, we investigated whether CDK12/13 inhibition altered the genomic distribution of sequencing reads. Prior to this analysis, we considered the various modalities of alternative splicing that may be affected by Pol II elongation defects, including exon skipping, alternative splice sites, and intron retention (Figure 30A).

Analysis of read distribution across genomic elements revealed a modest but statistically significant increase in the proportion of reads mapping to intronic regions in both SR4835- (paired *t*-test, $p = 0.021$) and THZ531-treated cells ($p = 0.023$) compared to DMSO controls (Figure 30B-C). This accumulation of intronic content is consistent with a defect in splicing efficiency or altered transcription termination, both of which are hallmark consequences of impaired Pol II elongation following CDK12/13 inhibition.

To directly quantify alternative splicing, rMATS analysis was performed across five distinct event types. A substantial number of significant splicing events were detected in both SR4835- and THZ531-treated cells, with skipped exons and retained introns emerging as the most frequent categories, especially after SR4835 treatment (Figure 30D). Reasoning that mechanistically relevant events should be reproducible across two structurally distinct inhibitors targeting the same kinases, I specifically examined events shared between both treatments.

While the overall number of shared splicing events was limited, the 38 common events identified across both inhibitor conditions represent high-confidence on-target effects (Figure 30E). These events exhibited high directional concordance (Spearman $\rho = 0.95$) suggesting they represent genuine on-target effects of CDK12/13 inhibition, with several genes affected with established roles in oncogenesis and hematological malignancies. Targets included *PAXBP1*, which bridges the transcription factors *PAX3* and *PAX7* to the histone methylation machinery, and has been linked to acute myeloid leukemia, and *DDX3X*, a known fusion partner in the high-risk DDX3X::MLLT10 rearrangement associated with aggressive, therapy-resistant AML.

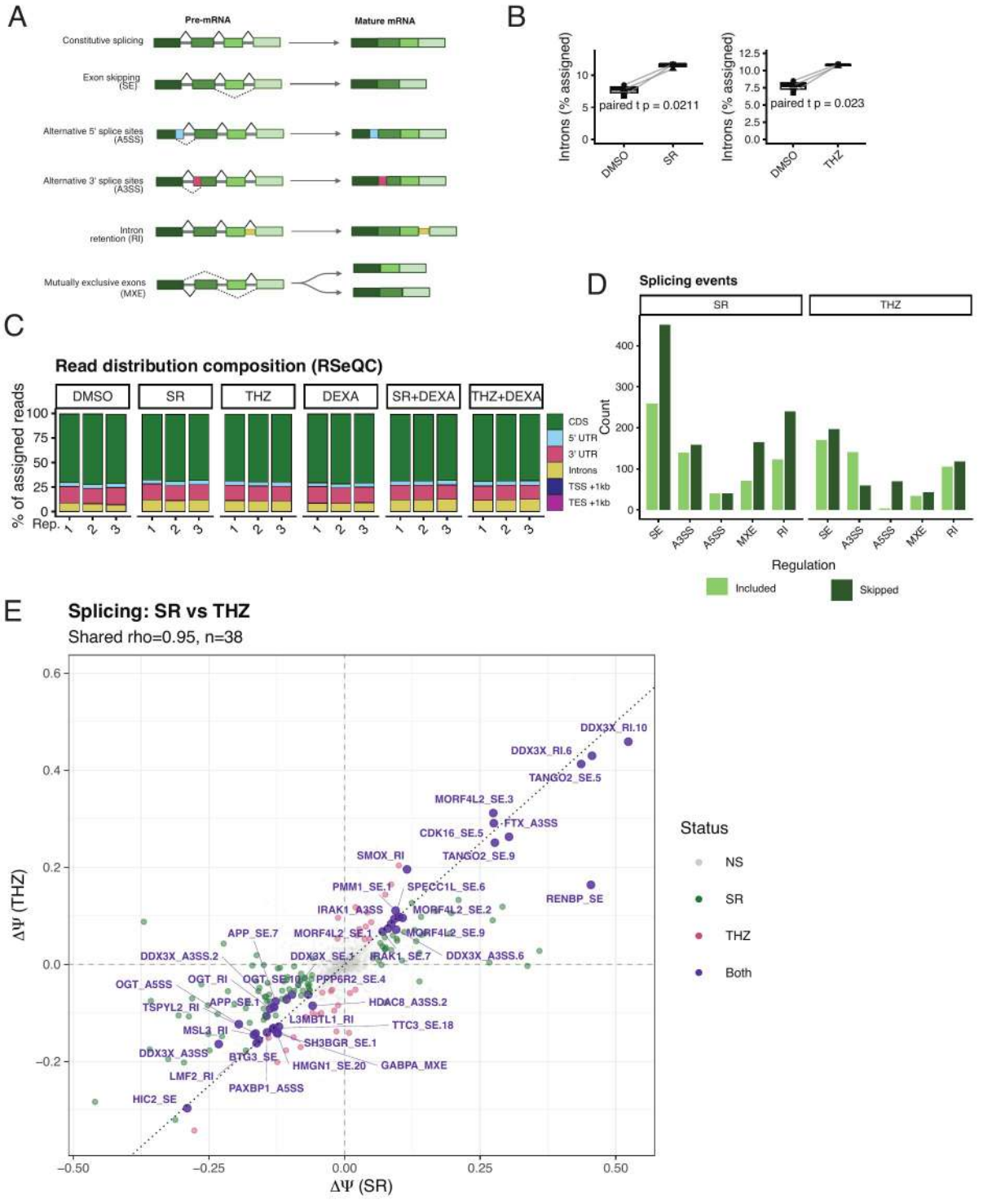

Figure 30. CDK12/13 inhibition leads to increased intronic read distribution and alternative splicing events. (A) Schematic representation of alternative splicing modalities, including exon skipping (SE), alternative 5' and 3' splice site usage (A5SS or A3SS), intron retention (RI), and mutually exclusive exons (MXE). (B) Statistical comparison of intronic read proportions. P-values were calculated using a paired t-test relative to the DMSO control. (C) Bar plots illustrating the distribution of RNA-seq reads across genomic features (exons, introns, intergenic, and untranslated regions). (D) Correlation of alternative splicing events common for both SR4835, and THZ531. Significant splicing changes were defined as FDR < 0.05 and |inclusion level difference (ΔΨ)| > 0.05. The concordance of splicing changes for shared events was assessed Spearman rank correlation. SR, SR4835; THZ, THZ531; UTR, untranslated region.

Furthermore, we identified splicing perturbations in *SH3BGR*, which is overexpressed in various AML cell lines, and *MORF4L2,* a component of the NuA4 histone acetyltransferase complex involved in DNA repair and *BRCA1* interaction.

The alternative splicing of these transcripts could result in either functional inactivation via nonsense-mediated decay or the production of isoforms with altered coding potential. While the specific consequences of these splicing events in B-ALL remain largely unexplored, CDK12/13 inhibition may modulate the leukemia landscape by targeting transcriptional and epigenetic regulators.

3.6.4 CDK12/13 inhibition potentiates the glucocorticoid-responsive transcriptional program

To identify the transcriptional basis for the observed synergy, I compared the gene expression profiles of single-agent treatments versus combinatorial settings. Initial analysis of the 50 most variable genes across all conditions revealed distinct clusters of treatment-responsive transcripts (Figure 31). I identified a subset of genes (indicated by red dashed outlines) that exhibited upregulation upon single-agent dexamethasone treatment but showed a marked, additive increase in expression within the combinatorial arms. This cluster was enriched for canonical steroid-responsive genes, including *TSC22D3* (*GILZ*) and *ZBTB16*. Parallel to this, a second cluster of genes (indicated by blue dashed outlines) was characterized by low induction by dexamethasone alone, but showed baseline upregulation following CDK12/13 inhibition, reaching even higher expression levels in the combination settings. This cluster was notably enriched for Immediate Early Genes (IEGs), such as *FOS, JUN, JUNB*, and *IER2*, as well as the pro-apoptotic factor *BMF*. The induction of this IEG stress signature by SR4835 and THZ531 suggests that CDK12/13 inhibition induces a primed, stress-responsive state. This observation is further supported by previous GSEA results, which demonstrated a positive enrichment of FOXO1 targets following CDK12/13 inhibition (Figure 27B, 28B). Given that FOXO1 and the glucocorticoid receptor often function as co-activators at shared genomic loci in lymphoid biology, it can be hypothesized that CDK12/13 inhibitors might partially engage the dexamethasone response program to lower the threshold for GR-mediated gene activation.

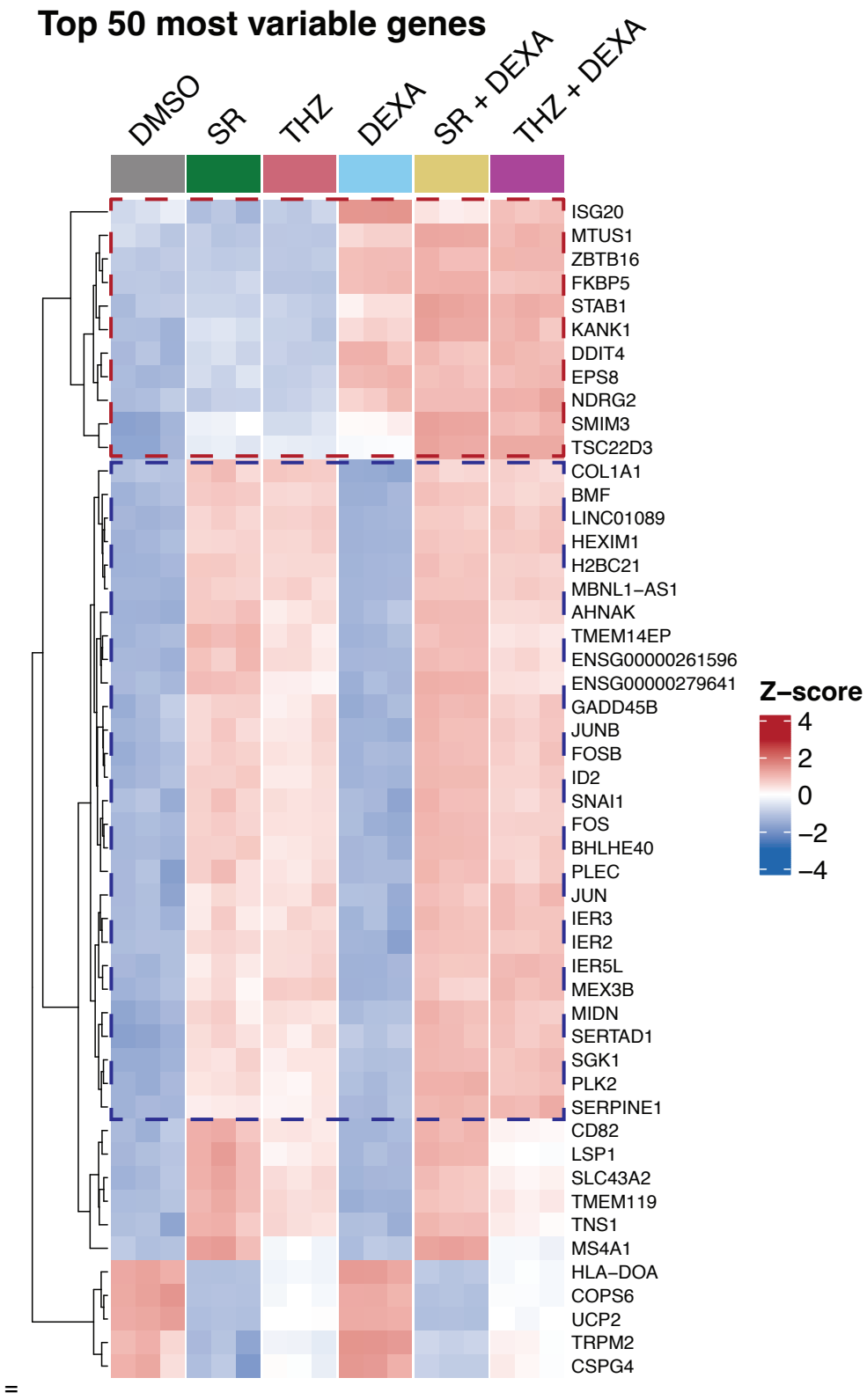

Figure 31. Combinatorial treatment differentially amplifies and primes gene expression clusters. Heatmap displaying the top 50 most variable genes across DMSO, single-agent (SR, THZ, DEXA), and combinatorial (SR+DEXA, THZ+DEXA) treatment settings. Red dashed boxes highlight a cluster of primary dexamethasone-responsive genes (e.g., TSC22D3, FKBP5) that are further amplified in the combination. Blue dashed boxes highlight a stress-responsive cluster primarily induced by CDK12/13 inhibition (e.g., FOS, JUN, SGK1) that shows enhanced expression upon co-treatment. Data represent Z-score normalized expression levels.

To test this, I assembled a curated set of 31 canonical GR-responsive genes and examined their expression across all conditions (Figure 32A). Strikingly, many well-established GR target genes, including *TSC22D3, PER1, TXNIP, BCL2L11 (BIM),* and *SGK1*, showed significant upregulation not only in DEXA-treated cells but also in SR4835- or THZ531-treated cells alone.

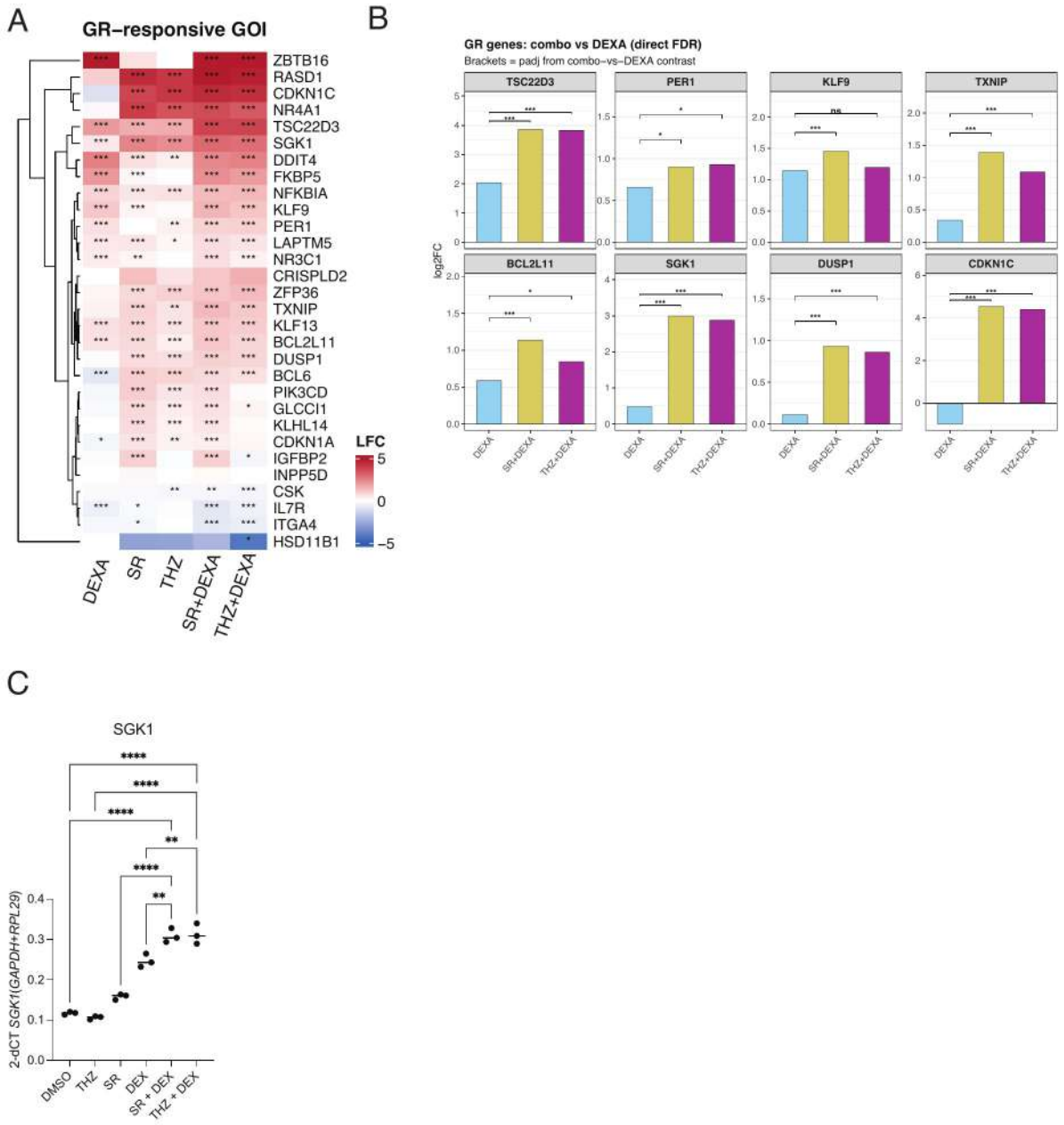

Figure 32. CDK12/13 inhibition potentiates the canonical glucocorticoid-responsive transcriptional program. (A) Heatmap analysis of a curated 31-gene canonical GR-responsive signature in SEMK2 cells following 24h treatment with DMSO, SR4835 (SR), THZ531 (THZ), dexamethasone (DEXA), or the indicated combinations. Data represent Z-score normalized expression levels. Asterisks indicate statistical significance relative to the DMSO control (adjusted $p < 0.05$). (B) Direct comparison of log_2(fold changes) for selected high-priority GR target genes. Statistical significance was determined by direct contrast between the combination arms (SR+DEXA or THZ+DEXA) and the dexamethasone monotherapy group (adjusted $p < 0.05$). (C) RT-qPCR validation of SGK1

expression levels. Data are presented as mean ± SD of three biological replicates. Statistical significance across groups was assessed via one-way ANOVA test ($p < 0.05$).

Heatmap analysis confirmed that a significant subset of the GR-responsive gene panel was induced by CDK12/13 inhibition, albeit generally to a lesser degree than by dexamethasone. Comparison of $\log_2$(fold changes) for these curated GR-responsive genes revealed that several key targets were expressed at significantly higher levels in the combination conditions (SR+DEXA, THZ+DEXA) than in DEXA alone. Specifically, *TSC22D3, PER1, BCL2L11, SGK1*, and *CDKN1C* showed statistically significant increase in one or both combination arms compared to the dexamethasone single-agent control (direct contrast adjusted $p < 0.05$; Figure 32B). To validate these transcriptomic findings, I performed RT-qPCR for *SGK1*, which showed a significant increase in expression upon combinatorial treatment compared to all single-agent groups (one-way ANOVA, $p < 0.05$; Figure 32C). Collectively, these results suggest that CDK12/13 inhibition transcriptionally primes B-ALL cells, leading to a synergistic induction of the glucocorticoid-responsive pro-apoptotic program.

3.7 Cellular and molecular mechanisms underlying the combination

3.7.1 Induction of apoptosis

To determine whether the reduced cell viability and synergistic drug interactions observed in preceding experiments were driven by apoptotic cell death, apoptosis was assessed using Annexin V and propidium iodide staining followed by flow cytometry (Figure 33A).

Single-agent treatment with dexamethasone, SR4835, or THZ531 induced variable levels of apoptosis across ALL cell lines, consistently reflecting the resistance profiles established in the initial IC_{50} assays and summarized heatmaps (Figure 33B). Notably, in responsive models, treatment resulted in an increased fraction of Annexin V-positive cells, whereas resistant models exhibited minimal apoptotic induction following single-agent dexamethasone exposure (Figure 33C).

To evaluate whether combined treatment enhanced apoptotic responses, drug combinations were tested in two representative B-ALL cell lines, SEMK2 and 697 (Figure 33C). In SEMK2 cells, combined treatment with dexamethasone and CDK12/13 inhibition resulted in a marked increase in apoptotic and necrotic cells compared with either single agent. This potentiation mirrors the synergistic effects

observed in preceding viability-based assays, suggesting that SR4835 effectively sensitizes otherwise dexamethasone-resistant SEMK2 cells to programmed cell death. In contrast, in 697 cells, dexamethasone alone induced near-complete apoptosis, limiting the capacity to detect additional enhancement by combination treatment.

Finally, dose-response analysis of apoptosis in SEMK2 cells treated with increasing concentrations of dexamethasone and SR4835 demonstrated a progressive increase in apoptotic cell fractions, supporting a dose-dependent induction of cell death by combined treatment (Figure 33D).

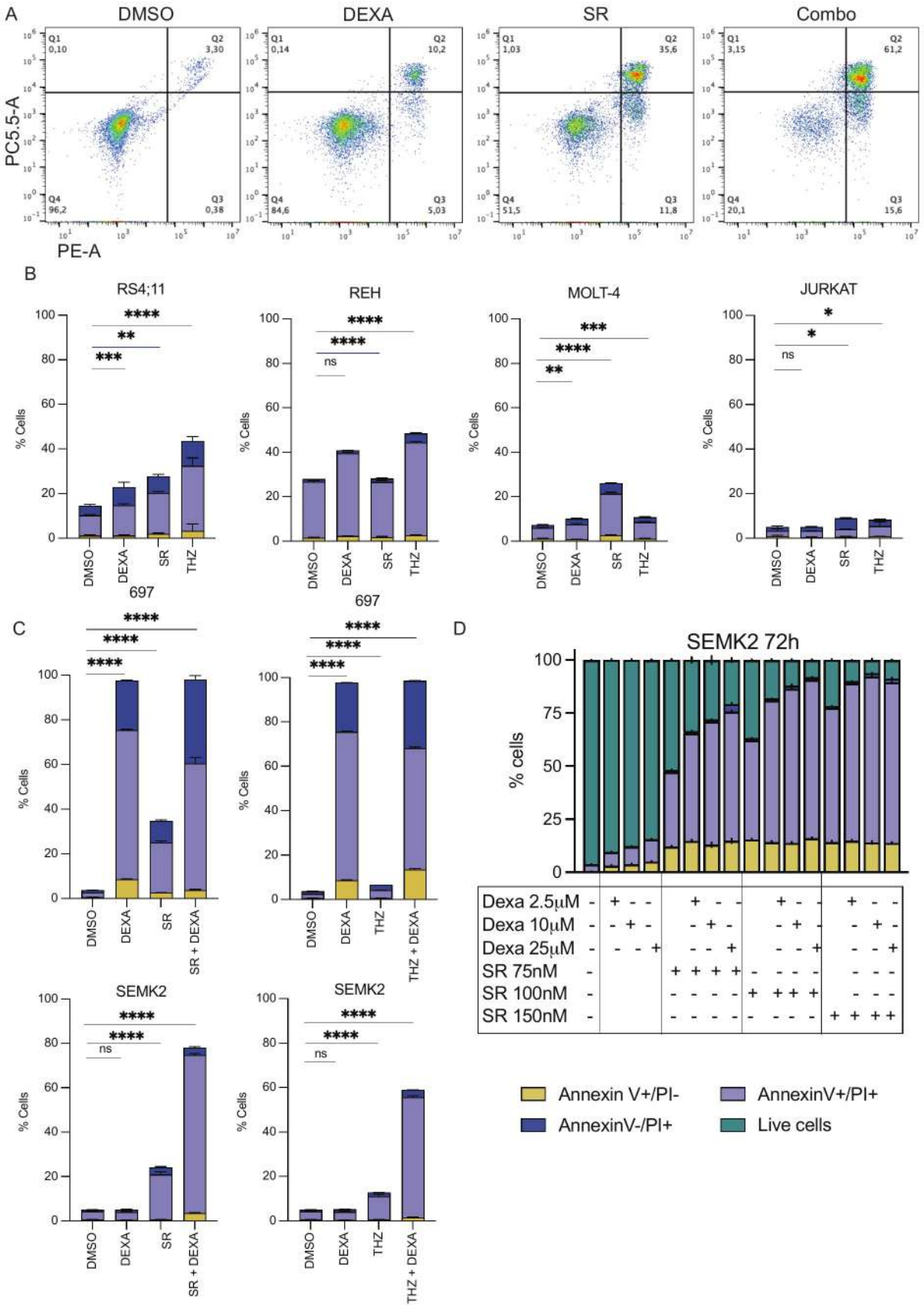

Figure 33. Induction of apoptosis by CDK12/13 inhibition and dexamethasone in ALL cell lines. (A) Representative flow cytometry density plots illustrating the gating strategy for Annexin V (PE-A) and propidium iodide (PC5.5-A) staining. SEMK2 cells were treated for 72 h with DMSO (control), dexamethasone, SR4835, or

the combination. Quadrants indicate viable (Annexin V-/PI-), early apoptotic (Annexin V+/PI-), late apoptotic (Annexin V+/PI+), and necrotic (Annexin V-/PI+) populations.
(B) Single agent apoptosis induction across a panel of ALL cell lines (RS4;11, REH, MOLT-4, and JURKAT). Cells were treated for 72h with SR4835 (75 nM), THZ531 (75 nM), or dexamethasone (2.5 µM). Statistical significance was assessed by one-way ANOVA with Tukey's multiple comparison test (n=2).
(C) Evaluation of apoptotic induction in representative B-ALL cell lines SEMK2 (dexamethasone-resistant) and 697 (dexamethasone-sensitive) under the treatment conditions described in (B). Statistical significance was assessed by one-way ANOVA with Tukey's multiple comparison test (n=2).
*(D) Dose-response analysis of apoptosis in SEMK2 cells following 72 h of treatment with increasing concentrations of dexamethasone, SR4835 or the combination. Data represent the mean ± SEM of n=2 independent experiments. Significance levels are indicated as: *p < 0.05, **p < 0.01, ***p < 0.001, ****p < 0.0001; ns, non-significant. SR, SR4835; THZ, THZ531; DEXA, dexamethasone.*

3.7.2 Modulation of cell cycle phases by SR4835 and dexamethasone

To investigate whether the observed synergistic growth inhibition was associated with specific alterations in cell cycle progression, the distribution of cells in G0/G1, S, and G2 phases was analyzed via flow cytometry following 36h of treatment.

In the 697 cell line, single-agent treatment with dexamethasone (1, 5, and 10 µM) resulted in an increased fraction of cells in the G0/G1 phase, consistent with a glucocorticoid-induced G1 arrest (Figure 34). Conversely, treatment with SR4835 alone induced a G2 arrest. Notably, the combination of SR4835 and dexamethasone led to a further enhancement of the G2 arrest population, which appeared to be the predominant effect over the G1 arrest observed with dexamethasone monotherapy.

In the SEMK2 cell line, dexamethasone treatment did not significantly alter the cell cycle distribution compared to the DMSO control, further confirming the dexamethasone-resistant phenotype of this model (Figure 34). While SR4835 monotherapy resulted in a marginal increase in the G0/G1 population, the combination of SR4835 and dexamethasone induced a distinct G2 arrest. These data suggest that CDK12/13 inhibition can modulate the cell cycle dynamics of dexamethasone-resistant cells, shifting the population toward G2 arrest when used in combination.

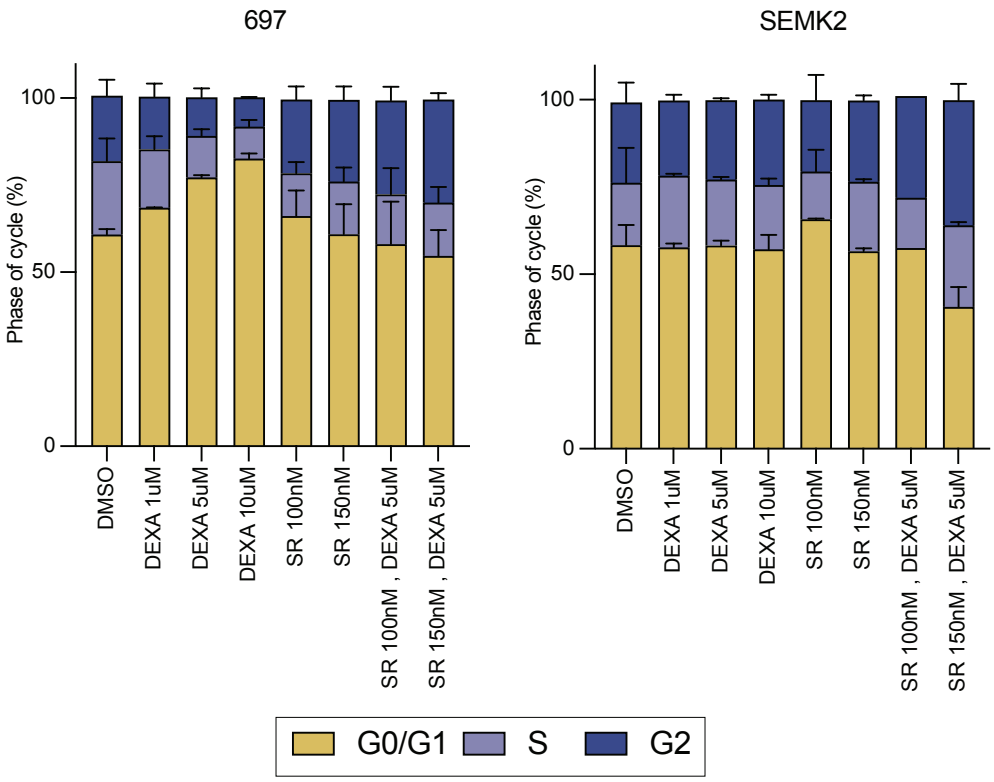

Figure 34. Impact of combined CDK12/13 inhibition and dexamethasone on cell cycle distribution.
Distribution of cells in G0/G1, S, and G2 phases was analyzed via flow cytometry following 36 h of treatment. The 697 cell line (left) and SEMK2 cell line (right) were treated with dexamethasone (DEXA; 1, 5, and 10 µM) or SR4835 (SR; 100 and 150 nM) as single agents, or in combination (SR 100/150 nM + DEXA 5 µM).

3.7.3 Evaluation of CDK12/13/Cyclin K levels and downstream transcriptional impact

To evaluate the baseline expression of the SR4835 targets across a broad panel of ALL cell lines, Western blot analysis was performed on total cell lysates under steady-state conditions (Figure 35). A high degree of heterogeneity in protein levels was observed across the 14 cell lines examined. Interestingly, the expression levels of CDK12 generally correlated with those of CDK13, with both kinases showing notably lower expression in MHH-CALL4, SD1, MOLT4, and JURKAT cells compared to the rest of the panel (Figure 35A, B). While CCNK levels partially mirrored the expression patterns of CDK12 and CDK13, most evidently in the low-expressing MHH-CALL4 and SD1 lines, this correspondence was not consistent across all models, suggesting potential cell line specific differences in the regulation of the CDK12/13-CCNK protein expression.

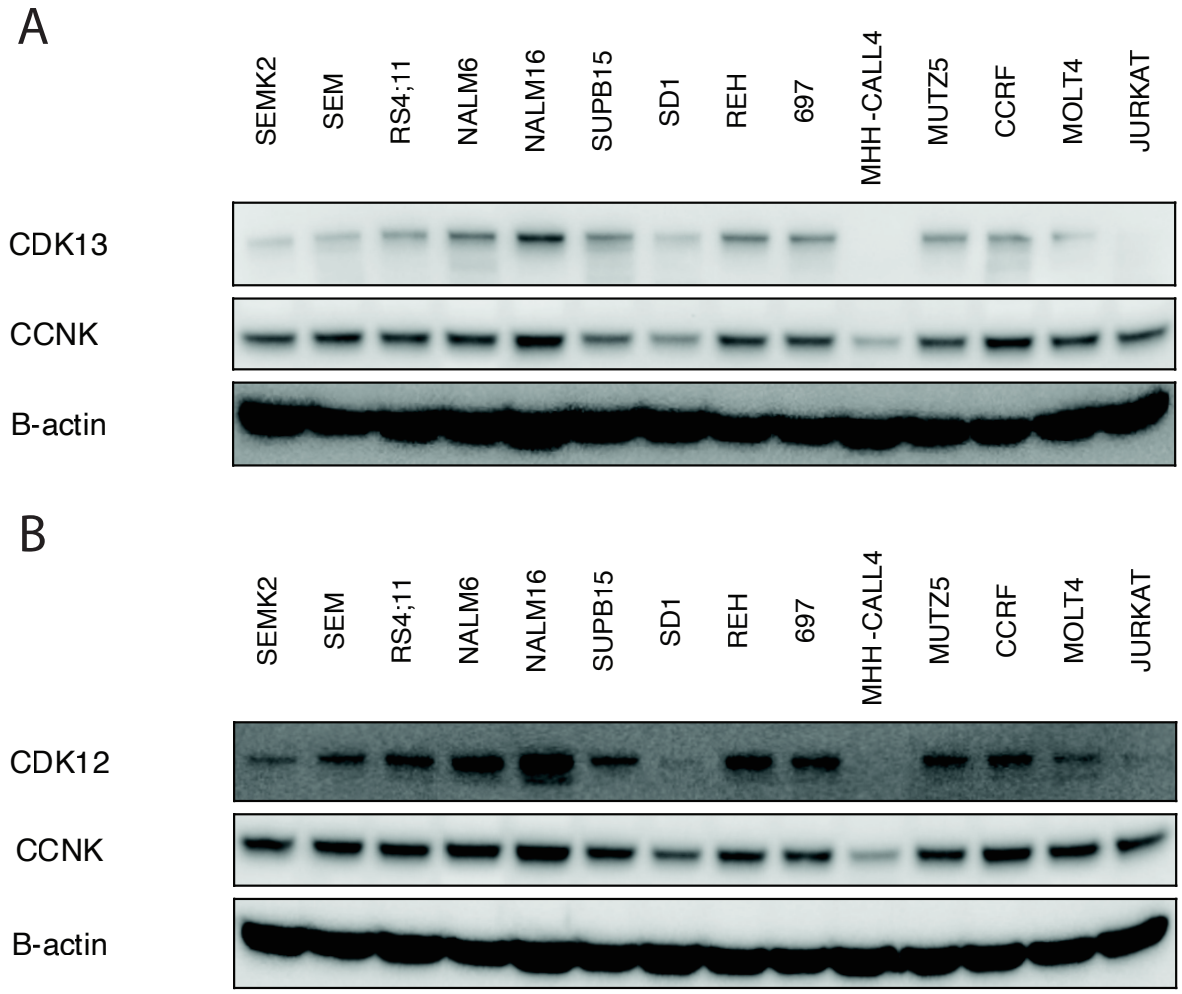

Figure 35. Baseline expression of CDK12, CDK13, and CCNK across ALL cell lines.
(A) Western blot analysis of CDK13 and CCNK protein levels across a panel of 14 ALL cell lines. (B) Western blot analysis of CDK12 and CCNK protein levels in the same cell line panel. Cell lines are ordered (left to right): SEMK2, SEMK, RS4;11, NALM6, NALM16, SUPB15, SD1, REH, 697, MHH-CALL4, MUTZ5, CCRF, MOLT4, and JURKAT. Blots are representative of 3 independent experiments. B-actin was used as a loading control. CDK12, cyclin-dependent kinase 12; CDK13, cyclin-dependent kinase 13; CCNK, cyclin K.

Building upon these baseline observations, the functional consequences of pharmacological CDK12/13 inhibition were subsequently investigated.

In NALM6 cells, acute treatment (3h) with SR4835, either as a single agent or in combination with dexamethasone, resulted in a marked reduction in Pol II C-terminal domain phosphorylation at the Serine 2 position (pSer2), while, consistent with the known function of CDK12/13, Serine 5 phosphorylation (pSer5) and total Pol II levels remained unchanged (Figure 36A). Additionally, a significant decrease in CCNK protein levels was observed following SR4835 exposure, reflecting its established mechanism of action. Total glucocorticoid receptor levels were not altered by any

treatment condition at this time point. Notably, the combination of SR4835 and dexamethasone did not further diminish pSer2 or CCNK levels beyond the effect observed with SR4835 monotherapy, suggesting that the early biochemical inhibition of CDK12/13 is driven primarily by the small molecule inhibitor.

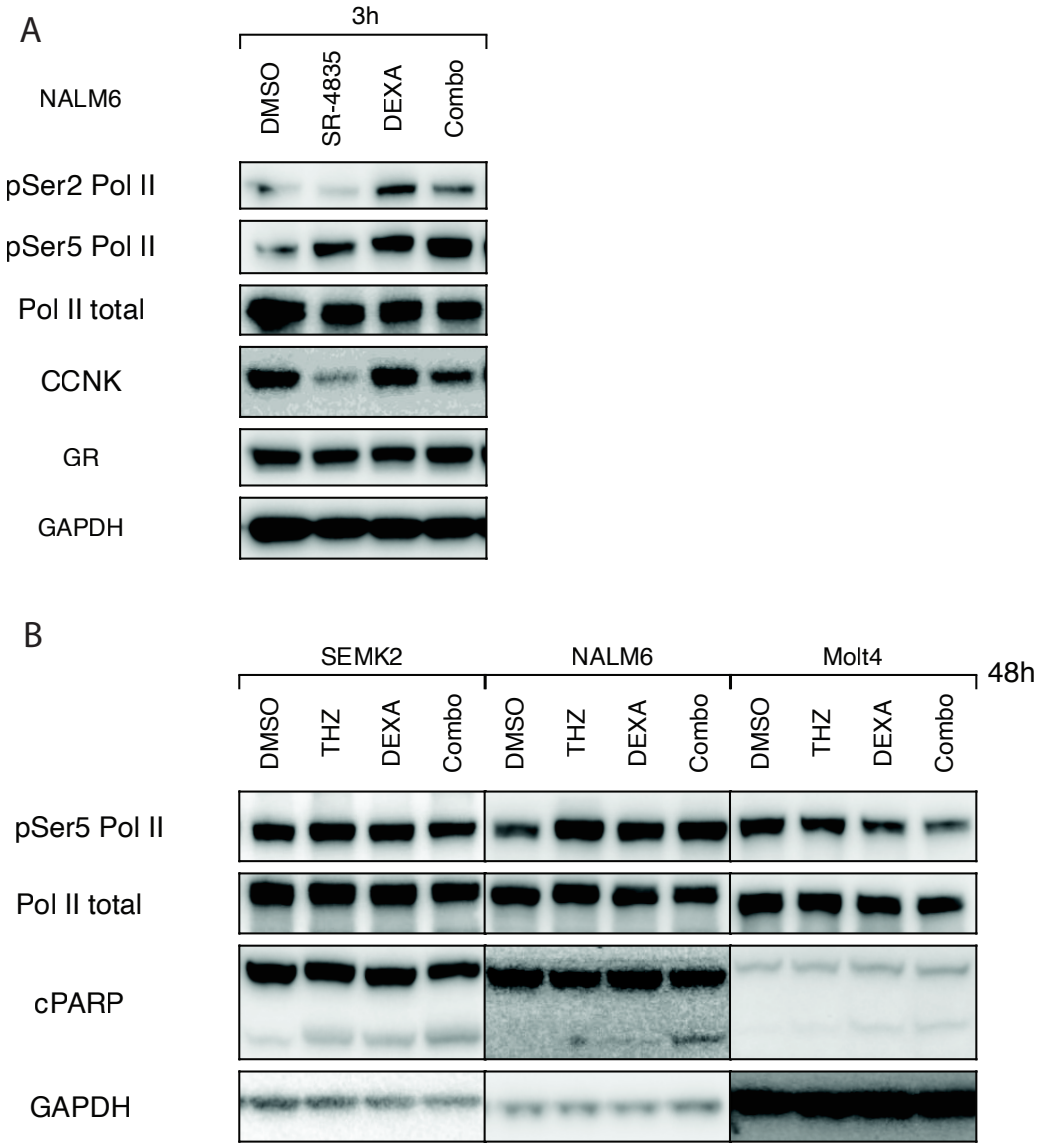

Figure 36. Biochemical inhibition of Pol II and induction of apoptotic markers following combined treatment.
(A) Western blot analysis of NALM6 cells following 3h of treatment with DMSO (control), SR4835, dexamethasone, or the combination. Protein levels of pSer2 Pol II, pSer5 Pol II, total Pol II, CCNK, and total GR were assessed, with GAPDH serving as a loading control. (B) Western blot analysis of SEMK2, NALM6, and MOLT4 cells following 48 h of treatment with DMSO, THZ531, dexamethasone, or the combination. Protein levels of pSer5 Pol II, total Pol II, and cleaved PARP (cPARP) were evaluated, with GAPDH utilized as a loading control.
THZ, THZ531; DEXA, dexamethasone; pSer2, phosphorylated Serine 2; pSer5, phosphorylated Serine 5; GR, glucocorticoid receptor; cPARP, cleaved Poly (ADP-ribose) polymerase.

To assess the long-term molecular consequences of this inhibition across different models, the apoptotic marker cleaved PARP (cPARP) was analyzed after 48 h of

treatment in SEMK2, NALM6, and MOLT4 cells (Figure 36B). Consistent with the early inhibition data, pSer5 and total Pol II levels remained stable. Importantly, a substantial increase in cPARP was detected in the combination treatment groups across all three cell lines, supporting the transition from CDK12/13-mediated transcriptional inhibition to the induction of programmed cell death. In summary, the baseline heterogeneity of CDK12 and CDK13 expression across ALL models provides a molecular context for varying drug sensitivities, while the depletion of pSer2 Pol II and CCNK confirms the potent biochemical activity of SR4835 and THZ531. The subsequent induction of cPARP across multiple cell lines demonstrates that this transcriptional disruption effectively translates into programmed cell death. Collectively, these findings suggest that the observed synergistic interactions with dexamethasone are supported by inhibition of the CDK12/13-mediated transcriptional machinery, thereby sensitizing ALL models to apoptosis.

3.7.4 Assessment of DNA damage via comet assay

To evaluate the extent of total DNA damage (including single- and double-strand breaks) following CDK12/13 inhibition, an alkaline comet assay was performed.

Treatment with SR4835 or THZ531 (130 nM) for 48 h resulted in a significant increase in DNA migration, as quantified by the tail-to-head ratio (%) (Figure 37A). In contrast to the compact, well-defined nuclei observed in DMSO-treated controls, cells treated with CDK12/13 inhibitors exhibited characteristic “comet” formation (Figure 37B). These data indicate that the inhibition of transcriptional kinases CDK12 and CDK13 leads to a marked accumulation of genomic DNA lesions, which likely contributes to the observed synergistic cell death when combined with dexamethasone.

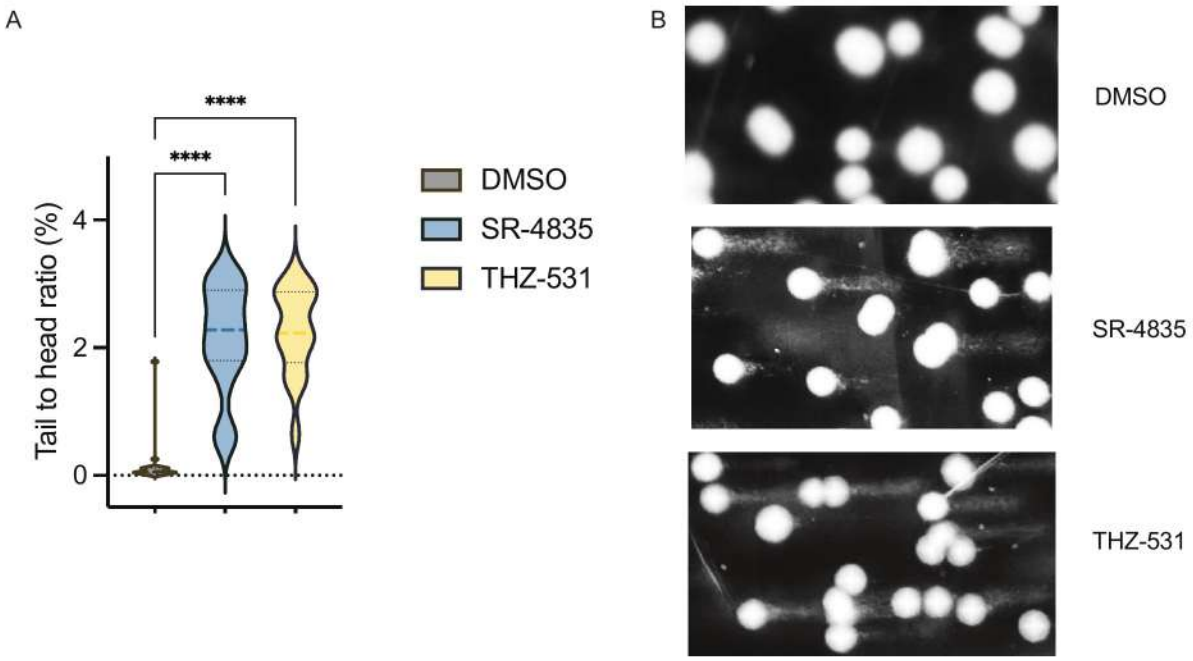

Figure 37. Induction of DNA damage following pharmacological inhibition of CDK12/13.
*(A) Quantitative analysis of DNA damage using the alkaline comet assay. Data represent tail-to-head ratio (%) in SEMK2 cells following 48 h of treatment with DMSO, SR4835 (130 nM), or THZ531 (130 nM). A minimum of 20 comets were analyzed per condition. Statistical significance was assessed by one-way ANOVA with Tukey's multiple comparison test (*p < 0.05, **p < 0.01, ***p < 0.001, ****p < 0.0001). (B) Representative fluorescence microscopy images of comets showing alkaline comet formations. The presence of prominent DNA tails in the SR4835 and THZ531 groups indicates the induction of total DNA strand breaks.*

Chapter 4. Discussion

4.1 Overcoming transcriptional addiction in acute lymphoblastic leukemia

Glucocorticoids have been a mainstay of ALL treatment for over seven decades, providing one of the earliest and most effective antileukemic therapies [175]. A poor initial response to GCs is a strong predictor of treatment failure, correlating with a significantly higher risk of relapsed or refractory disease [176]. The exact mechanisms driving glucocorticoid resistance remain incompletely understood. Resistance may arise from the positive selection of a resistant subclone already present at diagnosis that becomes dominant as GC-sensitive cells are eliminated, or it may evolve dynamically under selective pressure of GC therapy [175,177]. Because glucocorticoid-induced apoptosis relies heavily on the successful execution of a widespread transcriptional program mediated by the glucocorticoid receptor, the study hypothesized that the survival of GC-resistant leukemic blasts relies on the continuous, high-level transcription of pro-survival networks [175]. Consequently, it was proposed that this dependency could be disrupted by targeting the CDK12/CDK13/Cyclin K complex, a master regulator of RNA polymerase II that has been shown to drive oncogenesis across various malignancies, including ovarian and prostate cancers [144,157].

This thesis findings demonstrate that the CDK12/13/CCNK complex is a targetable vulnerability in ALL. Specifically, analysis of gene expression data from the MILE study, validated by immunohistochemical staining of primary patient biopsies, revealed that CDK13 is significantly upregulated in B-ALL blasts compared to healthy bone marrow (Figures 9-12). This overexpression translates into a functional dependency, as evidenced by genome-wide CRISPR/Cas9 and shRNA screens demonstrating that the survival of both B- and T-ALL models rely on the integrity of this complex (Figures 13-16). This dependency has been well documented in other malignancies, including ovarian, prostate, and renal cell carcinomas, underscoring that the dysregulation of the CDK12/13/CCNK complex is a fundamental driver of oncogenesis [141,144,178]. Consequently, pharmacological inhibition of CDK12 and CDK13 with the selective small molecules SR4835 and THZ531 yielded potent, low-micromolar to nanomolar cytotoxicity across a diverse panel of ALL cell lines and

primary patient samples (Figure 20). Crucially, this single-agent activity effectively bypassed intrinsic glucocorticoid resistance, indicating that CDK12/13 inhibition targets survival mechanisms distinct from canonical GR signaling.

4.2 Synergistic potential and the therapeutic window

While the single-agent efficacy of CDK12/13 inhibitors is promising, the most translationally significant finding of this study is the synergistic interaction between CDK12/13 inhibition and dexamethasone. Combinatorial treatment demonstrated positive ZIP synergy scores across a majority of the tested B-ALL models and patient samples, effectively restoring apoptotic sensitivity to the previously refractory SEMK2 cell line (Figure 25). The translational potential of targeting CDK12/13 is supported by recent preclinical studies demonstrating the anticancer effects of SR4835, both with cisplatin in triple-negative breast cancer and in combination with sorafenib in hepatocellular carcinoma [158,179]. Crucially, this study expands on this potential by demonstrating that the synergistic potentiation with dexamethasone is highly selective for malignant cells. The combination of SR4835 or THZ531 with dexamethasone did not yield synergistic cytotoxicity in healthy donor peripheral blood mononuclear cells (Figure 23). This differential response suggests a favorable therapeutic window, likely driven by the heightened baseline reliance of rapidly proliferating leukemic cells on the CDK12/13-mediated transcription of stress-response and DNA repair genes.

4.3 Mechanistic basis of synergy: the transcriptional priming model

To define the molecular underpinnings of this synergy, transcriptomic analyses revealed that CDK12/13 inhibition fundamentally rewires the leukemic intracellular state. Treatment with SR4835 or THZ531 suppressed growth-associated and biosynthetic programs, such as *mTORC1*, *MYC*, and *E2F* targets, while simultaneously downregulating mitochondrial respiratory pathways. More importantly, CDK12/13 inhibition independently triggered a distinct stress-responsive transcriptional program. Transcriptomic analysis revealed a robust induction of immediate early genes such as *FOS*, *JUN*, and *JUNB*, alongside the pro-apoptotic factor *BMF*. This was accompanied by a significant positive enrichment of *FOXO1* target genes (Figures 27-28). Given that *FOXO1* serves as a critical co-activator for the GR in lymphoid tissues, its activation suggests that CDK12/13 inhibition creates a

"primed" intracellular environment [180]. When dexamethasone is introduced to this primed state, the activation threshold for GR-mediated transcription is significantly lowered. This was validated by an observation that canonical GR target genes, including *TSC22D3 (GILZ), ZBTB16, SGK1*, and the pro-apoptotic *BCL2L11 (BIM),* were expressed at significantly higher, additive levels in the combinatorial treatment arms compared to dexamethasone monotherapy (Figure 32). Therefore, the synergy arises not from off-target toxicity, but from the intersection of therapy-induced cellular stress and amplified GR signaling. This mechanism of synergistic cell death aligns with previous studies describing the pro-apoptotic properties of SR4835 in other malignancies [158,179].

4.4 Genomic instability and alternative splicing

Beyond transcriptional priming, the inhibition of CDK12/13 compromised genomic integrity. RNA-seq data highlighted a marked downregulation of DNA repair pathways, including homologous recombination and nucleotide excision repair (Figure 29). Consistent with the established role of CDK12/13 in maintaining the expression of long, complex DNA damage response genes [140], alkaline comet assays confirmed an accumulation of DNA strand breaks in B-ALL cells following pharmacological inhibition. Furthermore, CDK12/13 inhibition altered read distributions and significantly increases alternative splicing events, such as intron retention and exon skipping. The combined burden of an impaired DNA repair machinery, widespread DNA damage, and the accumulation of aberrantly spliced transcripts imposes an unsustainable level of genomic stress, forcing the leukemic cell into the observed G2 cell cycle arrest and apoptosis. These findings align with similar observations reported in other malignancies, such as lung and prostate cancers [181,182], further solidifying the role of CDK12/13 as a critical guardian of genomic stability in cancer.

4.5 Limitations and future directions

While this study provides a strong preclinical rationale for dual CDK12/13 and GR targeting, several limitations must be acknowledged. First, the mechanistic insights were derived primarily from in vitro cell line models. Although the preservation of drug sensitivity in primary patient-derived B-ALL samples support the conclusions, the primary cohort size was small. The high molecular heterogeneity of ALL necessitates

the evaluation of this combination in larger, genetically diverse primary patient cohorts to identify definitive predictive biomarkers of response. In addition, while PBMC cytotoxicity testing might provide insight into the therapeutic window, it would be necessary to validate this in healthy donor CD34+ cord-blood HSPCs. Additionally, the functional consequences of the specific alternative splicing events induced by CDK12/13 inhibition remain to be fully elucidated. Future studies should investigate whether transcripts like aberrantly spliced *DDX3X* undergo nonsense-mediated decay or produce dominant-negative isoforms that actively contribute to leukemic cell death. Additionally, functional rescue experiments using a FOXO1 inhibitor in cells co-treated with SR4835 and dexamethasone are needed to determine if inhibiting FOXO1 reverses the upregulation of GR genes and prevents cell death. Finally, in vivo validation utilizing patient-derived xenograft murine models is the next step to assess the systemic tolerability, pharmacokinetics, and in vivo efficacy of combining SR4835 or THZ531 with standard-of-care induction regimens.

Chapter 5. Conclusions

In summary, this thesis establishes CDK12/13 as a potential therapeutic target in glucocorticoid-resistant B-cell acute lymphoblastic leukemia. By inhibiting DNA repair mechanisms, perturbing RNA splicing, and lowering the threshold for GR-mediated apoptosis, the pharmacological inhibition of CDK12 and CDK13 rewires the resistant leukemic cell. While these findings are compelling, future research incorporating additional dexamethasone-resistant cell lines and in vivo patient-derived xenograft models will be essential to fully validate this approach. Ultimately, the synergistic cell death observed upon combined treatment with dexamethasone provides a mechanistically rational, highly promising therapeutic strategy to overcome chemoresistance and improve clinical outcomes for patients with resistant/refractory ALL.

References

[1] Jaffe ES, Arber DA, Campo E, et al. Hematopathology. 3rd ed. Chantilly: Elsevier; 2024.

[2] Hematology. Elsevier; 2018. https://doi.org/10.1016/C2013-0-23355-9.

[3] Terwilliger T, Abdul-Hay M. Acute lymphoblastic leukemia: a comprehensive review and 2017 update. Blood Cancer J 2017;7:e577–e577. https://doi.org/10.1038/bcj.2017.53.

[4] Alaggio R, Amador C, Anagnostopoulos I, et al. The 5th edition of the World Health Organization Classification of Haematolymphoid Tumours: Lymphoid Neoplasms. Leukemia 2022;36:1720–48. https://doi.org/10.1038/s41375-022-01620-2.

[5] Maitra A, McKenna RW, Weinberg AG, et al. Precursor B-cell lymphoblastic lymphoma. A study of nine cases lacking blood and bone marrow involvement and review of the literature. Am J Clin Pathol 2001;115:868–75. https://doi.org/10.1309/Q5GV-3K00-WAC6-BBUB.

[6] Lin P, Jones D, Dorfman DM, et al. Precursor B-cell lymphoblastic lymphoma: a predominantly extranodal tumor with low propensity for leukemic involvement. Am J Surg Pathol 2000;24:1480–90. https://doi.org/10.1097/00000478-200011000-00003.

[7] PDQ Pediatric Treatment Editorial Board. Childhood Acute Lymphoblastic Leukemia Treatment (PDQ®): Health Professional Version. PDQ Cancer Information Summaries, Bethesda (MD): National Cancer Institute (US); 2002.

[8] Surveillance, Epidemiology, and End Results (SEER) Program, SEER Research Plus Data, 21 Registries, Nov 2023 Sub (2000-2021). U.S. Department of Health and Human Services, National Institutes of Health; 2024.

[9] Silverman LB, Stevenson KE, O'Brien JE, et al. Long-term results of Dana-Farber Cancer Institute ALL Consortium protocols for children with newly diagnosed acute lymphoblastic leukemia (1985–2000). Leukemia 2010;24:320–34. https://doi.org/10.1038/leu.2009.253.

[10] Wellbrock M, Zeeb H, Spix C, et al. Survival in Children Below the Age of 15 Years With Leukemia: Temporal Patterns in Eastern and Western Germany Since German Reunification. HemaSphere 2022;6:e755. https://doi.org/10.1097/HS9.0000000000000755.

[11] Pui C-H, Robison LL, Look AT. Acute lymphoblastic leukaemia. The Lancet 2008;371:1030–43. https://doi.org/10.1016/S0140-6736(08)60457-2.

[12] Cooper SL, Brown PA. Treatment of Pediatric Acute Lymphoblastic Leukemia. Pediatric Clinics of North America 2015;62:61–73. https://doi.org/10.1016/j.pcl.2014.09.006.

[13] Tasian SK, Loh ML, Hunger SP. Childhood acute lymphoblastic leukemia: Integrating genomics into therapy. Cancer 2015;121:3577–90. https://doi.org/10.1002/cncr.29573.

[14] Bienemann K, Burkhardt B, Modlich S, et al. Promising therapy results for lymphoid malignancies in children with chromosomal breakage syndromes (Ataxia teleangiectasia or Nijmegen-breakage syndrome): a retrospective survey. Br J Haematol 2011;155:468–76. https://doi.org/10.1111/j.1365-2141.2011.08863.x.

[15] Kohlmann A, Schoch C, Schnittger S, et al. Pediatric acute lymphoblastic leukemia (ALL) gene expression signatures classify an independent cohort of adult ALL patients. Leukemia 2004;18:63–71. https://doi.org/10.1038/sj.leu.2403167.
[16] Armstrong SA, Look AT. Molecular Genetics of Acute Lymphoblastic Leukemia. JCO 2005;23:6306–15. https://doi.org/10.1200/JCO.2005.05.047.
[17] Schmiegelow K, Lausten Thomsen U, Baruchel A, et al. High concordance of subtypes of childhood acute lymphoblastic leukemia within families: lessons from sibships with multiple cases of leukemia. Leukemia 2012;26:675–81. https://doi.org/10.1038/leu.2011.274.
[18] Williams DL, Tsiatis A, Brodeur GM, et al. Prognostic importance of chromosome number in 136 untreated children with acute lymphoblastic leukemia. Blood 1982;60:864–71.
[19] Raimondi SC. Current status of cytogenetic research in childhood acute lymphoblastic leukemia. Blood 1993;81:2237–51.
[20] Kalwinsky DK, Roberson P, Dahl G, et al. Clinical relevance of lymphoblast biological features in children with acute lymphoblastic leukemia. J Clin Oncol 1985;3:477–84. https://doi.org/10.1200/JCO.1985.3.4.477.
[21] Harris MB, Shuster JJ, Carroll A, et al. Trisomy of leukemic cell chromosomes 4 and 10 identifies children with B-progenitor cell acute lymphoblastic leukemia with a very low risk of treatment failure: a Pediatric Oncology Group study. Blood 1992;79:3316–24.
[22] Heerema NA, Nachman JB, Sather HN, et al. Hypodiploidy with less than 45 chromosomes confers adverse risk in childhood acute lymphoblastic leukemia: a report from the children's cancer group. Blood 1999;94:4036–45.
[23] Mullighan CG. Molecular genetics of B-precursor acute lymphoblastic leukemia. J Clin Invest 2012;122:3407–15. https://doi.org/10.1172/JCI61203.
[24] Holmfeldt L, Wei L, Diaz-Flores E, et al. The genomic landscape of hypodiploid acute lymphoblastic leukemia. Nat Genet 2013;45:242–52. https://doi.org/10.1038/ng.2532.
[25] Mühlbacher V, Zenger M, Schnittger S, et al. Acute lymphoblastic leukemia with low hypodiploid/near triploid karyotype is a specific clinical entity and exhibits a very high TP53 mutation frequency of 93%. Genes Chromosomes Cancer 2014;53:524–36. https://doi.org/10.1002/gcc.22163.
[26] Harrison CJ, Moorman AV, Schwab C, et al. An international study of intrachromosomal amplification of chromosome 21 (iAMP21): cytogenetic characterization and outcome. Leukemia 2014;28:1015–21. https://doi.org/10.1038/leu.2013.317.
[27] Faderl S, Kantarjian HM, Talpaz M, et al. Clinical significance of cytogenetic abnormalities in adult acute lymphoblastic leukemia. Blood 1998;91:3995–4019.
[28] Okuda T, van Deursen J, Hiebert SW, et al. AML1, the target of multiple chromosomal translocations in human leukemia, is essential for normal fetal liver hematopoiesis. Cell 1996;84:321–30. https://doi.org/10.1016/s0092-8674(00)80986-1.
[29] Wang LC, Swat W, Fujiwara Y, et al. The TEL/ETV6 gene is required specifically for hematopoiesis in the bone marrow. Genes Dev 1998;12:2392–402. https://doi.org/10.1101/gad.12.15.2392.

[30] Bernardin F, Yang Y, Cleaves R, et al. TEL-AML1, expressed from t(12;21) in human acute lymphocytic leukemia, induces acute leukemia in mice. Cancer Res 2002;62:3904–8.
[31] Douet-Guilbert N, Morel F, Le Bris MJ, et al. A fluorescence in situ hybridization study of TEL-AML1 fusion gene in B-cell acute lymphoblastic leukemia (1984-2001). Cancer Genet Cytogenet 2003;144:143–7. https://doi.org/10.1016/s0165-4608(02)00932-9.
[32] Borowitz MJ, Rubnitz J, Nash M, et al. Surface antigen phenotype can predict TEL-AML1 rearrangement in childhood B-precursor ALL: a Pediatric Oncology Group study. Leukemia 1998;12:1764–70. https://doi.org/10.1038/sj.leu.2401177.
[33] Zaliova M, Kotrova M, Bresolin S, et al. ETV6/RUNX1-like acute lymphoblastic leukemia: A novel B-cell precursor leukemia subtype associated with the CD27/CD44 immunophenotype. Genes Chromosomes Cancer 2017;56:608–16. https://doi.org/10.1002/gcc.22464.
[34] Schultz KR, Pullen DJ, Sather HN, et al. Risk- and response-based classification of childhood B-precursor acute lymphoblastic leukemia: a combined analysis of prognostic markers from the Pediatric Oncology Group (POG) and Children's Cancer Group (CCG). Blood 2007;109:926–35. https://doi.org/10.1182/blood-2006-01-024729.
[35] Loh ML, Rubnitz JE. TEL/AML1-positive pediatric leukemia: prognostic significance and therapeutic approaches. Curr Opin Hematol 2002;9:345–52. https://doi.org/10.1097/00062752-200207000-00013.
[36] Gale KB, Ford AM, Repp R, et al. Backtracking leukemia to birth: identification of clonotypic gene fusion sequences in neonatal blood spots. Proc Natl Acad Sci U S A 1997;94:13950–4. https://doi.org/10.1073/pnas.94.25.13950.
[37] Faderl S, Kantarjian HM, Talpaz M, et al. Clinical significance of cytogenetic abnormalities in adult acute lymphoblastic leukemia. Blood 1998;91:3995–4019.
[38] Wertheim JA, Miller JP, Xu L, et al. The biology of chronic myelogenous leukemia:mouse models and cell adhesion. Oncogene 2002;21:8612–28. https://doi.org/10.1038/sj.onc.1206089.
[39] Melo JV. The molecular biology of chronic myeloid leukaemia. Leukemia 1996;10:751–6.
[40] Uckun FM, Nachman JB, Sather HN, et al. Clinical significance of Philadelphia chromosome positive pediatric acute lymphoblastic leukemia in the context of contemporary intensive therapies: a report from the Children's Cancer Group. Cancer 1998;83:2030–9.
[41] Aricò M, Valsecchi MG, Camitta B, et al. Outcome of treatment in children with Philadelphia chromosome-positive acute lymphoblastic leukemia. N Engl J Med 2000;342:998–1006. https://doi.org/10.1056/NEJM200004063421402.
[42] Wetzler M, Dodge RK, Mrózek K, et al. Prospective karyotype analysis in adult acute lymphoblastic leukemia: the cancer and leukemia Group B experience. Blood 1999;93:3983–93.
[43] Schultz KR, Carroll A, Heerema NA, et al. Long-term follow-up of imatinib in pediatric Philadelphia chromosome-positive acute lymphoblastic leukemia: Children's Oncology Group study AALL0031. Leukemia 2014;28:1467–71. https://doi.org/10.1038/leu.2014.30.

[44] Hovorkova L, Zaliova M, Venn NC, et al. Monitoring of childhood ALL using BCR-ABL1 genomic breakpoints identifies a subgroup with CML-like biology. Blood 2017;129:2771–81. https://doi.org/10.1182/blood-2016-11-749978.
[45] Den Boer ML, van Slegtenhorst M, De Menezes RX, et al. A subtype of childhood acute lymphoblastic leukaemia with poor treatment outcome: a genome-wide classification study. Lancet Oncol 2009;10:125–34. https://doi.org/10.1016/S1470-2045(08)70339-5.
[46] Roberts KG, Li Y, Payne-Turner D, et al. Targetable kinase-activating lesions in Ph-like acute lymphoblastic leukemia. N Engl J Med 2014;371:1005–15. https://doi.org/10.1056/NEJMoa1403088.
[47] Behm FG, Raimondi SC, Frestedt JL, et al. Rearrangement of the MLL gene confers a poor prognosis in childhood acute lymphoblastic leukemia, regardless of presenting age. Blood 1996;87:2870–7.
[48] Parkin JL, Arthur DC, Abramson CS, et al. Acute leukemia associated with the t(4;11) chromosome rearrangement: ultrastructural and immunologic characteristics. Blood 1982;60:1321–31.
[49] Pui CH, Rubnitz JE, Hancock ML, et al. Reappraisal of the clinical and biologic significance of myeloid-associated antigen expression in childhood acute lymphoblastic leukemia. J Clin Oncol 1998;16:3768–73. https://doi.org/10.1200/JCO.1998.16.12.3768.
[50] Borowitz MJ, Hunger SP, Carroll AJ, et al. Predictability of the t(1;19)(q23;p13) from surface antigen phenotype: implications for screening cases of childhood acute lymphoblastic leukemia for molecular analysis: a Pediatric Oncology Group study. Blood 1993;82:1086–91.
[51] Rivera GK, Raimondi SC, Hancock ML, et al. Improved outcome in childhood acute lymphoblastic leukaemia with reinforced early treatment and rotational combination chemotherapy. Lancet 1991;337:61–6. https://doi.org/10.1016/0140-6736(91)90733-6.
[52] Pui CH, Raimondi SC, Hancock ML, et al. Immunologic, cytogenetic, and clinical characterization of childhood acute lymphoblastic leukemia with the t(1;19) (q23; p13) or its derivative. J Clin Oncol 1994;12:2601–6. https://doi.org/10.1200/JCO.1994.12.12.2601.
[53] Hogan TF, Koss W, Murgo AJ, et al. Acute lymphoblastic leukemia with chromosomal 5;14 translocation and hypereosinophilia: case report and literature review. J Clin Oncol 1987;5:382–90. https://doi.org/10.1200/JCO.1987.5.3.382.
[54] Grimaldi JC, Meeker TC. The t(5;14) chromosomal translocation in a case of acute lymphocytic leukemia joins the interleukin-3 gene to the immunoglobulin heavy chain gene. Blood 1989;73:2081–5.
[55] Wilson F, Tefferi A. Acute lymphocytic leukemia with eosinophilia: two case reports and a literature review. Leuk Lymphoma 2005;46:1045–50. https://doi.org/10.1080/10428190500085537.
[56] Schinnerl D, Mejstrikova E, Schumich A, et al. CD371 cell surface expression: a unique feature of DUX4-rearranged acute lymphoblastic leukemia. Haematologica 2019;104:e352–5. https://doi.org/10.3324/haematol.2018.214353.
[57] Alexander TB, Gu Z, Iacobucci I, et al. The genetic basis and cell of origin of mixed phenotype acute leukaemia. Nature 2018;562:373–9. https://doi.org/10.1038/s41586-018-0436-0.

[58] Shago M, Abla O, Hitzler J, et al. Frequency and outcome of pediatric acute lymphoblastic leukemia with ZNF384 gene rearrangements including a novel translocation resulting in an ARID1B/ZNF384 gene fusion. Pediatr Blood Cancer 2016;63:1915–21. https://doi.org/10.1002/pbc.26116.
[59] Gu Z, Churchman M, Roberts K, et al. Genomic analyses identify recurrent MEF2D fusions in acute lymphoblastic leukaemia. Nat Commun 2016;7:13331. https://doi.org/10.1038/ncomms13331.
[60] Wagener R, López C, Kleinheinz K, et al. IG-MYC + neoplasms with precursor B-cell phenotype are molecularly distinct from Burkitt lymphomas. Blood 2018;132:2280–5. https://doi.org/10.1182/blood-2018-03-842088.
[61] Brady SW, Roberts KG, Gu Z, et al. The genomic landscape of pediatric acute lymphoblastic leukemia. Nat Genet 2022;54:1376–89. https://doi.org/10.1038/s41588-022-01159-z.
[62] Raimondi SC, Behm FG, Roberson PK, et al. Cytogenetics of childhood T-cell leukemia. Blood 1988;72:1560–6.
[63] Ferrando AA, Neuberg DS, Staunton J, et al. Gene expression signatures define novel oncogenic pathways in T cell acute lymphoblastic leukemia. Cancer Cell 2002;1:75–87. https://doi.org/10.1016/s1535-6108(02)00018-1.
[64] Zhang J, Ding L, Holmfeldt L, et al. The genetic basis of early T-cell precursor acute lymphoblastic leukaemia. Nature 2012;481:157–63. https://doi.org/10.1038/nature10725.
[65] Neumann M, Coskun E, Fransecky L, et al. FLT3 mutations in early T-cell precursor ALL characterize a stem cell like leukemia and imply the clinical use of tyrosine kinase inhibitors. PLoS One 2013;8:e53190. https://doi.org/10.1371/journal.pone.0053190.
[66] Fang H, Wang W, El Hussein S, et al. B-cell lymphoma/leukaemia 11B (BCL11B) expression status helps distinguish early T-cell precursor acute lymphoblastic leukaemia/lymphoma (ETP-ALL/LBL) from other subtypes of T-cell ALL/LBL. Br J Haematol 2021;194:1034–8. https://doi.org/10.1111/bjh.17681.
[67] Montefiori LE, Bendig S, Gu Z, et al. Enhancer Hijacking Drives Oncogenic BCL11B Expression in Lineage-Ambiguous Stem Cell Leukemia. Cancer Discov 2021;11:2846–67. https://doi.org/10.1158/2159-8290.CD-21-0145.
[68] Di Giacomo D, La Starza R, Gorello P, et al. 14q32 rearrangements deregulating BCL11B mark a distinct subgroup of T-lymphoid and myeloid immature acute leukemia. Blood 2021;138:773–84. https://doi.org/10.1182/blood.2020010510.
[69] Weng AP, Ferrando AA, Lee W, et al. Activating mutations of NOTCH1 in human T cell acute lymphoblastic leukemia. Science 2004;306:269–71. https://doi.org/10.1126/science.1102160.
[70] Belver L, Ferrando A. The genetics and mechanisms of T cell acute lymphoblastic leukaemia. Nat Rev Cancer 2016;16:494–507. https://doi.org/10.1038/nrc.2016.63.
[71] Pagliaro L, Chen S-J, Herranz D, et al. Acute lymphoblastic leukaemia. Nat Rev Dis Primers 2024;10:41. https://doi.org/10.1038/s41572-024-00525-x.
[72] Brown P, Inaba H, Annesley C, et al. Pediatric Acute Lymphoblastic Leukemia, Version 2.2020, NCCN Clinical Practice Guidelines in Oncology. Journal of the National Comprehensive Cancer Network 2020;18:81–112. https://doi.org/10.6004/jnccn.2020.0001.

[73] Inaba H, Mullighan CG. Pediatric acute lymphoblastic leukemia. Haematol 2020;105:2524–39. https://doi.org/10.3324/haematol.2020.247031.
[74] Berry DA, Zhou S, Higley H, et al. Association of Minimal Residual Disease With Clinical Outcome in Pediatric and Adult Acute Lymphoblastic Leukemia: A Meta-analysis. JAMA Oncol 2017;3:e170580. https://doi.org/10.1001/jamaoncol.2017.0580.
[75] Bergeron BP, Diedrich JD, Zhang Y, et al. Epigenomic profiling of glucocorticoid responses identifies cis-regulatory disruptions impacting steroid resistance in childhood acute lymphoblastic leukemia. Leukemia 2022;36:2374–83. https://doi.org/10.1038/s41375-022-01685-z.
[76] Bhadri VA, Trahair TN, Lock RB. Glucocorticoid resistance in paediatric acute lymphoblastic leukaemia. J Paediatrics Child Health 2012;48:634–40. https://doi.org/10.1111/j.1440-1754.2011.02212.x.
[77] Den Boer ML, Harms DO, Pieters R, et al. Patient Stratification Based on Prednisolone-Vincristine-Asparaginase Resistance Profiles in Children With Acute Lymphoblastic Leukemia. JCO 2003;21:3262–8. https://doi.org/10.1200/JCO.2003.11.031.
[78] Kaspers GJ, Veerman AJ, Pieters R, et al. In vitro cellular drug resistance and prognosis in newly diagnosed childhood acute lymphoblastic leukemia. Blood 1997;90:2723–9.
[79] Pieters R, Huismans DR, Loonen AH, et al. Relation of cellular drug resistance to long-term clinical outcome in childhood acute lymphoblastic leukaemia. The Lancet 1991;338:399–403. https://doi.org/10.1016/0140-6736(91)91029-T.
[80] Dördelmann M, Reiter A, Borkhardt A, et al. Prednisone response is the strongest predictor of treatment outcome in infant acute lymphoblastic leukemia. Blood 1999;94:1209–17.
[81] Hunger SP, Mullighan CG. Acute Lymphoblastic Leukemia in Children. N Engl J Med 2015;373:1541–52. https://doi.org/10.1056/NEJMra1400972.
[82] Pui C-H. Genomic and pharmacogenetic studies of childhood acute lymphoblastic leukemia. Front Med 2015;9:1–9. https://doi.org/10.1007/s11684-015-0381-3.
[83] Holleman A, Cheok MH, Den Boer ML, et al. Gene-Expression Patterns in Drug-Resistant Acute Lymphoblastic Leukemia Cells and Response to Treatment. N Engl J Med 2004;351:533–42. https://doi.org/10.1056/NEJMoa033513.
[84] Bhojwani D, Pui C-H. Relapsed childhood acute lymphoblastic leukaemia. The Lancet Oncology 2013;14:e205–17. https://doi.org/10.1016/S1470-2045(12)70580-6.
[85] Choi J, Ceribelli M, Phelan JD, et al. Molecular targets of glucocorticoids that elucidate their therapeutic efficacy in aggressive lymphomas. Cancer Cell 2024;42:833-849.e12. https://doi.org/10.1016/j.ccell.2024.04.007.
[86] Weikum ER, Knuesel MT, Ortlund EA, et al. Glucocorticoid receptor control of transcription: precision and plasticity via allostery. Nat Rev Mol Cell Biol 2017;18:159–74. https://doi.org/10.1038/nrm.2016.152.
[87] Laane E, Panaretakis T, Pokrovskaja K, et al. Dexamethasone-induced apoptosis in acute lymphoblastic leukemia involves differential regulation of Bcl-2 family members. Haematologica 2007;92:1460–9. https://doi.org/10.3324/haematol.10543.

[88] Jing D, Bhadri VA, Beck D, et al. Opposing regulation of BIM and BCL2 controls glucocorticoid-induced apoptosis of pediatric acute lymphoblastic leukemia cells. Blood 2015;125:273–83. https://doi.org/10.1182/blood-2014-05-576470.
[89] Tamai M, Kasai S, Akahane K, et al. Glucocorticoid receptor gene mutations confer glucocorticoid resistance in B-cell precursor acute lymphoblastic leukemia. The Journal of Steroid Biochemistry and Molecular Biology 2022;218:106068. https://doi.org/10.1016/j.jsbmb.2022.106068.
[90] Buentke E, Nordström A, Lin H, et al. Glucocorticoid-induced cell death is mediated through reduced glucose metabolism in lymphoid leukemia cells. Blood Cancer Journal 2011;1:e31–e31. https://doi.org/10.1038/bcj.2011.27.
[91] Dyczynski M, Vesterlund M, Björklund A-C, et al. Metabolic reprogramming of acute lymphoblastic leukemia cells in response to glucocorticoid treatment. Cell Death Dis 2018;9:846. https://doi.org/10.1038/s41419-018-0625-7.
[92] Kruth KA, Fang M, Shelton DN, et al. Suppression of B-cell development genes is key to glucocorticoid efficacy in treatment of acute lymphoblastic leukemia. Blood 2017;129:3000–8. https://doi.org/10.1182/blood-2017-02-766204.
[93] Autry RJ, Paugh SW, Carter R, et al. Integrative genomic analyses reveal mechanisms of glucocorticoid resistance in acute lymphoblastic leukemia. Nat Cancer 2020;1:329–44. https://doi.org/10.1038/s43018-020-0037-3.
[94] López-Maury L, Marguerat S, Bähler J. Tuning gene expression to changing environments: from rapid responses to evolutionary adaptation. Nat Rev Genet 2008;9:583–93. https://doi.org/10.1038/nrg2398.
[95] Kohoutek J, Blazek D. Cyclin K goes with Cdk12 and Cdk13. Cell Div 2012;7:12. https://doi.org/10.1186/1747-1028-7-12.
[96] Marqués F, Moreau J-L, Peaucellier G, et al. A New Subfamily of High Molecular Mass CDC2-Related Kinases with PITAI/VRE Motifs. Biochemical and Biophysical Research Communications 2000;279:832–7. https://doi.org/10.1006/bbrc.2000.4042.
[97] Pellarin I, Dall'Acqua A, Favero A, et al. Cyclin-dependent protein kinases and cell cycle regulation in biology and disease. Sig Transduct Target Ther 2025;10:11. https://doi.org/10.1038/s41392-024-02080-z.
[98] Modi V, Dunbrack RL. A Structurally-Validated Multiple Sequence Alignment of 497 Human Protein Kinase Domains. Sci Rep 2019;9:19790. https://doi.org/10.1038/s41598-019-56499-4.
[99] Malumbres M. Cyclin-dependent kinases. Genome Biol 2014;15:122. https://doi.org/10.1186/gb4184.
[100] Blazek D, Kohoutek J, Bartholomeeusen K, et al. The Cyclin K/Cdk12 complex maintains genomic stability via regulation of expression of DNA damage response genes. Genes Dev 2011;25:2158–72. https://doi.org/10.1101/gad.16962311.
[101] Greenleaf AL. Human CDK12 and CDK13, multi-tasking CTD kinases for the new millenium. Transcription 2019;10:91–110. https://doi.org/10.1080/21541264.2018.1535211.
[102] Greifenberg AK, Hönig D, Pilarova K, et al. Structural and Functional Analysis of the Cdk13/Cyclin K Complex. Cell Reports 2016;14:320–31. https://doi.org/10.1016/j.celrep.2015.12.025.
[103] Hahn S, Young ET. Transcriptional Regulation in *Saccharomyces cerevisiae* : Transcription Factor Regulation and Function, Mechanisms of Initiation, and Roles

of Activators and Coactivators. Genetics 2011;189:705–36. https://doi.org/10.1534/genetics.111.127019.
[104] Payne JM, Laybourn PJ, Dahmus ME. The transition of RNA polymerase II from initiation to elongation is associated with phosphorylation of the carboxyl-terminal domain of subunit IIa. J Biol Chem 1989;264:19621–9.
[105] Adelman K, Lis JT. Promoter-proximal pausing of RNA polymerase II: emerging roles in metazoans. Nat Rev Genet 2012;13:720–31. https://doi.org/10.1038/nrg3293.
[106] Choi H, Jin S, Cho H, et al. CDK 12 drives breast tumor initiation and trastuzumab resistance via WNT and IRS 1-ErbB- PI 3K signaling. EMBO Reports 2019;20:e48058. https://doi.org/10.15252/embr.201948058.
[107] Choi SH, Martinez TF, Kim S, et al. CDK12 phosphorylates 4E-BP1 to enable mTORC1-dependent translation and mitotic genome stability. Genes Dev 2019;33:418–35. https://doi.org/10.1101/gad.322339.118.
[108] Chirackal Manavalan AP, Pilarova K, Kluge M, et al. CDK12 controls G1/S progression by regulating RNAPII processivity at core DNA replication genes. EMBO Reports 2019;20:e47592. https://doi.org/10.15252/embr.201847592.
[109] Lei T, Zhang P, Zhang X, et al. Cyclin K regulates prereplicative complex assembly to promote mammalian cell proliferation. Nat Commun 2018;9:1876. https://doi.org/10.1038/s41467-018-04258-w.
[110] Liu H, Liu K, Dong Z. Targeting CDK12 for Cancer Therapy: Function, Mechanism, and Drug Discovery. Cancer Research 2021;81:18–26. https://doi.org/10.1158/0008-5472.CAN-20-2245.
[111] Liu S, Wu J, Lu X, et al. Targeting CDK12 obviates the malignant phenotypes of colorectal cancer through the Wnt/β-catenin signaling pathway. Experimental Cell Research 2023:113613. https://doi.org/10.1016/j.yexcr.2023.113613.
[112] Wang Z, Himanen SV, Haikala HM, et al. Inhibition of CDK12 elevates cancer cell dependence on P-TEFb by stimulation of RNA polymerase II pause release. Nucleic Acids Research 2023;51:10970–91. https://doi.org/10.1093/nar/gkad792.
[113] Liu H, Shin SH, Chen H, et al. CDK12 and PAK2 as novel therapeutic targets for human gastric cancer. Theranostics 2020;10:6201–15. https://doi.org/10.7150/thno.46137.
[114] Houles T, Lavoie G, Nourreddine S, et al. CDK12 is hyperactivated and a synthetic-lethal target in BRAF-mutated melanoma. Nat Commun 2022;13:6457. https://doi.org/10.1038/s41467-022-34179-8.
[115] Dubbury SJ, Boutz PL, Sharp PA. CDK12 regulates DNA repair genes by suppressing intronic polyadenylation. Nature 2018;564:141–5. https://doi.org/10.1038/s41586-018-0758-y.
[116] Tien JF, Mazloomian A, Cheng S-WG, et al. CDK12 regulates alternative last exon mRNA splicing and promotes breast cancer cell invasion. Nucleic Acids Research 2017;45:6698–716. https://doi.org/10.1093/nar/gkx187.
[117] Pitolli C, Marini A, Guerra M, et al. MYC up-regulation confers vulnerability to dual inhibition of CDK12 and CDK13 in high-risk Group 3 medulloblastoma. J Exp Clin Cancer Res 2023;42:214. https://doi.org/10.1186/s13046-023-02790-2.
[118] Tadesse S, Duckett DR, Monastyrskyi A. The promise and current status of CDK12/13 inhibition for the treatment of cancer. Future Medicinal Chemistry 2021;13:117–41. https://doi.org/10.4155/fmc-2020-0240.

[119] Harlen KM, Churchman LS. The code and beyond: transcription regulation by the RNA polymerase II carboxy-terminal domain. Nat Rev Mol Cell Biol 2017;18:263–73. https://doi.org/10.1038/nrm.2017.10.
[120] Buratowski S. Progression through the RNA Polymerase II CTD Cycle. Molecular Cell 2009;36:541–6. https://doi.org/10.1016/j.molcel.2009.10.019.
[121] Fan Z, Devlin JR, Hogg SJ, et al. CDK13 cooperates with CDK12 to control global RNA polymerase II processivity. Sci Adv 2020;6:eaaz5041. https://doi.org/10.1126/sciadv.aaz5041.
[122] Lu H, Flores O, Weinmann R, et al. The nonphosphorylated form of RNA polymerase II preferentially associates with the preinitiation complex. Proc Natl Acad Sci U S A 1991;88:10004–8. https://doi.org/10.1073/pnas.88.22.10004.
[123] Robinson PJ, Trnka MJ, Bushnell DA, et al. Structure of a Complete Mediator-RNA Polymerase II Pre-Initiation Complex. Cell 2016;166:1411-1422.e16. https://doi.org/10.1016/j.cell.2016.08.050.
[124] Mayer A, Landry HM, Churchman LS. Pause & go: from the discovery of RNA polymerase pausing to its functional implications. Current Opinion in Cell Biology 2017;46:72–80. https://doi.org/10.1016/j.ceb.2017.03.002.
[125] Mayer A, di Iulio J, Maleri S, et al. Native elongating transcript sequencing reveals human transcriptional activity at nucleotide resolution. Cell 2015;161:541–54. https://doi.org/10.1016/j.cell.2015.03.010.
[126] Komarnitsky P, Cho EJ, Buratowski S. Different phosphorylated forms of RNA polymerase II and associated mRNA processing factors during transcription. Genes Dev 2000;14:2452–60. https://doi.org/10.1101/gad.824700.
[127] Schroeder SC, Schwer B, Shuman S, et al. Dynamic association of capping enzymes with transcribing RNA polymerase II. Genes Dev 2000;14:2435–40. https://doi.org/10.1101/gad.836300.
[128] Yu M, Yang W, Ni T, et al. RNA polymerase II–associated factor 1 regulates the release and phosphorylation of paused RNA polymerase II. Science 2015;350:1383–6. https://doi.org/10.1126/science.aad2338.
[129] Qiu M, Yin Z, Wang H, et al. CDK12 and Integrator-PP2A complex modulates LEO1 phosphorylation for processive transcription elongation. Sci Adv 2023;9:eadf8698. https://doi.org/10.1126/sciadv.adf8698.
[130] Curti L, Rohban S, Bianchi N, et al. CDK12 controls transcription at damaged genes and prevents MYC-induced transcription-replication conflicts. Nat Commun 2024;15:7100. https://doi.org/10.1038/s41467-024-51229-5.
[131] Oesterreich FC, Herzel L, Straube K, et al. Splicing of Nascent RNA Coincides with Intron Exit from RNA Polymerase II. Cell 2016;165:372–81. https://doi.org/10.1016/j.cell.2016.02.045.
[132] Braunschweig U, Gueroussov S, Plocik AM, et al. Dynamic Integration of Splicing within Gene Regulatory Pathways. Cell 2013;152:1252–69. https://doi.org/10.1016/j.cell.2013.02.034.
[133] Ko TK, Kelly E, Pines J. CrkRS: a novel conserved Cdc2-related protein kinase that colocalises with SC35 speckles. Journal of Cell Science 2001;114:2591–603. https://doi.org/10.1242/jcs.114.14.2591.
[134] Berro R, Pedati C, Kehn-Hall K, et al. CDK13, a New Potential Human Immunodeficiency Virus Type 1 Inhibitory Factor Regulating Viral mRNA Splicing. J Virol 2008;82:7155–66. https://doi.org/10.1128/JVI.02543-07.

[135] Eifler TT, Shao W, Bartholomeeusen K, et al. Cyclin-Dependent Kinase 12 Increases 3' End Processing of Growth Factor-Induced c-FOS Transcripts. Molecular and Cellular Biology 2015;35:468–78. https://doi.org/10.1128/MCB.01157-14.
[136] Liang K, Gao X, Gilmore JM, et al. Characterization of Human Cyclin-Dependent Kinase 12 (CDK12) and CDK13 Complexes in C-Terminal Domain Phosphorylation, Gene Transcription, and RNA Processing. Molecular and Cellular Biology 2015;35:928–38. https://doi.org/10.1128/MCB.01426-14.
[137] Panzeri V, Pieraccioli M, Cesari E, et al. CDK12/13 promote splicing of proximal introns by enhancing the interaction between RNA polymerase II and the splicing factor SF3B1. Nucleic Acids Research 2023;51:5512–26. https://doi.org/10.1093/nar/gkad258.
[138] Saldi T, Cortazar MA, Sheridan RM, et al. Coupling of RNA Polymerase II Transcription Elongation with Pre-mRNA Splicing. J Mol Biol 2016;428:2623–35. https://doi.org/10.1016/j.jmb.2016.04.017.
[139] Davidson L, Muniz L, West S. 3' end formation of pre-mRNA and phosphorylation of Ser2 on the RNA polymerase II CTD are reciprocally coupled in human cells. Genes Dev 2014;28:342–56. https://doi.org/10.1101/gad.231274.113.
[140] Krajewska M, Dries R, Grassetti AV, et al. CDK12 loss in cancer cells affects DNA damage response genes through premature cleavage and polyadenylation. Nat Commun 2019;10:1757. https://doi.org/10.1038/s41467-019-09703-y.
[141] Insco ML, Abraham BJ, Dubbury SJ, et al. Oncogenic *CDK13* mutations impede nuclear RNA surveillance. Science 2023;380:eabn7625. https://doi.org/10.1126/science.abn7625.
[142] Tullius TW, Isaac RS, Dubocanin D, et al. RNA polymerases reshape chromatin architecture and couple transcription on individual fibers. Molecular Cell 2024;84:3209-3222.e5. https://doi.org/10.1016/j.molcel.2024.08.013.
[143] Chu C, Geng Y, Zhou Y, et al. Cyclin E in normal physiology and disease states. Trends in Cell Biology 2021;31:732–46. https://doi.org/10.1016/j.tcb.2021.05.001.
[144] Popova T, Manié E, Boeva V, et al. Ovarian Cancers Harboring Inactivating Mutations in *CDK12* Display a Distinct Genomic Instability Pattern Characterized by Large Tandem Duplications. Cancer Research 2016;76:1882–91. https://doi.org/10.1158/0008-5472.CAN-15-2128.
[145] Juan H-C, Lin Y, Chen H-R, et al. Cdk12 is essential for embryonic development and the maintenance of genomic stability. Cell Death Differ 2016;23:1038–48. https://doi.org/10.1038/cdd.2015.157.
[146] Chen H-R, Juan H-C, Wong Y-H, et al. Cdk12 Regulates Neurogenesis and Late-Arising Neuronal Migration in the Developing Cerebral Cortex. Cereb Cortex 2016:bhw081. https://doi.org/10.1093/cercor/bhw081.
[147] Dai Q, Lei T, Zhao C, et al. Cyclin K-containing Kinase Complexes Maintain Self-renewal in Murine Embryonic Stem Cells. Journal of Biological Chemistry 2012;287:25344–52. https://doi.org/10.1074/jbc.M111.321760.
[148] Hamilton MJ, Caswell RC, Canham N, et al. Heterozygous mutations affecting the protein kinase domain of *CDK13* cause a syndromic form of developmental delay and intellectual disability. J Med Genet 2018;55:28–38. https://doi.org/10.1136/jmedgenet-2017-104620.

[149] Pitolli C, Marini A, Sette C, et al. Physiological and pathological roles of the transcriptional kinases CDK12 and CDK13 in the central nervous system. Cell Death Differ 2024. https://doi.org/10.1038/s41418-024-01413-3.
[150] Townsend LN, Clarke H, Maddison D, et al. Cdk12 maintains the integrity of adult axons by suppressing actin remodeling. Cell Death Discov 2023;9:348. https://doi.org/10.1038/s41420-023-01642-4.
[151] Pan L, Xie W, Li K-L, et al. Heterochromatin remodeling by CDK12 contributes to learning in *Drosophila*. Proc Natl Acad Sci USA 2015;112:13988–93. https://doi.org/10.1073/pnas.1502943112.
[152] Rodrigues F, Thuma L, Klämbt C. The regulation of glial-specific splicing of *Neurexin IV* requires HOW and Cdk12 activity. Development 2012;139:1765–76. https://doi.org/10.1242/dev.074070.
[153] Bradner JE, Hnisz D, Young RA. Transcriptional Addiction in Cancer. Cell 2017;168:629–43. https://doi.org/10.1016/j.cell.2016.12.013.
[154] Cesari E, Ciucci A, Pieraccioli M, et al. Dual inhibition of CDK12 and CDK13 uncovers actionable vulnerabilities in patient-derived ovarian cancer organoids. J Exp Clin Cancer Res 2023;42:126. https://doi.org/10.1186/s13046-023-02682-5.
[155] Lui GYL, Grandori C, Kemp CJ. CDK12: an emerging therapeutic target for cancer. J Clin Pathol 2018;71:957–62. https://doi.org/10.1136/jclinpath-2018-205356.
[156] Iniguez AB, Stolte B, Wang EJ, et al. EWS/FLI Confers Tumor Cell Synthetic Lethality to CDK12 Inhibition in Ewing Sarcoma. Cancer Cell 2018;33:202-216.e6. https://doi.org/10.1016/j.ccell.2017.12.009.
[157] Wu Y-M, Cieślik M, Lonigro RJ, et al. Inactivation of CDK12 Delineates a Distinct Immunogenic Class of Advanced Prostate Cancer. Cell 2018;173:1770-1782.e14. https://doi.org/10.1016/j.cell.2018.04.034.
[158] Quereda V, Bayle S, Vena F, et al. Therapeutic Targeting of CDK12/CDK13 in Triple-Negative Breast Cancer. Cancer Cell 2019;36:545-558.e7. https://doi.org/10.1016/j.ccell.2019.09.004.
[159] Bajrami I, Frankum JR, Konde A, et al. Genome-wide Profiling of Genetic Synthetic Lethality Identifies CDK12 as a Novel Determinant of PARP1/2 Inhibitor Sensitivity. Cancer Research 2014;74:287–97. https://doi.org/10.1158/0008-5472.CAN-13-2541.
[160] Frank S, Persse T, Coleman I, et al. Molecular consequences of acute versus chronic CDK12 loss in prostate carcinoma nominates distinct therapeutic strategies 2025. https://doi.org/10.7554/eLife.100081.2.
[161] Nguyen CB, Reimers MA, Perera C, et al. Evaluating Immune Checkpoint Blockade in Metastatic Castration-Resistant Prostate Cancers with Deleterious *CDK12* Alterations in the Phase 2 IMPACT Trial. Clinical Cancer Research 2024;30:3200–10. https://doi.org/10.1158/1078-0432.CCR-24-0400.
[162] Larsen TV, Maansson CT, Daugaard TF, et al. Trans-Regulation of Alternative PD-L1 mRNA Processing by CDK12 in Non-Small-Cell Lung Cancer Cells. Cells 2023;12:2844. https://doi.org/10.3390/cells12242844.
[163] Li T, Chen ZJ. The cGAS–cGAMP–STING pathway connects DNA damage to inflammation, senescence, and cancer. J Exp Med 2018;215:1287–99. https://doi.org/10.1084/jem.20180139.

[164] Bao Y, Chang Y, Tien JC-Y, et al. CDK12/13 inactivation triggers STING-mediated antitumor immunity in preclinical models. J Clin Invest 2025;135. https://doi.org/10.1172/JCI193745.
[165] Fan Z, Devlin JR, Hogg SJ, et al. CDK13 cooperates with CDK12 to control global RNA polymerase II processivity. Sci Adv 2020;6:eaaz5041. https://doi.org/10.1126/sciadv.aaz5041.
[166] Malcovati L, Della Porta MG, Pietra D, et al. Molecular and clinical features of refractory anemia with ringed sideroblasts associated with marked thrombocytosis. Blood 2009;114:3538–45. https://doi.org/10.1182/blood-2009-05-222331.
[167] Nathan DI, Feld J, El Jamal SM, et al. Myelodysplastic syndrome/myeloproliferative neoplasm with ring sideroblasts and thrombocytosis: Ringing in a new future. Leukemia Research 2022;115:106820. https://doi.org/10.1016/j.leukres.2022.106820.
[168] Lapidot-Lifson Y, Patinkin D, Prody CA, et al. Cloning and antisense oligodeoxynucleotide inhibition of a human homolog of cdc2 required in hematopoiesis. Proc Natl Acad Sci USA 1992;89:579–83. https://doi.org/10.1073/pnas.89.2.579.
[169] Savoy L, Long N, Lee H, et al. CDK12 /13 dual inhibitors are potential therapeutics for acute myeloid leukemia. Br J Haematol 2023;202:195–8. https://doi.org/10.1111/bjh.18843.
[170] Gíslason MH, Demircan GS, Prachar M, et al. BloodSpot 3.0: a database of gene and protein expression data in normal and malignant haematopoiesis. Nucleic Acids Research 2024;52:D1138–42. https://doi.org/10.1093/nar/gkad993.
[171] Arafeh R, Shibue T, Dempster JM, et al. The present and future of the Cancer Dependency Map. Nat Rev Cancer 2025;25:59–73. https://doi.org/10.1038/s41568-024-00763-x.
[172] Broad Institute DepMap. DepMap Public 25Q3 2025.
[173] Poulard C, Kim HN, Fang M, et al. Relapse-associated AURKB blunts the glucocorticoid sensitivity of B cell acute lymphoblastic leukemia. Proc Natl Acad Sci USA 2019;116:3052–61. https://doi.org/10.1073/pnas.1816254116.
[174] Ianevski A, Giri AK, Aittokallio T. SynergyFinder 3.0: an interactive analysis and consensus interpretation of multi-drug synergies across multiple samples. Nucleic Acids Research 2022;50:W739–43. https://doi.org/10.1093/nar/gkac382.
[175] Pourhassan H, Murphy L, Aldoss I. Glucocorticoid Therapy in Acute Lymphoblastic Leukemia: Navigating Short-Term and Long-Term Effects and Optimal Regimen Selection. Curr Hematol Malig Rep 2024;19:175–85. https://doi.org/10.1007/s11899-024-00735-w.
[176] Nguyen K, Devidas M, Cheng S-C, et al. Factors influencing survival after relapse from acute lymphoblastic leukemia: a Children's Oncology Group study. Leukemia 2008;22:2142–50. https://doi.org/10.1038/leu.2008.251.
[177] Van Der Zwet JCG, Smits W, Buijs-Gladdines JGCAM, et al. Recurrent NR3C1 Aberrations at First Diagnosis Relate to Steroid Resistance in Pediatric T-Cell Acute Lymphoblastic Leukemia Patients. HemaSphere 2021;5:e513. https://doi.org/10.1097/HS9.0000000000000513.
[178] Chen J, Liu H, Zhang Y, et al. CDK13 drives clear cell renal carcinoma through METTL16-mediated m6A modification of ACLY mRNA. Exp Mol Med 2026;58:472–86. https://doi.org/10.1038/s12276-025-01634-7.

[179] Houles T, Boucher J, Lavoie G, et al. The CDK12 inhibitor SR-4835 functions as a molecular glue that promotes cyclin K degradation in melanoma. Cell Death Discov 2023;9:459. https://doi.org/10.1038/s41420-023-01754-x.
[180] Cabrera-Ortega AA, Feinberg D, Liang Y, et al. The Role of Forkhead Box 1 (FOXO1) in the Immune System: Dendritic Cells, T Cells, B Cells, and Hematopoietic Stem Cells. Crit Rev Immunol 2017;37:1–13. https://doi.org/10.1615/CritRevImmunol.2017019636.
[181] Stern YE, Ghosh P, Peroza J, et al. Targeting CDK12/13 Drives Mitotic Arrest to Overcome Resistance to KRASG12C Inhibitors. Cancer Res 2025. https://doi.org/10.1158/0008-5472.CAN-25-0450.
[182] Frei K, Schecher S, Daher T, et al. Inhibition of the Cyclin K-CDK12 complex induces DNA damage and increases the effect of androgen deprivation therapy in prostate cancer. Intl Journal of Cancer 2024;154:1082–96. https://doi.org/10.1002/ijc.34778.

Appendix

Bioethical committee approval

Komisja Bioetyczna
przy Warszawskim Uniwersytecie Medycznym

Tel.: 022/ 57 - 20 -303
Fax: 022/ 57 - 20 -165

ul. Żwirki i Wigury nr 61
02-091 Warszawa

e-mail: komisja.bioetyczna@wum.edu.pl
www.komisja-bioetyczna.wum.edu.pl

Warszawa, dnia 05.02.2024

AKBE/ 36 / 2024

Lek. Julia Dudkiewicz
Zakład Metodologii Badań Naukowych
Centrum Badań Przedklinicznych WUM
ul. Banacha 1B,
02 – 097 Warszawa

OŚWIADCZENIE

Niniejszym oświadczam, że Komisja Bioetyczna przy Warszawskim Uniwersytecie Medycznym w dniu 05 lutego 2024 r. przyjęła do wiadomości informację na temat badania pt. "Inhibitor kinazy zależnej od cytokin 12 i 13 jako nowy potencjalny lek w ostrej białaczce limfoblastycznej."
Przedstawione badanie nie stanowi eksperymentu medycznego w rozumieniu art. 21ust.1 ustawy z dnia 5 grudnia 1996 r. o zawodach lekarza i lekarza dentysty (Dz.U. z 2018 r poz. 617) i nie wymaga uzyskania opinii Komisji Bioetycznej przy Warszawskim Uniwersytecie Medycznym, o której mowa w art. 29 ust.1 ww. ustawy.

Przewodnicząca Komisji Bioetycznej

Prof. dr hab. n. med. Magdalena Kuźma –Kozakiewicz